Department of Physics and Astronomy
Ruprecht-Karls-University Heidelberg

Diploma thesis
in Physics
submitted by
Kai Felix Mackenroth
born in Lübeck
2009

Multiphoton COMPTON scattering in ultra-short laser pulses

This diploma thesis was carried out by

Kai Felix Mackenroth

at the

Max-Planck-Institut for Nuclear Physics

under the supervision of

Prof. Christoph H. Keitel

Vielphotonen Compton-Streuung in ultra-kurzen Laserpulsen

Zusammenfassung:
Diese Arbeit ist der Berechnung von Emissionsspektren eines Elektrons, das an einem ultra-kurzen, hochintensiven Laserpuls streut, gewidmet. Als ultra-kurz bezeichnen wir Laserpulse, die nur eine Periode des elektrischen Laserfelds enthalten. Um hochintensive Laserfelder beschreiben zu können, berechnen wir die Emissionsspektren im sogenannten Furry Bild der Quantendynamik, in dem ein externes elektromagnetisches Feld exakt berücksichtigt wird. Für die Fälle eines sehr schwachen sowie eines ultra starken Laserpulses präsentieren wir analytische Ausdrücke für das Emissionsspektrum. Für den Fall mittelstarker Laserpulse präsentieren wir numerisch berechnete Spektren. Abschließend werden wir noch den Einfluss einer veränderten Träger-Einhüllenden-Phase auf die Emissionsspektren untersuchen.
Die Hauptergebnisse dieser Arbeit sind das Nachweisen klarer Unterschiede zwischen Elektronstreuung an einem ultra-kurzen und an einem langen Laserpuls, was bisher in der Literatur untersucht wurde. Außerdem weisen wir darauf hin, dass die Ergebnisse dieser Arbeit die Möglichkeit andeuten, aus den Winkelverteilungen der gestreuten Photonen Rückschlüsse auf die Träger-Einhüllenden-Phase zu ziehen.

Multiphoton Compton scattering in ultra-short laser pulses

Abstract:
This work is dedicated to the computation of emission spectra of an electron scattering off an ultra-short and highly intense laser pulse. By ultra-short we label pulses containing only a single cycle of the laser's electric field. To be able to describe highly intense laser fields we compute the emission spectra in the so called Furry picture of quantum dynamics taking an external electromagnetic field into account exactly. For weak and ultra-strong incident laser pulses we will present analytical expressions for the emission spectra. For intermediate laser intensities we are going to present numerically computed spectra. Finally we are going to investigate the influence of a changed carrier-envelope phase on the emission spectra.
The main results of this work concern the observation of distinct differences in electron scattering between an ultra-short and a long laser pulse what has been investigated in the literature so far. Furthermore we note that the results of this work indicate the possibility to infer the carrier-envelope-phase from the angular distribution of the scattered photons.

Contents

Chapter 1

Introduction

1.1 Implementation into the historical context

There are two basical trends in physics we track to motivate this work.
The first one of these are the theoretical studies of the interactions of unbound electrons with strong external electromagnetic fields.
The second development is the emergence of high intensity lasers which are needed to make experimental tests of the previously mentioned strong field effects feasible. Due to the remarkable progress in this latter area over the past decades theoretical interest in the former one has been revived. As introductory chapters we will sketch the historical developments in both fields of research.

1.1.1 Interaction of free electrons with radiation

According to classical electrodynamics radiation is composed of plane electromagnetic waves. These are characterized by their electric and magnetic fields $\boldsymbol{E}$ and $\boldsymbol{B}$, respectively, and their frequency ω [1]. In a plane wave in vacuum the modulus of $\boldsymbol{E}$ and $\boldsymbol{B}$ are the same. The interaction of an electron with charge $e < 0$ moving with the velocity vector $\boldsymbol{v}$ with a plane wave radiation field can then be thought of to be a force of the form

$$\boldsymbol{F} = e\left(\boldsymbol{E} + \frac{\boldsymbol{v}}{c} \times \boldsymbol{B}\right) \tag{1.1}$$

where c is the speed of light. From Eq. (1.1) we see that for electron velocities $|\boldsymbol{v}|$ much smaller than the speed of light the electron will exclusively feel the force applied to it by the electric field. Only for large velocities the electron will also feel the wave's magnetic field.
According to classical electrodynamics an accelerated charge emits radiation. This process of emission may be called *scattering* of the incident radiation by the electron. This very simple picture is called THOMSON scattering and was first theoretically described by THOMSON in 1906 [2]. The formula derived by him describes the scattering of radiation very well as long as the incident radiation field is of comparatively small amplitude and frequency. These conditions may be cast into mathematical form as

$$\frac{|e|\,E}{m\,\omega\,c} \ll 1 \qquad ; \qquad \frac{\hbar\omega}{m\,c^2} \ll 1. \tag{1.2}$$

Here the quantities are defined analogously to Eq. (1.1) with $E = |\boldsymbol{E}|$ and m is the electron mass.
In Eq. (1.2) the left inequality does not contain PLANCK's constant $\hbar$ and thus obviously is a classical condition for the smallness of the electric field amplitude. It states that the electric field within one period accelerates the electron only to velocities much smaller than the speed of light. In other words this first inequality ensures the electron to remain non-relativistic inside the radiation field. The right inequality ensures that the electromagnetic field quanta carry only an energy amount much smaller than the electron's rest mass. Therefore the quantum nature of light can be neglected in the interaction with the electron. If in the above approximations one now considers the incident radiation field to be periodic the motion of the accelerated electron will be periodic as well and it will emit radiation with identical frequency as the incident radiation.
There has been vast experimental proof for THOMSON scattering of low intensity light off free electrons. So the theory of low intensity light scattering is commonly accepted and can be found in any textbook of classical electrodynamics nowadays.
As we mentioned earlier, the classical THOMSON scattering is valid for small field amplitudes and frequencies only. For the former case, i.e. deviations from the THOMSON scattering predictions due to large field amplitudes, there even is a classical explanation available. If the incident radiation has a very large amplitude, the electron will be accelerated to very high velocities almost instantaneously. Although if the electron speed approaches the speed of light, from Eq. (1.1) we see that the magnetic force becomes important. The electron then will no longer be linearly accelerated along the electric field lines but much rather exhibit a complicated motion [3]. Additionally, it is obvious that the electron's velocity cannot grow linearly with the radiation field amplitude anymore as soon as it becomes of the order of the speed of light since it must not exceed c. In this regime necessarily nonlinear effects in the scattering will appear. Nonlinear in this sense means that quantities like for instance the scattering rate depend nonlinearly on the field intensity.
These and many further results have been obtained in numerous treatments of an electron scattering off an intense radiation field on the basis of classical calculations [3–8] as well as quantum considerations [9–14]. Throughout all of these works the strength of nonlinear effects is characterized by the relativistically invariant parameter

$$\xi = \frac{|e|\,E}{\omega\, m\, c}. \tag{1.3}$$

As soon as $\xi \sim 1$ the electron will attain relativistic speeds inside the radiation field. The electric field strengths needed to attain a relativistic parameter equal to unity for optical radiation and for X-rays would be $E\,(\hbar\omega \sim 1\mathrm{eV})|_{\xi=1} \sim 10^{10}\,\mathrm{V/cm}$ and $E\,(\hbar\omega \sim 1\mathrm{keV})|_{\xi=1} \sim 10^{13}\,\mathrm{V/cm}$, respectively, corresponding to laser intensities

$$I\,(\hbar\omega \sim 1\mathrm{eV})|_{\xi=1} \approx 10^{18}\frac{\mathrm{W}}{\mathrm{cm}^2} \qquad ; \qquad I\,(\hbar\omega \sim 1\mathrm{keV})|_{\xi=1} \approx 10^{24}\frac{\mathrm{W}}{\mathrm{cm}^2}. \tag{1.4}$$

In the optical regime $\hbar\omega \sim 1$ eV laser intensities of these orders have already been obtained during the last decade [15].
The parameter ξ is often referred to as the *nonlinearity* or *intensity parameter* and it is well fit to distinguish the onset of nonlinear interactions [12, 13]. The effects introduced above are

equally referred to as either *nonlinear* or *relativistic* THOMSON scattering and there has already been a variety of undisputable experimental proof of nonlinear THOMSON scattering [16–21]. In these works laser systems were employed reaching nonlinearity parameters on the order of up to $\xi \sim 1 - 10$.

There exists another possible physical interpretation for the nonlinear dependence of the scattering rates on the field intensity besides being due to the electron attaining relativistic velocities: When in the beginning of the past century the quantum hypothesis was developed people began to consider radiation as streams of photons [22]. In the photon picture of radiation the intensity of the radiation field is connected to the photon number density. That means that for a not too intense radiation field the electron will basically always scatter only one photon from it. This facilitates the interpretation that as long as the electron scatters only one photon from the radiation field the scattering rates will depend linearly on its intensity. On the other hand if the incident radiation is very intense i.e. its photon flux is very high the electron absorbs not only one but many photons from the radiation field. Thus, the scattering rate will no longer depend linearly on the number of photons in the radiation field but it will exhibit a more complex dependency. In this picture of radiation the parameter ξ gives the ratio of energy absorbed by the electron over one COMPTON wavelength $\lambda_C = \hbar/mc$ in units of the incident photon energy. In this sense as soon as $\xi \gtrsim 1$ the electron absorbs more than one photon from the laser what again yields nonlinear effects.

Moreover, besides offering an elegant interpretation for deviations from classical THOMSON scattering for high field strengths quantum theory is inevitably needed to explain what happens when an electron scatters of high frequency radiation fields. Already from the second inequality of Eq. (1.2) we could guess that it would take quantum mechanical considerations to understand what happens if $\hbar\omega \sim mc^2$. This is the second possible path how the realm of classical THOMSON scattering may be left. In addition while the case of large field amplitudes could still be described in terms of classical electrodynamics in the case of high frequency incident radiation this is no longer possible. In that case COMPTON could show in 1923 that the scattered radiation will no longer have the same frequency as the incident radiation [23]. To derive COMPTON's results theoretically one has to take quantum mechanical considerations into account. In this theory radiation is composed of single photons [22] each carrying a momentum of

$$p_\gamma = \frac{\hbar\omega}{c}. \tag{1.5}$$

From this formula we derive an interpretation of the onset of COMPTON scattering: If the photon frequencies become very large, so does their momentum. COMPTON scattering may then be interpreted as the scattering of an electron with a photon carrying such a large momentum that it kicks back the electron. In fact the essential difference between THOMSON and COMPTON scattering is the recoil of the involved electron which classical electrodynamics cannot explain. So whenever in this work we will mention differences between classical and quantum mechanical effects we equally well could have called this differences between THOMSON and COMPTON scattering or between processes in which the electron does or does not experience a recoil. Furthermore we point out that it is unimportant if the electron recoils from the absorbed or the emitted photon. So even for a low-energy incident photon there may arise the necessity to take quantum effects into account for in certain conditions the emitted photon may carry a large momentum. Actually this effect may arise by employing nowadays available

lasers. As we pointed out an electron may absorb far more than one photon upon scattering from a highly intense laser field. The photon flux in state-of-the-art laser facilities may now become so dense that the electron absorb up to millions of photons resulting in the emission of one single high energetic photon. This photon may then cause the electron to recoil even though in every respective absorption process of a photon from the laser the recoil is negligible. This combination of effects are called *nonlinear quantum effects*.
Indeed there have been numerous works on the theoretical description of multiphoton scattering as well in terms of classical electrodynamics (THOMSON scattering) [3,6–8] as in terms of quantum electrodynamics (COMPTON scattering) [10–14]. Throughout these works the strength of these nonlinear quantum effects is described by a dimensionless parameter

$$\chi = |e| \frac{\hbar \sqrt{\left(F_{\mu\nu} p^{\nu}\right)^2}}{c^3 m^3}$$

where p_μ is the electron's initial four momentum and $F_{\mu\nu}$ the electromagnetic field amplitude. The parameter χ is a measure for the radiation's field amplitude [10, 13]. It is always possible to consider the scattering of an electron with a photon in a reference frame in which both particles are initially counter-propagating and in that frame the resulting formulas have a simplified structure. In this special reference frame $\chi = \gamma_0 \left(1 + \beta\right) \mathcal{E}/E_{\mathrm{cr}}$ expresses the ratio of the incident radiation's electric field and the critical field of QED E_{cr} evaluated in the reference frame in which the incident electron initially is at rest. The critical field is defined as

$$E_{\mathrm{cr}} = \frac{m^2 c^3}{|e| \hbar} = 1.3 \cdot 10^{16} \frac{\mathrm{V}}{\mathrm{cm}} \tag{1.6}$$

performing a work $\Delta\mathscr{E} = mc^2$ over one electron COMPTON wavelength. Creating an electric field of that amplitude would demand a laser intensity of

$$I_{\mathrm{cr}} = \frac{c}{8\pi} E_{\mathrm{cr}}^2 = 2.3 \cdot 10^{29} \frac{\mathrm{W}}{\mathrm{cm}^2}. \tag{1.7}$$

The physical relevance of this quantity is that in an electric field of the critical field strength there arises the possibility of creating electron positron pairs from vacuum [24, 25]. So if the parameter χ approaches unity the electron will feel an electric field strength at which there are nonlinear QED effects expected to happen. However, the parameter χ does not constitute a measure for the importance of quantum effects i.e. the COMPTON effect in general. For instance in single photon COMPTON scattering corresponding to $\xi \ll 1$ there definitely are quantum effects observable. But still $\chi \ll 1$ holds and this process is linear in the electric field intensity. The parameter χ really is a measure for the existence of *nonlinear* quantum effects which may arise by either letting nonlinear effects become quantum mechanical or by having quantum effects becoming nonlinear. Analogously it has be pointed out that for small intensity parameters $\xi \ll 1$ quantum effects scale with the photon energy while for the opposite case $\xi \gg 1$ they scale with the parameter χ i.e. rather with the electric field strength [13].
All available electric and magnetic fields fall short of reaching the critical field strength by at least three or four orders of magnitude. However, the condition $\chi \sim 1$ has already been realized in an experimental setup where a beam of ultra-relativistic electrons with a kinetic energy of

$\epsilon_{\text{kin}} \approx 250$ GeV impinges on a crystal [26, 27]. A crystal is used because under certain incident angles of the electron beam the electric fields of the periodically arranged atomic nuclei in a crystal will add up to make the incident electron feel a very strong electromagnetic field. The tremendous electron energies utilized in this experiment have exclusively been achieved at the *Super Proton Synchrotron* (SPS) at *CERN*.

As we pointed out another possible realization of nonlinear quantum effects is becoming more and more feasible through the advent of high intensity laser systems. The use of a laser instead of a crystal would be preferable for the electric field created by a laser is much better controllable and better known than the field inside a crystal where the literally unavoidable lattice defects and impurities lead to deviations from perfect periodicity. Additionally for high precision calculations in a crystal one would have to consider a whole class of perturbations of the electric field rising from the finite size of the atomic nuclei such as form factors or even QCD effects. Summed up a plane wave laser field provides a much cleaner and ideal experimental environment than a crystal.

To the best of the author's knowledge due to lack of sufficiently intense laser systems so far nonlinear COMPTON scattering in a laser field has been verified in only one experimental setup [28]. There the authors were taking advantage of the unique experimental facility of the *Stanford Linear Accelerator* (SLAC) and could compensate the lack of intense laser radiation by the use of a highly relativistic electron beam with energies of $\epsilon \approx 50$ GeV. But with the development of laser systems to ever higher peak intensities more experimental tests for nonlinear COMPTON scattering seem to be in reach.

As a final remark we emphasize that all theoretical works done so far on nonlinear COMPTON scattering mostly considered a perfectly monochromatic laser wave [10–13]. However, there has been some work published on electron scattering from a laser pulse of duration τ and period T [14] but there the authors considered a pulse fulfilling the condition

$$\frac{\tau}{T} \gg 1. \tag{1.8}$$

This corresponds to the demand that the laser pulse contains many cycles of the electric field and would look like exemplary shown in Fig. 1.1

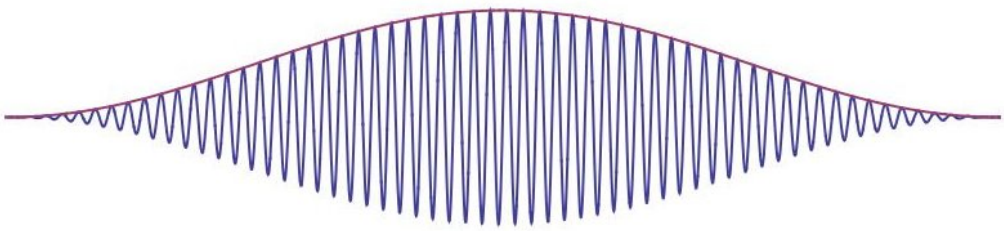

Figure 1.1: A typical laser pulse fulfilling condition (1.8)

Here the blue line is the actual electric field of the laser and the purple line gives the envelope function shaping the pulse.

1.1.2 Increase of laser peak intensities

There has been a tremendous increase in available peak laser intensities over the past decades as can be viewed in Fig. 1.2 which we took from [15].

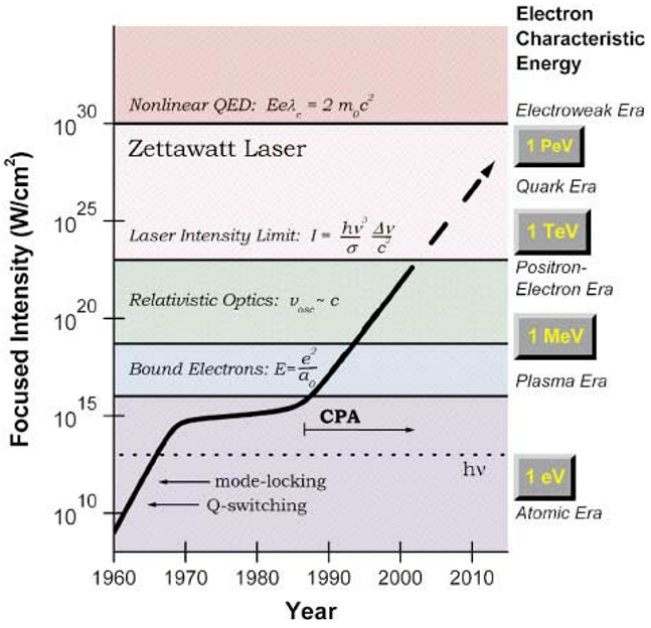

Figure 1.2: Evolution of laser intensities over the past decades according to [15]

It can be seen that all technical inventions leading to considerable improvements in available laser intensities such as Q-switching, modelocking or Chirped Pulse Amplification (CPA) involved ever shorter laser pulses. So the importance of the possibilities given by shortening pulse lengths is remarkable.
However, all lasers available up to now reach peak intensities far below the SCHWINGER limit (1.7). The highest optical laser intensities reported are on the order of $2 \cdot 10^{22}\,\mathrm{W/cm^2}$ achieved by the HERCULES laser system at the University of Michigan [29]. This laser system operates at pulse durations of roughly 30 fs. Even though there are a couple of Petawatt laser systems under construction promising focussed laser intensities of $\sim 10^{23}\,\mathrm{W/cm^2}$ these facilities still fall short of creating the critical field strength in a laboratory reference frame. More promising is the proposed *Extreme Light Infrastructure* (ELI) aiming at peak intensities of $10^{25} - 10^{26}\,\mathrm{W/cm^2}$ [30]. This facility is planned to operate at pulse durations of only 5 fs.

1.2 Topic of this work

The task of this thesis is to combine the results of the two previous sections into one framework. In section 1.1.1 we traced the efforts that have been made to understand the dynamics of electrons in strong external electromagnetic fields. We pointed out that interest in this kind of research has been rising in the past years due to tremendous increases in available laser intensities. In section 1.1.2 in turn we recapitulated the development of lasers towards such high peak intensities. This development basically was achieved by improved spatial and temporal confinement of the laser's radiation power. Thus, under realistic conditions a highly intense laser pulse may not be approximated to be monochromatic. Put in quantitative terms relation (1.8) can no longer be assumed to hold. It even has already been accomplished to generate single-cycle laser pulses in the mid-infrared [31] as well as in the extreme ultra-violet (XUV) regime [32]. Such pulses containing one or only a few cycles of the electric field will be distinguished by the condition

$$\frac{\tau}{T} \sim 1 \tag{1.9}$$

with the symbol definitions from Eq. (1.8).
We will label laser pulses fulfilling condition (1.9) *ultra-short*.
To combine the extensive efforts spent in obtaining a quantum mechanical treatment of electron dynamics inside a strong external field with the state-of-the-art techniques of attaining highest field strengths we will present an exemplary treatment of electron dynamics inside an external electromagnetic field we specifically choose to model an ultra-intense, single-cycle, linearly polarized laser pulse. To distinguish the lasers intensities we will use the nonlinearity parameter defined in Eq. (1.3). Our main interest will be focussed on the case of large ξ for only there our calculations will exhibit features of multiphoton scattering. So a visualization of the scattering process we are going to be considered in terms of a FEYNMAN diagram would look like shown in Fig. 1.3.

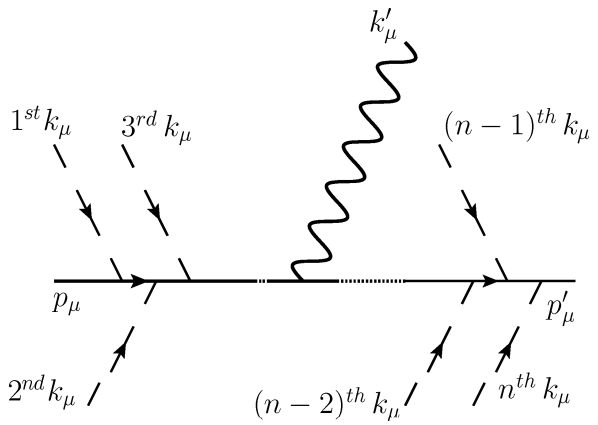

Figure 1.3: Typical FEYNMAN diagram of multiphoton scattering

The electron enters the scattering process with an initial four momentum p_μ. During the interaction time with the laser pulse it may absorb or reemit n photons from or into the laser's photon field all sharing the same wave vector k^μ and at some point the electron emits a single final photon with wave vector k'_μ. In Fig. 1.3 n may be an arbitrarily large natural number

what we represent by the dots inserted into the electron line. After the scattering the electron will propagate with a changed four momentum p'_μ.
So apparently we seem to be urged to compute a process involving $n+1$ single photon absorption or emission processes. To circumvent this tedious task instead of computing these $n+1$ vertices all separately we will take the laser's photon field into account exactly. This task is accomplished by performing the calculations in the FURRY picture for quantum dynamics as described in section 2.1. Investigating a process in this picture will basically relieve us of the duty to consider the n laser photons explicitly by providing us with an exact wave function of an electron propagating inside an external plane wave of arbitrary shape and amplitude. This simplification also becomes evident in the graphical display. Drawn in the FURRY picture the process shown in Fig. 1.3 will look like shown in Fig. 1.4.

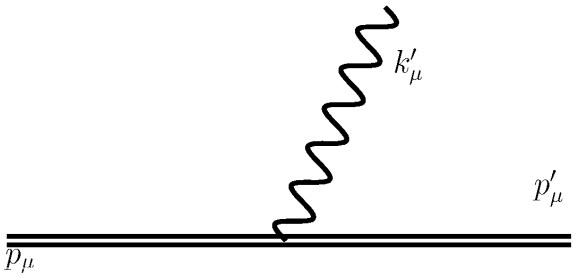

Figure 1.4: FEYNMAN diagram of multiphoton scattering in the FURRY picture

In this figure the double solid line represents the electron inside the external plane wave. In comparison with Fig. 1.3 we can imagine this as incorporating the solid line and all the dashed lines into the double solid line in Fig. 1.4. The only remaining vertex in the FURRY picture is the emission of the single photon with wave vector k'_μ. The interaction of the electron with this radiation field we will treat by perturbation theory.
We are going to treat the process depicted in Fig. 1.4 in three different intensity regimes. More precisely we will show that in the cases of weak ($\xi \ll 1$) or ultra-intense lasers ($\xi \gg 1$) it is possible to obtain analytical approximations for the electron's energy emission spectra (see sections 3, 4.1 and 4.2). To obtain these analytical expressions in the low intensity limit we will expand the emission probability into a TAYLOR series in orders of the small parameter ξ. In this treatment we are going to consider terms up to quadratic order in ξ. Such an expansion corresponds precisely to treating the laser perturbatively. This is why we will call this intensity regime *perturbative regime*.
In the limit of very high intensities $\xi \gg 1$ we are going to expand the defining integrals of the transition amplitude asymptotically.
For the case of $\xi \sim 1$ we will present the results of numerical simulations in section 5.
Finally in section 6 we are going to investigate the effect of changing the carrier-envelope-phase (CEP) on the scattering process. In the scattering of electrons with few-cycle laser pulses the CEP is a quantity of great experimental interest because it has significant influence on the electron dynamics. For strong fields up to now it is an experimentally challenging task to measure the CEP. However, our analysis suggests that it might be possible to determine the CEP from emission spectra of an electron scattered off the laser pulse.

1.3 Units and symbol conventions

Except from these introductory chapters in this work we are going to employ natural units where the speed of light c and the reduced PLANCK constant $\hbar$ are set equal to unity

$$c = \hbar = 1.$$

The vacuum permittivity is defined to be $\epsilon_0 = 1/4\pi$. Resulting from this there will remain only one physical dimension which we choose to be the energy unit electron volt eV. Additionally it follows that the electron's charge e becomes dimensionless and is expressible in terms of the fine structure constant α_{QED} and looks like $e = -\sqrt{\alpha_{\mathrm{QED}}} \approx -\frac{1}{\sqrt{137}}$.
Furthermore we will use the following conventions

- spatial vectors will be denoted by bold letters such as the three-dimensional position vector $\boldsymbol{r} = (r_1, r_2, r_3)$
- contravariant four-dimensional vectors will be denoted by a letter with an upper Greek index and are expressible as the four-vectors time component and its spatial components which form a three-vector $a^\mu = (a^0, \boldsymbol{a})$; the same vector's covariant components are denoted by the same small letter with a lower index attached to it a_μ
- Greek indices run from $0 \ldots 3$ and wherever in an expression the same index occurs twice it has to be summed over according to EINSTEIN's summation convention
- we use the metric with the signature $(+,-,-,-)$ such that the product of two four vectors reads $a_\mu b^\mu = a_0 b_0 - \boldsymbol{ab}$ and covariant four vectors may consequently be written as $a_\mu = (a^0, -\boldsymbol{a})$
- the DIRAC matrices in standard representaion are γ^μ
- the product of any four-vector a^μ with the four-vector of DIRAC matrices γ_μ will be denoted by FEYNMAN's slash notation $\not{a} = \gamma_\mu a^\mu$
- general quantum mechanical state vectors will be denoted in bra-ket notation $\langle\psi| = |\psi\rangle^\dagger$ while wave functions will be written without brackets ψ
- for a wave function ψ the DIRAC conjugate is denoted by a bar $\bar{\psi} = \psi^* \gamma^0$
- taking the trace of a matrix is denoted by tr
- quantum mechanical operators will be denoted by a capital letter with a hat such as $\hat{A}$ and the commutator of two operators $\hat{A}$ and $\hat{B}$ will be written as $\left[\hat{A}, \hat{B}\right]$
- the dotted equal sign $\doteq$ indicates a TAYLOR expansion with higher orders possibly already dropped
- the symbol $\sim$ denotes the asymptotic behaviour of a variable i.e. $\mathcal{Q} \sim x^n$ for a large quantity x is to be read as $\mathcal{Q} \propto x^n + \mathcal{O}\left(x^{n-1}\right)$

Chapter 2

General scattering theory

2.1 Quantum dynamics in the FURRY picture

The Lagrangian of quantum electrodynamics in the presence of an external potential $A_{\mu,\text{ext}}$ is written [33]

$$\mathcal{L}_{\text{QED}} = \bar{\psi}\left(\mathrm{i}\,\partial\!\!\!/ - m\right)\psi - \frac{1}{4}\left(F_{\mu\nu}\right)^2 \quad - \quad e\bar{\psi}\gamma^\mu\psi A_\mu \quad - \quad e\bar{\psi}\gamma^\mu\psi A_{\mu,\text{ext}} \tag{2.1}$$

with the electric field strength tensor $F_{\mu\nu} = \partial_\mu A_\nu - \partial_\nu A_\mu$ and the electromagnetic vector potential of the radiation field A_μ.
Eq. (2.1) can be written as

$$\mathcal{L} = \mathcal{L}_{\text{free}} + \mathcal{L}_{\text{ext}} + \mathcal{L}_{\text{rad}} \tag{2.2}$$

with Lagrangians of the free DIRAC and photon field $\mathcal{L}_{\text{free}}$ and the interaction Lagrangians with the external and the radiation field $\mathcal{L}_{\text{ext}}$ and $\mathcal{L}_{\text{rad}}$, respectively. The interactions usually are treated by means of perturbation theory as long as they are weak. In case that the external perturbation is strong it can no longer be treated in this way unless one considers all orders of perturbation theory. This is impractical. Thus one combines the free Lagrangian and the interaction Lagrangian of the strong external field to form a common Lagrangian $\mathcal{L}_{\text{free,ext}} = \mathcal{L}_{\text{free}} + \mathcal{L}_{\text{ext}}$. By using this combination as a free Lagrangian one can quantize the DIRAC field inside the external field which then is taken into account exactly. The remaining perturbation by the radiation field of photons emitted by the electron is described by $\mathcal{L}_{\text{rad}}$ and can be treated perturbatively. This is called the FURRY picture of quantum dynamics [34].

2.2 VOLKOV solutions and the question of normalization

Working in the Furry picture requires wave functions for an electron inside an external electromagnetic potential A_μ. Since our external field is a laser beam for simplicity we can choose A_μ to be a plane wave. The four potential then is a function of only one variable

$$A_\mu = A_\mu(\phi)$$

where $\phi = k_\mu x^\mu$ is the wave's invariant phase with a four vector k_μ fulfilling the condition $k_\mu k^\mu = 0$ and the gauge condition $k_\mu A^\mu = 0$.

The desired electron wave functions then are solutions of the Dirac equation in the external potential $A_\mu(\phi)$

$$\left(\gamma_\mu \left(-\mathbb{i}\, \partial_\mu - \mathrm{e}A^\mu\right) - m\right)\psi = 0 \tag{2.3}$$

For the case of A_μ being a plane waves such a solution was found by VOLKOV already in 1935 [35].
These solutions nowadays are commonly used and their derivation can be found in e.g. [36].

$$\psi_p(x) \;=\; \left[1 + e\frac{\not{k}\not{A}}{2(kp)}\right] \frac{u_p}{\sqrt{2p_0\,V}} \exp\left[-\mathbb{i}\int_{-\infty}^{kx}\left(e\frac{pA(\phi)}{pk} - \frac{e^2A(\phi)^2}{2\,pk}\right)\mathrm{d}\phi - \mathbb{i}\;px\right]. \tag{2.4}$$

Here V is a normalization volume that drops out in the end of our calculations and u_p is a constant spinor that will be discussed below.
The VOLKOV solutions are distinguished by p_μ which is the electron's four momentum fulfilling $p_\mu p^\mu = m^2$.
For a vanishing four potential $A_\mu = 0$ these solutions turn into the solutions for a free plane-wave electron

$$\psi_p(x)\Big|_{A=0} \;=\; \frac{u_p}{\sqrt{2p_0\,V}}\mathrm{e}^{-\mathbb{i}\;px} \tag{2.5}$$

where p_μ can be interpreted as the electrons four-momentum. We normalize the spinors according to

$$\bar{u}_p u_p = 2m. \tag{2.6}$$

as is usual for free spinors.
But this choice leads to inevitable difficulties in comparing the results of this quantum calculation with classical considerations. These occur since the VOLKOV wave functions are plane waves stretching out over all space. Thus the interaction time between the electron and the laser pulse will be overestimated in comparison to a pointlike classical electron. In earlier quantum mechanical treatments of electron-laser-scattering (e.g. [13]) this problem did not occur explicitly for when considering an infinite, monochromatic wave train the interaction time is infinite also in classical electrodynamics.
However, we need to compensate in the normalization of the solutions (2.4) for the finite interaction time which classically lasts from the electron's incidence into the laser pulse until its emergence but want to keep the normalization (2.6). So we introduce an additional factor n compensating for the finite interaction time.
Let's assume that in the laboratory frame the pulse has a duration Δt. We consider an electron with energy ϵ and momentum P incident to this pulse along its direction of propagation. The time a classical electron will sojourn inside the pulse then is found by simply adding the speed of the electron to that of the laser pulse and dividing the pulse duration by this velocity. By this computation we find the interaction time as the time a classical electron would stay inside the laser pulse

$$t_{\mathrm{int}} \;=\; \frac{\Delta t}{1 + \frac{P}{\epsilon}} = \Delta t \frac{\epsilon}{\epsilon + P}.$$

Thus we conclude that the factor by which the quantum calculation overestimates the interaction time is $\Delta t/t_{\text{int}} = (\epsilon + P)/\epsilon$. So we found the correct normalization factor n for the spinors (2.6) to compensate for the finite interaction time

$$n = \frac{\epsilon}{\epsilon + P}. \tag{2.7}$$

In order to be able to keep up the textbook calculations for summing and averaging over spin states it is desirable to keep up the normalization of the free spinors (2.6). This can be achieved by multiplying the spinor contained in the wave function (2.4) by the normalization factor n

$$\psi_p(x) \to \psi_p(x) \cdot \frac{\epsilon}{\epsilon + P}.$$

Since the final transition probability will involve the modulus squares of any numerical prefactor in Eq. (2.4) the quantum transition number will be diminished by

$$\left(\frac{\epsilon}{\epsilon + P}\right)^2 \begin{cases} = 1 & \text{if} \quad \gamma_0 = 1 \\ \to \frac{1}{4} & \text{if} \quad \gamma_0 \to \infty \end{cases} \tag{2.8}$$

where $\gamma_0 = \epsilon/m$ is the electron's initial γ-factor. The quantity n^2 will be between these two limiting values for any incoming electron momentum.
Having now the solutions to describe electrons in a short laser pulse at hand we turn to specify the pulse itself.

2.3 The model pulse

To describe a single-cycle pulse we employ the model function for the pulse's four potential

$$A^\mu(\phi) \quad = \quad a^\mu \frac{1}{\cosh(\phi)} \tag{2.9}$$

with the amplitude four-vector $a^\mu = \mathcal{A} \cdot n^\mu$. We use the gauge freedom to put $A_0(\phi) = 0$.
In a reference frame where the laser pulse propagates along the z-axis its wave vector can be written like

$$k^\mu = \frac{1}{T}(1, 0, 0, 1) \tag{2.10}$$

where the parameter T is connected to the pulse duration and will be discussed further below. The invariant phase then can be written like

$$\phi = \frac{t - z}{T}. \tag{2.11}$$

This four potential will lead to electric and magnetic fields of the form

$$\mathbf{E} \quad = \quad \frac{\xi\, m}{T|e|} \frac{\tanh(\phi)}{\cosh(\phi)} \mathbf{n} \tag{2.12}$$

$$\mathbf{B} \quad = \quad -\frac{\xi\, m}{T|e|} \frac{\tanh(\phi)}{\cosh(\phi)} \begin{pmatrix} -n_y \\ n_x \\ 0 \end{pmatrix} \tag{2.13}$$

with $\boldsymbol{n}$ the spatial part of the normalized direction vector n^μ.
We note that both the electric and the magnetic field have the same amplitudes E and B, respectively, namely

$$E = B = \frac{\xi\, m}{T|e|} \frac{|\tanh(\phi)|}{\cosh(\phi)}$$

One conclusion we draw from Eq. (2.12) respecting

$$\max\big|_{\phi\in\mathbb{R}} \left(\frac{\tanh(\phi)}{\cosh(\phi)}\right) = \frac{1}{2}$$

is that the maximal amplitude $\mathcal{E}$ of the electric field vector $\mathbf{E}$ is related to the maximal amplitude of the four potential $\mathcal{A}$ by

$$\mathcal{A} = 2\,T\mathcal{E}$$

and accordingly the invariant intensity parameter becomes

$$\xi = -\frac{e\mathcal{A}}{m} = -\frac{2e\,\mathcal{E}T}{m}. \tag{2.14}$$

To get an idea of the physical pulse described by Eq. (2.12) we plot the normalized electric field amplitude $(\mathcal{E}\,T)/\mathcal{A}$ with respect to z/T at $t = 0$ in Fig. 2.1.

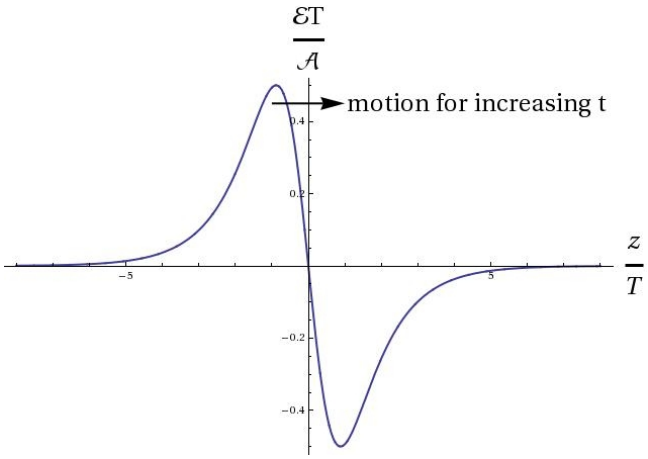

Figure 2.1: The normalized electric field amplitude in dependency of $\frac{z}{T}$

From the electric field's shape depicted in Fig. 2.1 we may infer a physical duration of the pulse described by Eq. (2.9). We define the duration of the pulse as the time τ during which the pulse exceeds one tenth of its peak strength:

$$\tau = 2 \cdot t_{Max} \approx 7 \cdot T \tag{2.15}$$

This is clarified in Fig. 2.2.

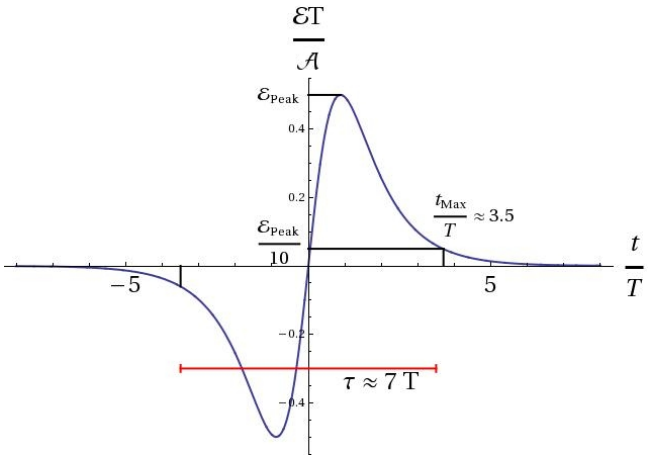

Figure 2.2: Pulse duration of (2.12)

To find the dominant frequency of the incident laser field we investigate the energy distribution of the incident electric field in frequency space. This is calculated as the FOURIER transform of the incoming time-dependent electric field $\mathbf{E}(\phi(t))$ which we know from Eq. (2.12).
The FOURIER transform is calculated as usually for an arbitrary time-dependent function $f(t)$

$$\widetilde{\mathbf{E}}(\omega) \;=\; \frac{1}{\sqrt{2\pi}}\int_{-\infty}^{\infty}\mathbf{E}(t)\,\mathrm{e}^{-\mathbb{i}\,\omega\,t}\mathrm{d}t = -\frac{\mathbb{i}\,m\sqrt{\frac{\pi}{2}}T\xi\omega\mathrm{sech}\left(\frac{\pi T\omega}{2}\right)}{e}\mathbf{n} \tag{2.16}$$

at the fixed space point $z = 0$.
The corresponding energy distribution is proportional to the modulus square of Eq. (2.16)

$$\mathscr{E}(\omega) \propto \omega^2\mathrm{sech}^2\left(\frac{\pi T\omega}{2}\right) \tag{2.17}$$

and looks like Fig. 2.3.

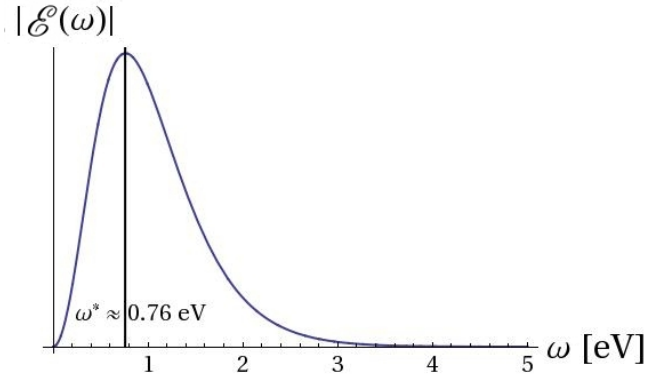

Figure 2.3: Distribution of incoming frequencies for a pulse with $T = 1\,\mathrm{eV}^{-1}$

As we aim to describe optical lasers we may choose

$$T = 1\frac{1}{\mathrm{eV}}. \tag{2.18}$$

for then the incoming laser frequencies ω are on the order of unity and the central frequency is

$$\omega^* \approx 0.76\,\mathrm{eV} (\approx 1600\,\mathrm{nm})$$

which is close to the optical regime.
Second we state that the choice (2.18) corresponds to a pulse duration of

$$\tau = 7\,T \hat{=}\, 4.6\,10^{-15}\,\mathrm{s} \tag{2.19}$$

i.e. roughly 5 fs. This is exactly the order of magnitude of pulse duration experimentally feasible nowadays.
To still further characterize the model pulse (2.9) we connect it to the corresponding laser intensity as this is a laboratory-controllable quantity. To this end we recall Eq. (2.12) and calculate the resulting POYNTING vector $\mathbf{S}$ from which we may easily obtain the instantaneous laser intensity $I_{\max}$ as the POYNTING vector's modulus. It holds

$$\begin{aligned} \mathbf{S} &= \tfrac{\mathbf{E}\times\mathbf{B}}{4\,\pi} &&= \frac{1}{4\,\pi}\left(\frac{\xi\,m}{e\,T}\right)^2 \frac{\tanh^2\left(\frac{t-z}{T}\right)}{\cosh^2\left(\frac{t-z}{T}\right)}\,\hat{\mathbf{z}} \\ \Rightarrow I &= |\mathbf{S}| &&= \frac{1}{4\,\pi}\left(\frac{\xi\,m}{e\,T}\right)^2 \frac{\tanh^2\left(\frac{t-z}{T}\right)}{\cosh^2\left(\frac{t-z}{T}\right)} \end{aligned} \tag{2.20}$$

This quantity is still dependent on the phase ϕ and has the shape shown in Fig. 2.4.

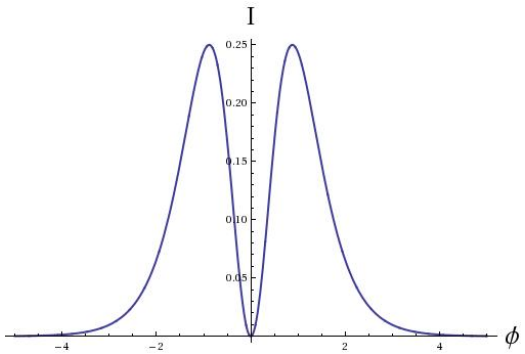

Figure 2.4: Shape of (2.20) in arbitrary units

This function has a maximum at $t_{\max} = \pm T\,\mathrm{arsech}\left[\sqrt{1/2}\right] \approx \pm 0.9\,T$ leading to

$$I_{\max} = \frac{m^2\,\xi^2}{4\,e^2\,\pi\,T^2}. \tag{2.21}$$

We may now state a formula for the intensity parameter ξ in dependence of the intensity I

$$\xi = \sqrt{\frac{I_{\max}\,4\,e^2\,\pi\,T^2}{m^2}} = -\frac{2\,e\,T}{m}\sqrt{I_{\max}\,\pi} \tag{2.22}$$

2.4 General derivation of the transition probability

By inserting our model pulse (2.9) into Eq. (2.4) we can integrate the argument of the exponential in the VOLKOV solutions to obtain

$$\begin{aligned}\psi_p(x) &= \left[1 + e\frac{\not{k}\not{a}}{2(kp)}\frac{1}{\cosh\left(\frac{t-z}{T}\right)}\right]\frac{u_p}{\sqrt{2p_0\,V}}\cdot n \\ &\times \exp\left[-\mathbb{i}\,e\frac{pa}{pk}\left(\frac{\pi}{2} + 2\arctan\left(\tanh\left(\frac{t-z}{2T}\right)\right)\right) + \mathbb{i}\,\frac{e^2\,a^2}{2\,(kp)}\left(\tanh\left(\frac{t-z}{T}\right)+1\right) - \mathbb{i}\;p_\mu x^\mu\right].\end{aligned} \tag{2.23}$$

Here in the wave function for the incoming electron n is the additional normalization factor as obtained in section 2.2. We did not write indices σ and σ' denoting the spin states of the electron because we are going to compute the transition probability averaged over initial and summed over final spin states anyway.
From Eq. (2.23) we are prepared to calculate the scattering matrix element as described in appendix A

$$\begin{aligned}S_{fi} &= -\mathbb{i}\,\frac{e\sqrt{4\pi}\,n}{\sqrt{8\omega'\,p_0'\,p_0\,V^3}}\int \mathrm{d}^4x\;\bar{u}_{p'}\left[\not{\epsilon}'^* + A_1\,\mathrm{sech}\left(\frac{t-z}{T}\right) - A_2\,\mathrm{sech}^2\left(\frac{t-z}{T}\right)\right]u_p \\ &\times \exp\left[\mathbb{i}\left[\alpha\left(\frac{\pi}{2} + 2\arctan\left(\tanh\left(\frac{t-z}{2T}\right)\right)\right) - \beta\left(\tanh\left(\frac{t-z}{T}\right)+1\right) + \left(p_\mu' + k_\mu' - p_\mu\right)x^\mu\right]\right].\end{aligned} \tag{2.24}$$

We defined the abbreviations

$$\begin{aligned}A_1 &:= e\left(\frac{\not{a}\not{k}\not{\epsilon}'^*}{2(kp')} + \frac{\not{\epsilon}'^*\not{k}\not{a}}{2(kp)}\right) \quad ; \quad A_2 := \frac{e^2\,a^2\;(k\epsilon'^*)\,\not{k}}{2(kp)(kp')} \\ \alpha &:= e\left(\frac{p'a}{p'k} - \frac{pa}{pk}\right) \quad ; \quad \beta := \frac{e^2\,a^2}{2}\left(\frac{1}{kp'} - \frac{1}{kp}\right).\end{aligned}$$

The integrations over x and y are now easy. To perform the integration over z and t it is convenient to introduce the new integration variables $C_\pm := (t \pm z)\,/\,(2\,T)$. The integrations in Eq. (2.24) then reduce to a one dimensional integral and we can write

$$\begin{aligned}S_{fi} &= -\mathbb{i}\,\frac{e\sqrt{4\pi}\,n}{\sqrt{8\omega'\,p_0'\,p_0\,V^3}}\,2T^2\,(2\pi)^2\delta_\perp^{(2)}\,(p' + k' - p)\left(\frac{2\pi}{T}\delta\,(p_0' + \omega' - p_0 - (p_3' + k_3' - p_3))\right) \\ &\quad \bar{u}_{p'}\left[\not{\epsilon}'^*\;f_0 + A_1\;f_1 - A_2\;f_2\right]u_p.\end{aligned} \tag{2.25}$$

With the auxiliary functions f_i, $i \in \{0,1,2\}$

$$\boxed{\begin{aligned}f_0 &= \mathrm{e}^{\mathbb{i}\left(\frac{\pi}{2}\alpha-\beta\right)}\int_{-\infty}^{\infty} \mathrm{e}^{\mathbb{i}\,[2\,\alpha\,\arctan(\tanh(x))-\beta\,\tanh(2\,x)]}\mathrm{e}^{i\,K_3 x}\mathrm{d}x \\ f_1 &= \mathrm{e}^{\mathbb{i}\left(\frac{\pi}{2}\alpha-\beta\right)}\int_{-\infty}^{\infty} \mathrm{sech}\,(2x)\;\mathrm{e}^{\mathbb{i}\,[2\,\alpha\,\arctan(\tanh(x))-\beta\,\tanh(2\,x)]}\mathrm{e}^{i\,K_3 x}\mathrm{d}x \\ f_2 &= \mathrm{e}^{\mathbb{i}\left(\frac{\pi}{2}\alpha-\beta\right)}\int_{-\infty}^{\infty} \mathrm{sech}^2\,(2x)\;\mathrm{e}^{\mathbb{i}\,[2\,\alpha\,\arctan(\tanh(x))-\beta\,\tanh(2\,x)]}\mathrm{e}^{i\,K_3 x}\mathrm{d}x\end{aligned}} \tag{2.26}$$

where K_3 is defined as

$$K_3 := T\left(p_0' + \omega' - p_0 + (p_3' + k_3' - p_3)\right) \tag{2.27}$$

Most of the upcoming analysis will be analyzing these parameter functions.
The δ-functions in Eq. (2.25) state the energy momentum conservation in the considered process. In these conservation laws we face a deep difference between the scattering of an electron off a long and off an ultra-short laser pulse. In the former case it is possible to expand the transition matrix element (2.25) into a FOURIER series in which the s^{th} summand contains a four-dimensional energy momentum conserving δ-function of the form $\delta^{(4)}\left(sk_\mu + q_\mu - q_\mu' - k_\mu'\right)$. Here k_μ and k_μ' are laser pulse's and the emitted photon's wave vectors, respectively. Then the δ-functions can be interpreted as energy-momentum conservation laws for an electron absorbing s photons from the laser pulse and emitting a single photon of wave vector k_{mu}'. The quantities $q_\mu = p_\mu - e^2a^2/\left(2(k_\mu p^\mu)\right)k_\mu$ and $q_\mu' = p_\mu' - e^2a^2/\left(2(k_\mu p'^\mu)\right)k_\mu$, however, are the so-called quasi-momentum of the electron before and after scattering (see [13]). The square of these quasi-momenta is not equal to the squared electron mass but much rather to the square of a dressed mass $m^* = m\sqrt{1+\xi^2/2}$. From the fact that in our conservation laws there occurs no quasi-momentum we conclude that an electron scattering off an ultra-short laser pulse inside this pulse unlike in the scattering off a long pulse will not behave as if it had a dressed mass. This prediction could experimentally be tested by measuring not only the final photon's but also the electron's momentum after scattering and checking the energy momentum conservation laws.
The integrals (2.26) are not analytically solvable. To evaluate the expressions for the f_i we apply approximation techniques in the limiting cases $\xi \gg 1$ and $\xi \ll 1$. In these treatments the second and third parameter function f_1 and f_2 are easy to evaluate since these integrals converge. However, f_0 is divergent. Nonetheless in appendix B we show that it is possible to decompose f_0 into a convergent part and a part proportional to a δ-function. When multiplying f_0 with the δ-functions present in (2.25) this latter part is proportional to $\delta^{(4)}\left(p_\mu - p_\mu' - k_\mu'\right)$. This corresponds to the energy conservation law of a free photon emitting a single photon. This process can never occur because it cannot fulfill momentum conservation. Thus this term can be dropped. Consequently the first parameter function may be written like

$$\begin{aligned} f_0 &= -\mathrm{e}^{\mathrm{i}\left(\frac{\pi}{2}\alpha-\beta\right)}\frac{2}{K_3}\int_{-\infty}^{\infty}\mathrm{d}x\ \mathrm{e}^{\mathrm{i}\left(2\,\alpha\,\arctan(\tanh(x))-\beta\,\tanh(2\,x)\right)}\ \mathrm{e}^{\mathrm{i}\,K_3\,x} \\ &\quad \times\operatorname{sech}(2x)(\alpha-\beta\operatorname{sech}(2x)) \\ &= -\frac{2}{K_3}\left(\alpha\,f_1 - \beta\,f_2\right). \end{aligned} \tag{2.28}$$

The photon and electron spin summed and averaged modulus square of the scattering matrix element S_{fi} is computed in appendix C. The transition probability is then of the form $W = \int \mathrm{d}W/\left(\mathrm{d}\Omega\mathrm{d}\omega'\right)\mathrm{d}\Omega\mathrm{d}\omega'$ with the integrand being the differential emission probability per solid angle element $\mathrm{d}\Omega$ and frequency interval $\mathrm{d}\omega'$. From this quantity we derive the differentially emitted energy $\mathrm{d}\mathscr{E}/\left(\mathrm{d}\Omega\mathrm{d}\omega'\right) = \mathrm{d}W/\left(\mathrm{d}\Omega\mathrm{d}\omega'\right)\cdot\omega'$. This quantity is equally called the *energy spectrum* of the scattering and in the present case reads

$$
\begin{aligned}
\frac{\mathrm{d}\mathscr{E}}{\mathrm{d}\omega' \mathrm{d}\mathcal{T} \mathrm{d}\varphi} &= \frac{\omega'^2 e^2 T^2 n^2}{\pi^2 \left(\epsilon - \omega' + \frac{\omega'(\epsilon + P\mathcal{T})}{\epsilon + P - \omega'(1-\mathcal{T})}\right) \epsilon} \\
&\times \left[\left(\epsilon \left(\epsilon - \omega' + \frac{\omega'\left(\epsilon + P\mathcal{T}\right)}{\epsilon + P - \omega'(1-\mathcal{T})}\right)\right.\right. \\
&+ P \left(\frac{\omega'\left(\epsilon + P\mathcal{T}\right)}{\epsilon + P - \omega'(1-\mathcal{T})} - P - \omega'\mathcal{T}\right) - 2m^2 \Bigg) |f_0|^2 \\
&+ \mathcal{A} e\, \omega' \sqrt{1-\mathcal{T}^2} \cos(\varphi) \left(\frac{\epsilon + P}{\epsilon + P - \omega'\left(1-\mathcal{T}\right)} - 1\right) \Re\left(f_0 f_1^*\right) \\
&- e^2 \mathcal{A}^2 \Re\left(f_0 f_2^*\right) \\
&\left. + \frac{e^2 \mathcal{A}^2}{2} \left[\frac{\epsilon + P - \omega'\left(1-\mathcal{T}\right)}{\epsilon + P} + \frac{\epsilon + P}{\epsilon + P - \omega'\left(1-\mathcal{T}\right)}\right] |f_1|^2\right] \qquad (2.29)
\end{aligned}
$$

Here we defined $\mathcal{T} = \cos(\vartheta)$ and it holds $\mathrm{d}\Omega = -\,\mathrm{d}\mathcal{T}\mathrm{d}\varphi$.
To obtain Eq. (2.29) we evaluated the energy spectrum in the reference frame where the electron and the laser beam are initially counter-propagating and the laser pulse being linearly polarized along the x-axis

$$
\begin{aligned}
p_\mu &= \left(\epsilon = \sqrt{m^2 + P^2}, 0, 0, -P\right) \\
k_\mu &= \left(\frac{1}{T}, 0, 0, \frac{1}{T}\right) \\
a_\mu &= \mathcal{A}\,(0, 1, 0, 0) \\
p'_\mu &= (\epsilon', p'_1, p'_2, p'_3) \\
k'_\mu &= (\omega', k'_1, k'_2, k'_3)\,. \qquad (2.30)
\end{aligned}
$$

This choice of coordinates is visualized in Fig. 2.5.

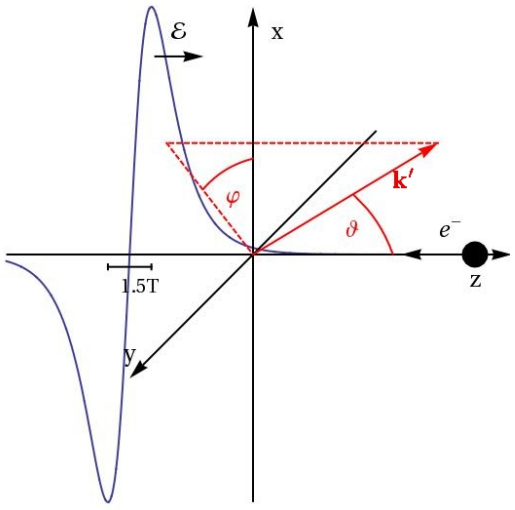

Figure 2.5: The special coordinate system

Here the outgoing photon's spatial wave vector $\mathbf{k}'$ is depicted in solid red and characterized by

its polar angle ϑ and its azimuthal angle φ.
In this reference frame due to the momentum conserving δ-functions there exist relations between the momentum of the outgoing electron and photon

$$\begin{aligned} p_1' = & \quad -k_1' & = -\omega' \sin(\vartheta)\cos(\varphi) \\ p_2' = & \quad -k_2' & = -\omega' \sin(\vartheta)\sin(\varphi) \\ \epsilon' - p_3' = & \quad \epsilon + P - \omega' + k_3' & = \epsilon + P - \omega'(1-\cos(\vartheta)). \end{aligned} \tag{2.31}$$

The last line of (2.31) states the difference between the total energy of the outgoing electron and the third component of its spatial momentum and as such always has to be positive. But this is true only for frequencies smaller than

$$\boxed{\omega_{\mathrm{Max}} = \frac{\epsilon + P}{1-\cos(\vartheta)}.} \tag{2.32}$$

Eq. (2.32) is an important result of our quantum mechanical calculations since it gives a cutoff frequency which will show up in the energy spectra.
The important process parameters α, β and K_3 can be written as

$$\begin{aligned} \alpha &= -m\,\xi\,T\frac{\omega'\,\sin(\vartheta)\,\cos(\varphi)}{\epsilon + P - \omega'(1-\cos(\vartheta))} \\ \beta &= -\frac{m^2\,\xi^2\,T}{2}\frac{\omega'(1-\cos(\vartheta))}{(\epsilon + P - \omega'(1-\cos(\vartheta)))(\epsilon + P)} \\ K_3 &= 2\,T\frac{\omega'(\epsilon + P\cos(\vartheta))}{\epsilon + P - \omega'(1-\cos(\vartheta))} \end{aligned} \tag{2.33}$$

The quantum parameter χ in the special reference frame we have chosen becomes

$$\chi = \gamma_0(1+\beta)\frac{\mathcal{E}}{E_{\mathrm{cr}}}. \tag{2.34}$$

with E_{cr} the critical field strength of QED.

2.5 The classical limit

For later use we will establish the classical limit of (2.29). Since we consider the incident laser beam to be optical the classical limit will hold whenever

$$\omega' \ll \epsilon.$$

This allows for some major simplifications in Eq. (2.29).

$$\frac{\mathrm{d}\mathscr{E}}{\mathrm{d}\omega'\mathrm{d}\mathcal{T}\,\mathrm{d}\varphi} \overset{\omega' \ll \epsilon}{\approx} \frac{\omega'\,e^2\,T^2\,n^2}{\pi^2\,\gamma_0^2}\left[\xi^2\left(|f_1|^2 - \Re\left(f_0 f_2^*\right)\right) - |f_0|^2\right] \tag{2.35}$$

This is precisely the structure of the energy spectrum as can be found by inserting the solutions of the classical equations of motion [6]

$$\begin{aligned}\mathbf{r}(\phi) &= \mathbf{r}_0 + \frac{1}{k}\int_{\phi_0}^{\phi}\left[\frac{\gamma_0 m\boldsymbol{v}_0 + \frac{e}{c}\boldsymbol{A}(\phi')}{\gamma_0 mc\left(1-\frac{\boldsymbol{k}\cdot\boldsymbol{v}_0}{|\boldsymbol{k}|c}\right)}\right]\mathrm{d}\phi' \\ &\quad + \frac{\boldsymbol{k}}{|\boldsymbol{k}|^2}\int_{\phi_0}^{\phi}\left[\frac{\frac{1}{2}\left(\frac{e\boldsymbol{A}(\phi')}{\gamma_0 mc^2}\right)^2 + \left(\frac{e\boldsymbol{A}(\phi')}{\gamma_0 mc^2}\right)\cdot\left(\frac{\boldsymbol{v}_0}{c}\right)}{\left(1-\frac{\boldsymbol{k}\cdot\boldsymbol{v}_0}{|\boldsymbol{k}|c}\right)}\right]\mathrm{d}\phi' \qquad (2.36)\end{aligned}$$

$$\boldsymbol{\beta}(\phi) = \frac{\boldsymbol{\beta}_0 + \frac{e}{\gamma_0 mc^2}\boldsymbol{A}(\phi) + \frac{\boldsymbol{k}}{|\boldsymbol{k}|}\left[\frac{\frac{1}{2}\left(\frac{e\boldsymbol{A}(\phi)}{\gamma_0 mc^2}\right)^2 + \left(\frac{e\boldsymbol{A}(\phi)}{\gamma_0 mc^2}\right)\cdot\boldsymbol{\beta}_0}{1-\frac{\boldsymbol{k}}{|\boldsymbol{k}|}\cdot\boldsymbol{\beta}_0}\right]}{1+\left[\frac{\frac{1}{2}\left(\frac{e\boldsymbol{A}(\phi)}{\gamma_0 mc^2}\right)^2 + \left(\frac{e\boldsymbol{A}(\phi)}{\gamma_0 mc^2}\right)\cdot\boldsymbol{\beta}_0}{1-\frac{\boldsymbol{k}}{|\boldsymbol{k}|}\cdot\boldsymbol{\beta}_0}\right]}. \qquad (2.37)$$

into the classical expression for the energy spectrum [1]

$$\frac{\mathrm{d}\mathscr{E}}{\mathrm{d}\omega'\mathrm{d}\Omega} = \frac{e^2\omega'^2}{4\pi^2 c}\left|\int_{-\infty}^{\infty}\boldsymbol{n}\times(\boldsymbol{n}\times\boldsymbol{\beta}(t))\,\mathrm{e}^{\mathrm{i}\,\omega'(t-\boldsymbol{n}\boldsymbol{r}(t)/c)}\mathrm{d}t\right|^2. \qquad (2.38)$$

We will compute classical energy spectra via this formula in this work.

2.6 The special case of forward scattering

We first consider the special case of a photon emitted into the initial propagation direction of the laser pulse $\vartheta = 0$. This case is special as essentially no scattering takes place. First we show this analytically.
From Eq. (2.33) we derive expressions for the parameters α, β and K_3 at $\vartheta = 0$

$$\alpha = \beta = 0 \qquad (2.39)$$

$$K_3 = 2\,T\omega' \qquad (2.40)$$

So in this case the parameter functions (2.26) and (2.28) turn into

$$f_0 = 0 \qquad (2.41)$$

$$f_i = \int_{-\infty}^{\infty}\mathrm{d}x\;\mathrm{e}^{i\,K_3 x}\mathrm{sech}^i(2x) = \frac{1}{2}\pi\mathrm{sech}\left(\frac{K_3\pi}{4}\right). \qquad (2.42)$$

and the energy spectrum is found to be

$$\frac{\mathrm{d}\mathscr{E}}{\mathrm{d}\omega'\mathrm{d}\mathcal{T}} = \frac{\pi\omega'^2\,e^2\,T^2\,n^2\,\xi^2}{2\,\gamma_0^2}\mathrm{sech}^2\left(\frac{T\omega'\pi}{2}\right). \qquad (2.43)$$

where the dependency on the azimuthal angle φ has been integrated out and we defined $\mathcal{T} = \cos(\vartheta)$. Formula (2.43) tracks the initial frequency distribution of the laser pulse as can be guessed already from a plot of the power spectrum at $\vartheta = 0$ given in Fig. 2.6.

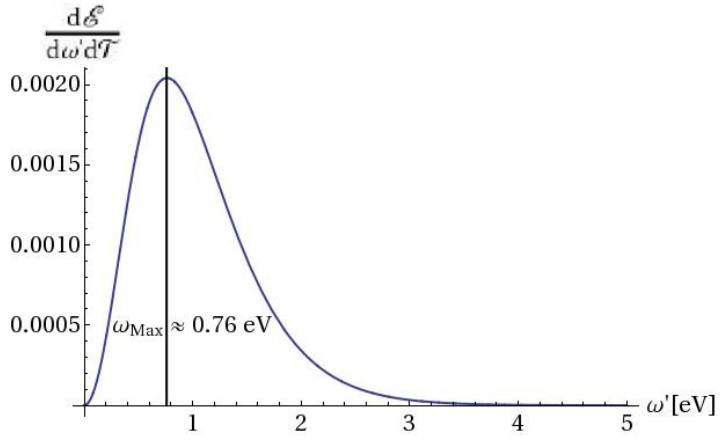

Figure 2.6: Emission spectrum at $\vartheta = 0$

This figure is strongly reminiscent of Fig. 2.3 as it is peaked at the same frequency $\omega^* \approx 0.763$. So we conclude that in the onward propagation direction of the incoming laser pulse the emitted radiation will have the same spectral distribution as the incident laser pulse.
This can also be understood from physical considerations as argued in [13] as well:
In our special coordinate frame for the involved energies and momenta there hold the conservation laws (2.31) whence follows for $\vartheta = 0$

$$\epsilon + P = \epsilon' - p'_3. \tag{2.44}$$

Additionally it follows that for $\vartheta = 0$ it holds $p'_{1,2} = 0$. But for an electron described by VOLKOV wave functions its quantum state is uniquely defined by the quantum numbers p_1, p_2 and $\epsilon - p_3$ [36]. The previous statements show that none of these quantum number changes during a scattering process where a photon is emitted into its initial direction of propagation $\vartheta = 0$. The electron's initial quantum state therefore remains unchanged in the process. However, the electromagnetic field cannot change its state without changing the electron field and it consequently also remains in its initial state. This corresponds to emission of only first harmonic radiation.

Chapter 3

Low intensity regime

3.1 Physical implications

We distinguish the low intensity regime by the condition $\xi \ll 1$. This is equivalent to the statement that over one COMPTON wavelength the laser imparts much less energy on the electron than it could by one single photon. Thus the transition probability will by far be dominated by the probability of single photon scattering of the electron. So unlike Fig. 1.3 the diagramatic illustration of the scattering process in the regime of small ξ will look as is visualized in Fig. 3.1.

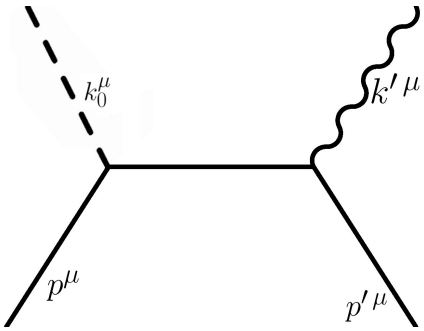

Figure 3.1: FEYNMAN diagram of single photon scattering

This FEYNMAN diagram symbolizes the absorption of a single photon from the laser by the electron with subsequent emission of another photon with wave vector k'^μ. So the limit of small ξ is equivalent to the well known limit of single photon COMPTON scattering.
In this section we are going to consider laser intensities of $I = 10^{16}\,\mathrm{W/cm^2}$ as are commonly available nowadays. However, in order to observe quantum mechanical effects we consider very high initial electron energies of up to $\epsilon = 250$ GeV. Such tremendous electron momenta are actually attained exclusively at the SPS at CERN as already stated in the introduction.

3.2 Parameter functions

To further evaluate Eq. (2.29) we now need to find analytical expressions for the parameter functions f_i. We remind ourselves of Eq. (2.26)

$$f_i \;=\; \mathrm{e}^{\mathrm{i}\left(\frac{\pi}{2}\alpha-\beta\right)}\int_{-\infty}^{\infty}\mathrm{e}^{\mathrm{i}\,[2\,\alpha\,\arctan(\tanh(x))-\beta\,\tanh(2\,x)]}\mathrm{e}^{i\,K_3 x}\mathrm{sech}^{\,i}\,(2x)\;\,\mathrm{d}x$$

In the perturbative regime distinguished by the condition $\xi \ll 1$ we may simplify the integrand notably by expanding the exponential into a power series in ξ up to second order. The Taylor expansion of an exponential in two variables is written as

$$\exp\left[\mathrm{i}\;\;(K_1\,\alpha - K_2\beta)\right] \doteq \left[1+\mathrm{i}\;K_1\,\alpha-\mathrm{i}\;K_2\,\beta-\frac{\alpha^2}{2}K_1^2\right]+\mathcal{O}\left(\alpha^3,\beta^2,\alpha\beta\right)$$

In this expansion we respected the fact that $\alpha \propto \xi$ and $\beta \propto \xi^2$ and we defined

$$K_1 = 2\arctan\left(\tanh\left(x\right)\right) \qquad ; \qquad K_2 = \tanh\left(2\,x\right).$$

Inserting this approximation into Eq. (2.26) and neglecting all terms that would lead to contributions of order ξ^3 or higher in Eq. (2.29) the relevant combinations of the parameter functions needed in Eq. (2.29) are

$$|f_0|^2 \;\approx\; \frac{\alpha^2\,\pi^2}{K_3^2}\mathrm{sech}^2\left(\frac{K_3\pi}{4}\right) \tag{3.1}$$

$$|f_1|^2 \;\approx\; \frac{\pi^2}{4}\mathrm{sech}^2\left(\frac{K_3\pi}{4}\right) \tag{3.2}$$

$$\Re\left(f_0 f_1^*\right) \;\approx\; \frac{\alpha\,\pi^2}{2}\mathrm{sech}^2\left(\frac{K_3\pi}{2}\right) \tag{3.3}$$

$$\Re\left(f_0 f_2^*\right) \;\approx\; \frac{\alpha\,\pi^2}{4}K_3\mathrm{csch}\left(\frac{K_3\pi}{2}\right). \tag{3.4}$$

We realize that the decay of the parameter functions with increasing frequency is basically due to the appearance of the hyperbolic secans and thus is quite fast. This decreasing of the f_i ensures the spectrum to go to zero for larger outgoing frequencies.

3.3 Energy spectrum

Now that we found approximations for the parameter functions f_i in the perturbative regime we may insert these forms into Eq. (2.29) to obtain the transition number in our special reference frame. If we additionally respect the expressions (2.33) we obtain an expression for the differential transition probability which is solely dependent of ϵ, P, T, ω', ϑ and φ. Since in

the resulting expression the dependency on φ is rather simple and we can integrate it to obtain

$$\begin{aligned}
\frac{\mathrm{d}\,\mathscr{E}}{\mathrm{d}\omega'\mathrm{d}\mathcal{T}} = \quad & \frac{\pi e^2 T^2\, n^2 \omega'^2 m^2 \xi^2}{(\epsilon+P)\,(\epsilon+P-\omega'(1-\mathcal{T}))} \\
& \left(\frac{\left(\epsilon\,(\epsilon+P-\omega'(1-\mathcal{T})) + P\left(\frac{\omega'(\epsilon+P\mathcal{T})}{\epsilon+P-\omega'(1-\mathcal{T})} - P - \omega'\mathcal{T}\right) - 2m^2\right)}{4\,(\epsilon+P\mathcal{T})^2} \right. \\
\times \quad & \left(1-\mathcal{T}^2\right) \operatorname{sech}^2\left(T\frac{\pi\omega'\,(\epsilon+P\mathcal{T})}{2\,(\epsilon+P-\omega'(1-\mathcal{T}))}\right) \\
+ \quad & \frac{T\omega'^2\left(\frac{\epsilon+P}{\epsilon+P-\omega'(1-\mathcal{T})}-1\right)}{2\,(\epsilon+P-\omega'(1-\mathcal{T}))}\left(1-\mathcal{T}^2\right)\operatorname{sech}^2\left(T\frac{\pi\omega'\,(\epsilon+P\mathcal{T})}{\epsilon+P-\omega'(1-\cos(\theta))}\right) \\
+ \quad & \frac{1}{4}\left(\frac{\epsilon+P}{\epsilon+P-\omega'(1-\mathcal{T})} + \frac{\epsilon+P-\omega'(1-\mathcal{T})}{\epsilon+P}\right) \\
\times \quad & \left.\operatorname{sech}^2\left(T\frac{\pi\omega'\,(\epsilon+P\mathcal{T})}{2\,(\epsilon+P-\omega'(1-\mathcal{T}))}\right)\right)
\end{aligned} \tag{3.5}$$

with $\mathcal{T} = \cos(\vartheta)$. As metioned in the beginning of this section we choose the laser's intensity to be $I = 10^{16}\,\mathrm{W/cm^2}$. With Eq. (2.22) we then find $\xi \approx 0.07$ which is well in the perturbative regime. For this parameter ξ we plot the energy distributions (3.5) for different momenta of the incoming electron and for different angles ϑ as well.
We are going to show several emission spectra in Figs. 3.2-3.5. Every figure displays emission spectra for a particular initial γ-factor of the incoming electron and consists of three individual plots for the polar angles $\vartheta = 0, \pi/2$ and π. Below and above every diagram there are frequencies printed we will use to interpret the spectra. The upper frequency ω_{Peak} is the numerically found frequency of the actual maximum of the plotted spectrum. The lower frequency ω_{Theo} is the blue shifted central frequency of the initial laser pulse's frequency distribution. If the electron moves with a considerable fraction of the speed of light towards the detector any photon emitted by the electron will be blue shifted. Now reminding ourselves of the discussion in section 2.3 below relation (2.18) we know the dominant energy of the incoming photons to be

$$\omega^* \approx 0.76\,\mathrm{eV}$$

in the present case of $\omega \equiv 1\,\mathrm{eV}$. The relativistic dopplershift now is well known to be

$$\omega' = \gamma_0 \omega\,(1 - \mathbf{n}\cdot\boldsymbol{\beta}) \tag{3.6}$$

with ω and ω' the frequency in the observer's rest frame and in the frame moving relative to it, respectively. The vectors $\boldsymbol{\beta}$ and $\mathbf{n}$ denote the relative velocity of the two inertial systems and the observation direction in the observer's rest frame, respectively. In our case we have

$$\begin{aligned}
\boldsymbol{\beta} &= (0, 0, -\beta) \\
\mathbf{n} &= (\cos(\varphi)\sin(\vartheta), \sin(\varphi)\sin(\vartheta), \cos(\vartheta))
\end{aligned}$$

Next we need to consider that in the rest frame of the electron the predominantly emitted frequency will be the incoming laser frequency. We thus need to transform the incoming laser

frequency which is ω^* in the laboratory frame to the electrons rest frame via

$$\begin{aligned} \omega' &= \gamma_0 \omega^* \left(1 - \frac{\mathbf{k} \cdot \boldsymbol{\beta}}{|\mathbf{k}|}\right) \\ &= \gamma_0 \omega^* (1 + \beta) \end{aligned} \tag{3.7}$$

The second equality holds because $\boldsymbol{k} = (0, 0, k)$ is the wave vector of the laser pulse propagating in z-direction. This frequency now needs to be transformed back into the laboratory frame to find the observed frequency for each incoming electron momentum and observation angle. After recasting Eq. (3.6) and inserting ω' from (3.7) into it one finds as the theoretically predicted frequency of the spectrum's maximum

$$\omega_{\text{Theo}} = \omega^* \frac{1 + \beta}{1 + \beta \cos(\vartheta)} \tag{3.8}$$

We begin presenting the results with three plots for an initial $\gamma_0 = 1$ (electron initially at rest).

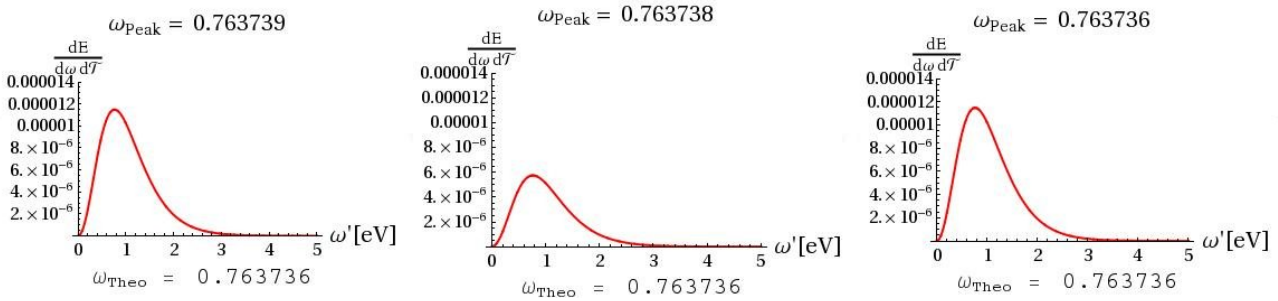

Figure 3.2: Emitted frequency spectra for $\gamma_0 = 1$ for the polar angles from left to right $\vartheta = 0, \frac{\pi}{2}, \pi$

In these plots we can easily recognize a pattern reminiscent of THOMSON scattering for non-relativistic particles. Since the incoming laser pulse is polarized in the x-direction, the electron is accelerated along this direction and radiates most energy symmetrically perpendicular to the direction of its acceleration. Thus we find the same amplitudes in the emission spectra for the angles $\vartheta = 0$ and $\vartheta = \pi$. In the direction of the electron's propagation $\vartheta = \pi/2$ there is least emission.
Next we show the emission spectra of an electron initially moving with a momentum of $P \approx 10^5$ eV in Fig. 3.3. This case is on the edge to a relativistic incoming electron.

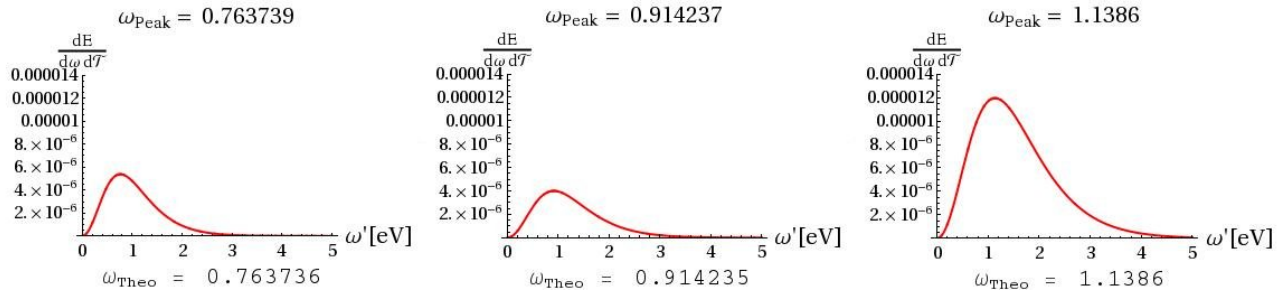

Figure 3.3: Emitted frequency spectra for $\gamma_0 = 1.02 \Leftrightarrow P \approx 10^5\,\mathrm{eV}$ and polar angles from left to right $\vartheta = 0, \frac{\pi}{2}, \pi$

These plots exhibit a different radiation pattern in comparison to Fig. 3.2. First of all we notice that the amplitude of the spectra has increased which proves that the overall emitted energy increases with electron energy as it has to be. Next we note that in Fig. 3.3 there is no symmetry in the emission spectra between the angles $\vartheta = 0$ and $\vartheta = \pi$ but the spectrum at the latter polar angle is significantly more pronounced. We conclude that the electron emits preferentially to its initial direction of propagation. This observation is easily interpreted classically. Since a relativistic electron initially carries an amount of energy much larger than it can absorb from the laser it will not change its initial direction of propagation significantly. An electron moving with relativistic velocities (e.g.$\beta \gtrsim 0.1$), however, emits radiation mainly around its propagation direction [1]. We may therefore regard the concentration of emitted radiation to angles close to $\vartheta = \pi$ for high γ_0 as relativistic focussing. But still in Fig. 3.3 the emission probability at the polar angle $\vartheta = 0$ is higher than at $\vartheta = \pi/2$. This observation proves that at an initial electron momentum of approximately $P = 10^5$ eV still the THOMSON scattering pattern dominates over the relativistic focussing. For higher incoming electron momenta we expect these two features to exchange importance and relativistic focussing to be the dominant feature in the emission spectra.
Next we show spectra for an incoming electron momentum equal to its rest mass $P = m$ in Fig. 3.4.

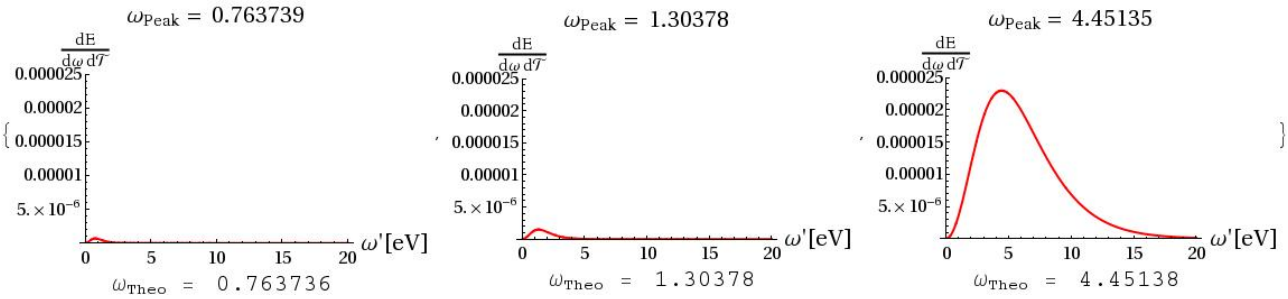

Figure 3.4: Emitted frequency spectra for $\gamma_0 = \sqrt{2} \Leftrightarrow P = m$ and polar angles from left to right $\vartheta = 0, \frac{\pi}{2}, \pi$.

In the diagrams Fig. 3.4 we find the emission amplitude at $\vartheta = \pi/2$ to be larger than at $\vartheta = 0$ and the relativistic focussing starts to dominate the emission spectra over the THOMSON scattering pattern. Hence the spectrum of emitted energy at $\vartheta = \pi$ is overly pronounced and

features a considerably higher amplitude than the emission spectra at the other two angles. For even higher initial electron momenta relativistic focussing will increase this discrepancy in emission amplitudes and at smaller scattering angles the observable emission will become ever less.
Up to now we found very good agreement between the frequencies ω_{Peak} and ω_{Theo} plotted above and below every spectrum, respectively. We therefore claim the shift of these spectra's maxima to be due to a relativistic DOPPLER shift. However, this does not hold for arbitrarily high initial electron momenta. To choose a very large γ-factor we take the largest electron momentum achieved at SLAC up to now [37]. This would be a momentum of $P \approx 50$ GeV corresponding to $\gamma_0 \approx 10^5$. In Fig. 3.5 we plot the resulting emission spectrum exclusively at $\vartheta = \pi$ for at smaller angles there is no emission.

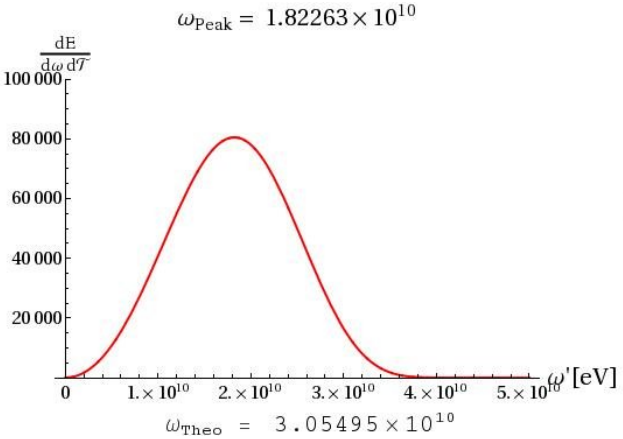

Figure 3.5: The emission spectrum for $\gamma_0 = 10^5 \Leftrightarrow P \approx 50\,\text{GeV}$ at $\vartheta = \pi$

In this spectrum we find not only the theoretically predicted frequency ω_{Theo} to differ from the actual spectrum's maximum frequency by almost a factor 2 but also has the shape of the spectrum changed obviously with respect to Fig. 3.2. To understand this deviation between ω_{Peak} and the prediction from Eq. (3.8) we analyze the quantity ω_{Peak} for very large $\gamma_0 \gg 1$ and at $\vartheta = \pi$. In that case we may approximate $\beta = \sqrt{1-\gamma_0^{-2}} \approx 1 - (2\gamma_0^2)^{-1}$ and express Eq. (3.8) as

$$\omega_{\text{Theo}} \approx 4\omega^* \gamma_0^2$$

The blue shifted central frequency of the incident laser pulse thus is growing quadratically in γ_0. Now looking back at Eq. (2.32) we see that there exists a maximally allowed emission frequency which for large γ_0 and $\vartheta = \pi$ reads as

$$\omega_{\text{Max}} \approx m\,\gamma_0$$

i.e. is growing linearly in γ_0. So from comparing the latter two equalities we already infer that at some value of γ_0 the blue shifted central frequency of the incident laser pulse will exceed the maximally allowed emission frequency. And indeed if we plot the quantities ω_{Theo} and ω_{Max} in dependency of γ_0 we find Fig. 3.6.

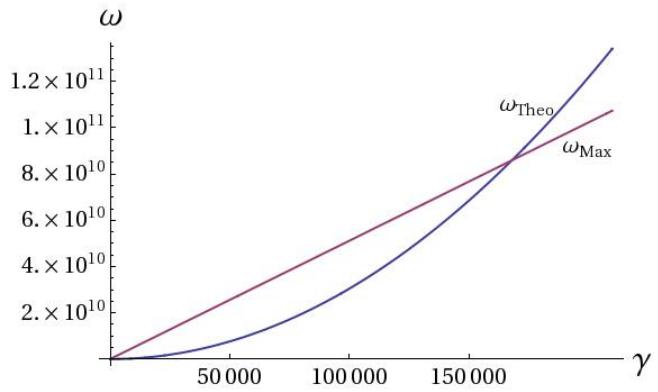

Figure 3.6: Evolution of Eqs. (2.32) and (3.8) for large γ_0

Here we note that for $\gamma_0 = 10^5$ what we identified as the largest γ-factor attainable at SLAC the laser's blue shifted central frequency ω_{Theo} lies already close to ω_{Max}. For such large γ_0 the high energy parts of the spectrum consequently may not be emitted any more which will distort the emission spectrum just as seen in Fig. 3.5. This effect is further enhanced at an initial γ-factor of $\gamma_0 = 0.5 \cdot 10^6$. This corresponds to an electron energy of $\epsilon \approx 250$ GeV which up to date has been achieved only at the SPS at CERN [26]. The resulting emission spectrum is shown in Fig. 3.7

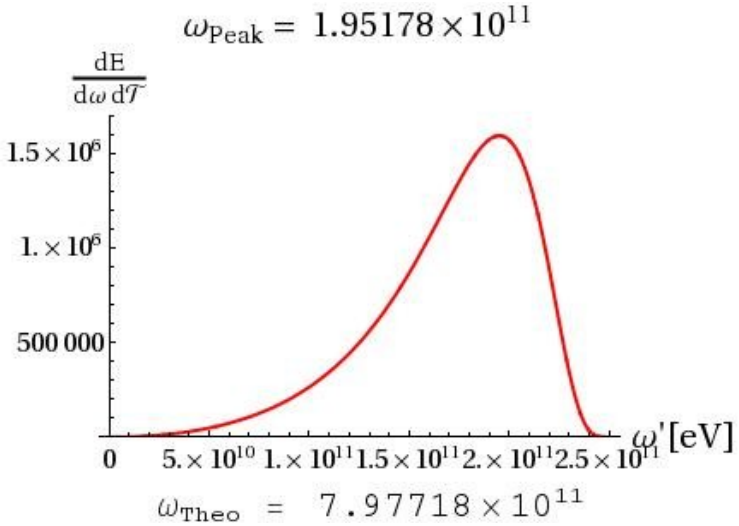

Figure 3.7: The emission spectrum at $\vartheta = \pi$ for $\gamma_0 = 511000 \Leftrightarrow P \approx 260\,\text{GeV}$

We see that the factor by which ω_{Theo} exceeds ω_{Peak} has increased to four. So for very large γ_0 the emission spectra will not have their maxima at the blue shifted central frequency of the incident laser but at smaller frequencies. Furthermore the spectra will change their shapes to be more and more peaked towards their high energy cutoff. This latter effect was already discovered by HARTEMANN et al. who labelled it *kinematic pileup* [38].
We can put this discussion on mathematical grounds. Looking back at section 3.2 to the

equations (3.1-3.4) and their derivations we find that the parameter functions are of the form

$$f_i \propto \int_{-\infty}^{\infty} \dots \, \mathrm{e}^{\mathrm{i}\, K_3 x} \mathrm{d}x. \tag{3.9}$$

That means they are expressible as FOURIER transformations of some function of the variable x represented by the dots in Eq. (3.9). This transformation can be seen as a transformation from the time space to the variable K_3. This variable in turn is written for $\vartheta = \pi$

$$K_3 = 2\,T \frac{\omega' \left(\epsilon - P\right)}{\epsilon + P - 2\omega'}. \tag{3.10}$$

As long as $\omega' \ll \epsilon$ from (3.10) we find $K_3 \propto \omega'$. So in that case Eq. (3.9) can be interpreted as a FOURIER transform into frequency space. Hence it is obvious that the emission spectra will reproduce the blue shifted incident frequency distribution. Instead if $\omega' \to \omega_{\mathrm{Max}}$ it will be $K_3 \to \infty$ and the rapidly oscillating exponential in Eq. (3.9) will let the paramter functions f_i go to zero. This causes the distortions of the energy spectra for large emission frequencies. We will actually analyze this behaviour closer in section 5.

Chapter 4

High intensity regime

The opposite case of the low intensity regime is that of highly relativistic laser intensities characterized by an intensity parameter $\xi \gg 1$. We are going to consider values of the nonlinearity parameter up to $\xi = 1000$. For optical radiation this corresponds to a laser intensity of $I \approx 10^{24}\,\mathrm{W/cm^2}$. Even though such high intensities are not available nowadays they will be reached within the next few years for instance at the ELI [30]. In addition we will consider initial electron energies of $\epsilon \approx 500$ MeV. Such high energetic electrons can be produced at a number of experimental facilities as e.g. in Germany DESY in Hamburg or BESSY in Berlin [39, 40]. Of course electrons can also be accelerated to such high energies at CERN or SLAC. However, there exist different parameter regimes considering the incident electron's relativistic factor γ_0 and the pulse duration T.

4.1 Strong field approximation

The first parameter regime we consider is called *strong field approximation* and covers parameter configurations in which γ_0 is allowed to be of the same order as the nonlinearity parameter ξ and the pulse duration T is fixed. From Eq. (2.14) we know that the amplitude of the electric field depends on the intensity parameter ξ via

$$\mathcal{E} = -\frac{m\,\xi}{2eT}.$$

From the fact that in the strong field approximation we consider the pulse duration T to be independent of ξ we conclude that in the limit $\xi \to \infty$ the electric field amplitude grows like

$$\mathcal{E} \sim \xi.$$

This is the reason for naming this approximation *strong field approximation*. In the strong field limit we consider γ_0 to grow asymptotically like the nonlinearity parameter ξ and thus the electron absorbs an amount of energy from the laser comparable to its initial energy. Then from classical calculations it is known that in this case the dynamics of the electron when scattered by the laser pulse is very rich and interesting.

4.1.1 Asymptotic behaviour of the process parameters

From solving the classical equations of motion of an electron inside a plane wave one can deduce a few scaling properties in the limit of very strong lasers [1,6,41]: Since we are allowed to consider growing initial electron energies in the limit of large laser intensities the sum $\epsilon + P$ which occurs frequently in our calculations will scale linearly in ξ. Furthermore an electron with no initial momentum in y-direction scattered off a laser pulse which is linearly polarized in the x-z-plane classically will move exclusively in this plane. Solving the classical equations of motion we find it to move on a typical trajectory as shown in Fig. 4.1

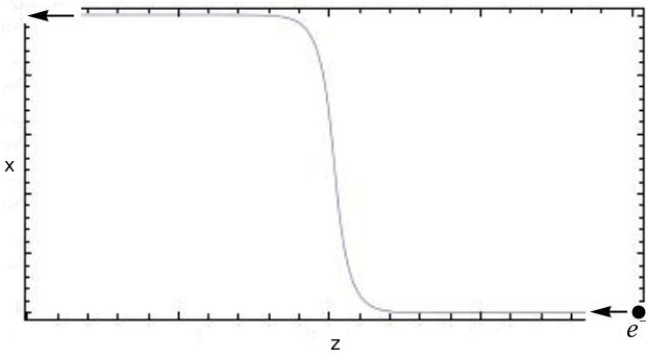

Figure 4.1: Classical electron trajectory

which points towards positive x values in our special reference frame only. Due to relativistic focussing the emission thus will be confined to azimuthal angles of the order $\varphi \sim \gamma^{-1}$ which scales as the inverse of ξ.
Written as asymptotic relations the previous statements read

$$\begin{aligned} \epsilon + P &\sim \xi \\ \varphi &\sim \xi^{-1}. \end{aligned} \tag{4.1}$$

In our calculations quantum effects play an important role as soon as the electron experiences a considerable recoil. Eq. (2.32) states that this will happen if the emitted photon frequencies ω' approach ω_{Max}. Thus we distinguish the two regimes $\omega' \ll \omega_{\mathrm{Max}}$ and $\omega' \lesssim \omega_{\mathrm{Max}}$ where quantum effects are negligible and have to be considered, respectively. In the first regime there are a few more additional asymptotic properties to be concluded from classical considerations. The most important result is that the frequency of the predominantly emitted photons will scale as the initial photon frequency ω^* times $\gamma^3 \sim \xi^3$ [1]. Then with the first and second line of Eq. (2.31) we conclude the scaling properties in the case $\omega' \ll \omega_{\mathrm{Max}}$ to be

$$\begin{aligned} \omega' \sim \omega^* \gamma^3 &\sim \xi^3 \\ p_1' = -k_1' &\sim \xi^3 \\ p_2' = -k_2' &\sim \xi^2 \\ \epsilon' - p_3' &\sim \xi. \end{aligned} \tag{4.2}$$

Here we have to point out that classically the electron momentum components are expected to scale as $p_1' \sim \xi$ and $p_2' \sim$ const. for $\xi \to \infty$. This difference is due to the energy momentum

conservation apparent in quantum electrodynamics.
In the regime $\omega' \lesssim \omega_{\mathrm{Max}}$ the scaling property $\omega' \sim \xi^3$ will no longer be valid. Investigating the asymptotic properties of ω_{Max} we find this maximal emitted frequency to scale linearly in the nonlinearity parameter ξ as it holds

$$\omega_{\mathrm{Max}} = \frac{\epsilon + P}{|1 - \cos(\vartheta)|} \sim \xi. \tag{4.3}$$

So at some critical value of the nonlinearity parameter ξ the predominantly emitted frequencies will be close to the cutoff. From then on they will scale linearly in ξ rather than with its third power since they must not exceed ω_{max}. The phenomenon that the predominantly emitted frequencies of the emission spectra will grow like $\omega' \sim \xi^3$ while the cutoff frequency scales as $\omega_{\mathrm{Max}} \sim \xi$ is reminiscent of the kinematic pileup as discussed in section 3.3 where we already reasoned that it is this difference in the scaling properties that will lead to the typical distortions of the emission spectra in the parameter regime where quantum effects become important. We derive the asymptotics in the regime $\omega' \lesssim \omega_{\mathrm{Max}}$

$$\begin{aligned} \omega' &\sim \xi \\ p_1' = -k_1' &\sim \xi \\ p_2' = -k_2' &\sim \text{const.} \\ \epsilon' - p_3' \sim &\to 0. \end{aligned} \tag{4.4}$$

Having the approximations (4.2), (4.4) and $\gamma_0 \sim \xi$ at hand we state the asymptotics for the parameters α, β and K_3 in the case $\omega' \ll \omega_{\mathrm{Max}}$

$$\begin{aligned} \alpha = -m\,\xi\,T\frac{k_1'}{\epsilon' - p_3'} &\sim \xi^3 \\ \beta = -\frac{m^2\,\xi^2\,T}{2}\frac{\omega'\,(1-\cos(\vartheta))}{(\epsilon' - p_3')\,(\epsilon + P)} &\sim \xi^3 \\ K_3 = 2\,T\frac{\omega'\,(\epsilon + P\cos(\vartheta))}{\epsilon' - p_3'} &\sim \xi^3 \end{aligned} \tag{4.5}$$

as well as in the case $\omega' \lesssim \omega_{\mathrm{Max}}$

$$\begin{aligned} \alpha &\sim \frac{\xi^2}{\epsilon' - p_3'} \\ \beta &\sim \frac{\xi^2}{\epsilon' - p_3'} \\ K_3 &\sim \frac{\xi^2}{\epsilon' - p_3'}. \end{aligned} \tag{4.6}$$

Here it is important to note that in both cases the third asymptotic relation cannot hold if $1 + \cos(\vartheta) \sim \xi^{-1}$ i.e. $\cos(\vartheta)$ is very close to negative unity. Thus we will have to restrict our calculations to angles ϑ not too close to π.
So in the strong field approximation in both frequency regimes the parameters α, β and K_3 scale

with a power law of the large nonlinearity parameter ξ. Since these parameters consequently are very large in the strong field limit so will be the phase of the parameter functions (see Eqs. (2.26)). Then we can obtain analytic approximations for the parameter functions by applying the *method of stationary phase*. The idea of this method is to approximate the integral over a highly oscillating function by its function values at the stationary points of the integrand's phase. It is explained thoroughly e.g. in [42].

4.1.2 Parameter functions

We recall that the parameter functions are

$$f_i = \mathrm{e}^{\mathrm{i}\left(\frac{\pi}{2}\alpha-\beta\right)} \int_{-\infty}^{\infty} \mathrm{d}x\, G_i(x)\, \mathrm{e}^{g(x)}. \tag{4.7}$$

with the exponential argument function

$$g(x) = \mathrm{i}\,\left(2\,\alpha \arctan\left[\tanh(x)\right] - \beta\,\tanh(2x) + K_3\,x\right). \tag{4.8}$$

and the preexponential functions $G_i(x)$

$$\begin{aligned} G_0(x) &= -\frac{2}{K_3}\left(\alpha\, G_1(x) - \beta\, G_2(x)\right) \\ G_1(x) &= \operatorname{sech}(2x) \\ G_2(x) &= \operatorname{sech}^2(2x). \end{aligned} \tag{4.9}$$

We mention already at this point that the preexponential functions are easily evaluated at the stationary point x_0. In appendix D we find that the condition $g'(x_0) = 0$ distinguishing this point can be written as

$$\operatorname{sech}\left(2\,x_0\right) = \frac{\alpha}{2\,\beta} - \mathrm{i}\,\frac{\sigma_0}{\xi} \tag{4.10}$$

where σ_0 is defined in Eq. (D.5). The asymptotic behaviours are $\alpha/\left(2\beta\right) \sim$ const. and $\sigma_0 \sim$ const. In the limit $\xi \to \infty$ this returns a real stationary point only if

$$0 < \frac{\alpha}{2\,\beta} \leq 1 \tag{4.11}$$

is fulfilled. Hence we conclude $\varphi \geq 0$. Since a complex stationary point would lead to exponential damping of the parameter functions the main region of emission will be

$$\boxed{\begin{aligned} \vartheta \geq \vartheta_{\min} &= 2\ \operatorname{arccot}\left(\frac{\xi}{2\,\gamma_0}\right) \\ \pi - \vartheta &\gg \frac{1}{\xi}. \end{aligned}} \tag{4.12}$$

Considering $\xi = \gamma_0$ gives the sample value $\vartheta_{\min} \approx\ 126°$.
Another important consequence from Eq. (4.12) is that in order to have the laser pulse to reflect the electron - i.e. $\vartheta_{\min} \leq 90°$ - we need to have $\xi \geq 2\,\gamma_0$. This condition corresponds exactly to

the condition for electron reflection found classically [3].
It is possible to find a classical analogue for the condition (4.12). The classical trajectory of an electron in an external laser field described by Eq. (2.12) was depicted in Fig. 4.1. We have to pay attention that for $\xi \gg 1$ and $\gamma_0 \gg 1$ the electron will already move at relativistic speed when it enters the pulse and there it is even further accelerated. The electron then will emit radiation only into a very narrow cone around its instantaneous direction of motion [1]. If we now have a look at Fig. 4.1 we find that there should be a maximal angle of deviation from the electron's initial direction of propagation. In Fig. 4.2 this angle is labelled θ_0.

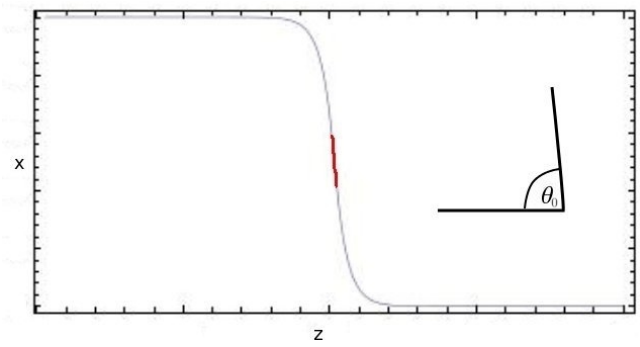

Figure 4.2: Maximal angle of deviation from the electron's initial direction of propagation

While the electron propagates inside the laser pulse its velocity vector never points to a polar angle smaller than $\pi - \theta_0$. Hence there will be no radiation detectable at smaller polar angles. This minimal observation angle $\pi - \theta_0$ corresponds exactly to $\vartheta_{\min}$ defined in Eq. (4.12).
In the sense of the method of stationary phase the oscillating function will only contribute appreciably to the integral in the very vicinity of the stationary point. We make use of this behaviour by expanding the argument function of the exponential into a TAYLOR series around the stationary point

$$g(x) \doteq \sum_{n=0}^{N} \frac{1}{n!} \frac{\mathrm{d}^{(n)}}{\mathrm{d}x^{(n)}} g(x)\Big|_{x=x_0} (x - x_0)^n. \tag{4.13}$$

The term $(x - x_0)$ may be considered to be small for the integrand oscillates heavily if evaluated far away from the stationary point x_0. In fact we are going to show that it is only necessary to consider values of x lying so close to the stationary point that $x - x_0 \sim \xi^{-1}$ will be the effective region of integration. So in some sense in the limit of large ξ we expand the transition probability in powers of the small quantity ξ^{-1} while in contrast to that in the limit of small ξ we expanded the transition probability in orders of ξ itself.
For convenience we define the TAYLOR expansion of $g(x)$ up to third order as another function

$$g_{\mathrm{T}}(x) = g_0 + \frac{1}{2} g_0'' \, (x - x_0)^2 + \frac{1}{6} g_0''' \, (x - x_0)^3 \tag{4.14}$$

with the definitions $g_0 := g(x_0)$, $g_0'' := g''(x_0)$ and $g_0''' := g'''(x_0)$.
In the expansion (4.14) the first derivative does not show up because x_0 is a stationary point distinguished by $g'(x_0) = 0$. The third derivative needs to be taken into account since the terms $g_0'' \, (x - x_0)^2$ and $g_0''' \, (x - x_0)^3$ yield contributions of the same order in the limit $\xi \to \infty$. To

verify this statement we make use of the relations (D.10) and (D.11) which state $g_0'' \sim \xi^2$ and $g_0''' \sim \xi^3$. In the spirit of the method of stationary phase we need to consider only such values of x in the integral which yield no highly oscillating exponentials what can be understood as the demand that the argument of the exponential has to be of order unity. So we only have to take values of the integration variable x into account so close to the stationary point x_0 that it holds $(x - x_0) \sim (g_0'')^{-1/2} \sim \xi^{-1}$. Considering only values of x fulfilling this demand we immediately notice that $g_0''' \, (x - x_0)^3 \sim 1$ holds as well. Every higher derivative of $g(x)$ evaluated at the stationary point is proportional to ξ^3 as well and for $n > 3$ it holds $g^{(n)}(x - x_0)^n \sim \xi^{3-n} \xrightarrow{\xi \to \infty} 0$. We consequently drop every higher derivative in (4.14).
By the same token we replace the preexponential functions by their expansions around the stationary point.

$$G_i(x) \approx G_{i,0} + G_{i,0}'(x - x_0) + \frac{1}{2} G_{i,0}'' \, (x - x_0)^2 \,. \tag{4.15}$$

Once again for reasons of convenience we defined $G_i(x_0) =: G_{i,0}$, $G_i'(x_0) =: G_{i,0}'$ and $G_i''(x_0) =: G_{i,0}''$.
The general form for the asymptotically expanded parameter function we are going to consider then looks like

$$f_i \sim \mathrm{e}^{\mathbb{i}\left(\frac{\pi}{2}\alpha - \beta\right)} \int_{-\infty}^{\infty} \mathrm{d}x \left(G_{i,0} + G_{i,0}'(x - x_0) + \frac{1}{2} G_{i,0}'' \, (x - x_0)^2 \right) \mathrm{e}^{g_\mathrm{T}(x)} \tag{4.16}$$

correct up to terms $(x - x_0)^3$ in the preexponential and up to $(x - x_0)^4$ in the exponential function.
A simplified form of Eq. (4.16) can be written as

$$f_i \sim \mathrm{e}^{\mathbb{i}\left(\frac{\pi}{2}\alpha - \beta\right)} \left[G_{i,0} \mathcal{I}_0 + G_{i,0}' \mathcal{I}_1 + \frac{1}{2} G_{i,0}'' \mathcal{I}_2 \right] \tag{4.17}$$

where we defined the integrals

$$\mathcal{I}_i := \int_{-\infty}^{\infty} (x - x_0)^i \, \mathrm{e}^{g(x)} \, \mathrm{d}x. \tag{4.18}$$

Their computation is possible on grounds of the method of stationary phase and performed in appendix D. The in the limit $\xi \to \infty$ asymptotically correct results are

$$\begin{aligned} \mathcal{I}_0 &\sim 4 \cos\left(\Im(g_0)\right) \left(-\frac{2\,\pi^3}{g} \right)^{\frac{1}{3}} \mathrm{Ai}\left(\eta\right) \\ \mathcal{I}_1 &= \mathbb{i} \, \frac{g}{2\,h} \, \mathcal{I}_2 \\ \mathcal{I}_2 &\sim 8 \cos\left(\Im(g_0)\right) \left(-\frac{2}{g} \right)^{\frac{1}{3}} \frac{\pi}{h} \left(\eta^{\frac{3}{2}} \, \mathrm{Ai}\left(\eta\right) + \eta \, \mathrm{Ai}'\left(\eta\right) \right) \end{aligned} \tag{4.19}$$

with the first AIRY function $\mathrm{Ai}(x)$ and the definitions

$$\eta = \left(-\frac{h^3}{2\,g^2} \right)^{\frac{2}{3}} \quad ; \quad h = g_0''\,|_{\xi \to \infty} \quad ; \quad g = \mathbb{i}\, g_0'''\,|_{\xi \to \infty} \,.$$

4.1.3 Energy spectrum

To obtain emission spectra in the strong field approximation we insert the asymptotic expansions (4.17) into the general formula (2.29). However, we will not plot the actual energy spectra but much rather their envelope functions. We choose to do so because in the actual spectra there will occur numerous minima and maxima lying very close to each other. These structures are due to destructive interferences as we will show in section 5.
We begin with presenting the energy spectrum for the parameters $\gamma_0 = \xi = 100$. According to Eq. (2.34) this corresponds to a quantum parameter of $\chi \approx 0.02$. From Eq. (4.12) we find that with this choice the minimal angle where radiation is expected is $\vartheta_{\text{min}} \approx 126°$.

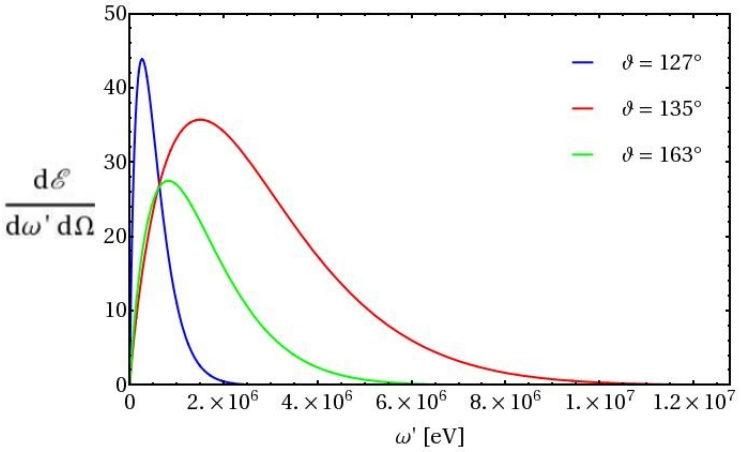

Figure 4.3: Power spectra for different scattering angles and $\xi = \gamma_0 = 100$.

In this figure we plot $\vartheta = 127°$ as the smallest scattering angle. At this observation angle the energy spectrum extends to substantially smaller emission frequencies than at larger angles. Closer to ϑ_{min} this shift of the energy spectra to smaller frequencies and higher amplitudes becomes even more pronounced. The maximal polar observation angle the emission spectrum is plotted for in Fig. 4.3 is $\vartheta \approx 163°$. The reason for this is that as discussed below Eq. (4.6) for larger ϑ the approximation $\alpha \sim \beta \sim K_3$ does not hold any more. At $\vartheta \approx 164°$ e.g. we find $|\beta/K_3| \approx 9$ and for growing angles this ratio quickly exceeds ten. So to maintain the assumptions (4.5,4.6) we are allowed to consider only smaller angles.
Because for the above parameter choice the quantum nonlinearity parameter χ is rather small a classical calculation gives an emission spectrum comparable to ours. To verify this in Fig. 4.4 we compare our quantum electrodynamical to a classical spectrum obtained as outlined in section 2.5. Both spectra share the same labelling of the axes as given in the left plot.

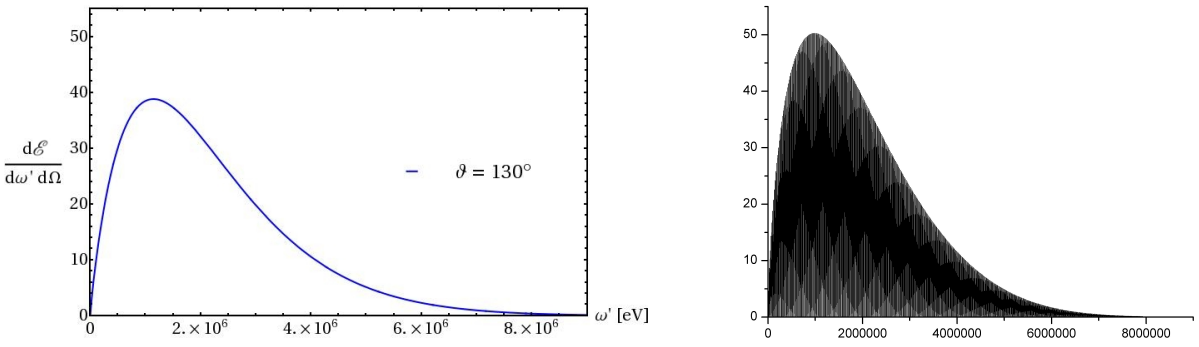

Figure 4.4: Comparison of quantum electrodynamical and classical emission spectra for $\xi = \gamma_0 = 100$ at $\vartheta = 130°$

Here one finds the structure of many nearby minima and maxima described at the beginning of this chapter in the classical spectrum. The envelopes of the spectra, however, look quite similar concerning the position of their maximum at roughly $\omega' \approx 10^6$ eV and their smooth decay towards higher emission frequencies. The fact that the amplitude of the classical spectrum which is calculated exactly slightly exceeds the amplitude of the spectrum obtained in our calculation only by a factor of approximately 1.2 is clear evidence for the validity of the stationary phase approximation.
If according to Eq. (2.32) we calculate the maximum frequency that may be emitted from an electron under the given process parameters we find

$$\omega_{\mathrm{Max}}(\gamma_0 = 100) = \begin{cases} 6.38 \cdot 10^7 & \text{eV for } \vartheta = 127° \\ 5.22 \cdot 10^7 & \text{eV for } \vartheta = 167° \end{cases}$$

and the maximum frequencies at all other angles in the range $\vartheta \in [\vartheta_{\mathrm{min}}, \vartheta_{\mathrm{max}}]$ lie between these two frequencies. The frequencies actually emitted in the spectra in Fig. 4.3 are approximately one order of magnitude below the maximally allowed emission frequency as one could have guessed since in the investigated scattering process it holds $\chi \ll 1$.
To investigate a process in which quantum effects are important we increase the relativistic parameters by a factor of ten to $\xi = \gamma_0 = 1000$. According to Eq. (2.34) this yields a quantum parameter of $\chi \approx 2$ hinting at the importance of quantum effects. But from Eq. (4.12) and the fact that we still have $\gamma_0 = \xi$ as before we find the polar angular observation range unchanged. The resulting emission spectra are shown in Fig. 4.5.

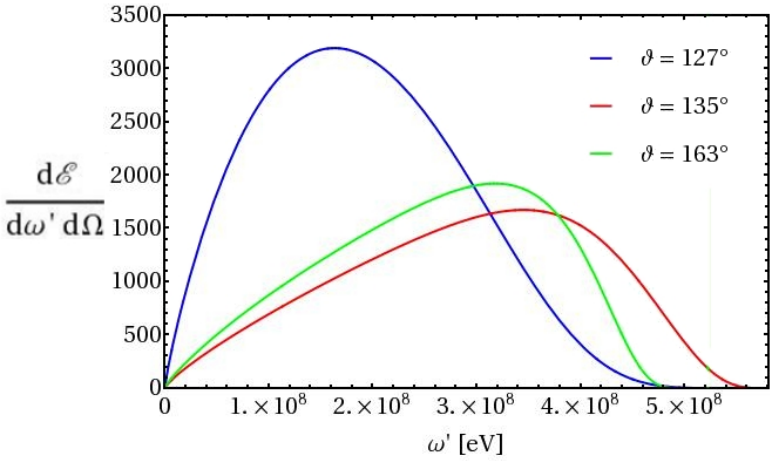

Figure 4.5: Power spectra for different scattering angles and $\xi = \gamma_0 = 1000$.

In the spectra plotted we find clear differences with respect to Fig. 4.3. Not only do the scales of emitted frequencies and of the spectra's amplitudes differ by several orders of magnitude but also the shapes of the spectra look distinctly different. So in Fig. 4.5 we find a fast decay of the emitted energy when the emitted frequencies approach the maximally emitted photon energy. While in Fig. 4.3 the spectra exhibited a much more moderate decrease. This again is evidence for the effect of kinematic pile up as described in section 3.3. Computing again the maximally allowed emitted photon frequency according to Eq. (2.32) we find it to be on the order of the frequency where the fast drop off in Fig. 4.5 occurs

$$\omega_{\mathrm{Max}}(\gamma_0 = 1000) = \begin{cases} 6.38 \cdot 10^8 & \text{eV for } \vartheta = 127° \\ 5.22 \cdot 10^8 & \text{eV for } \vartheta = 163.5°. \end{cases}$$

So we conclude that as soon as the quantum parameter χ becomes of order unity the emitted photons will approach their maximally allowed frequencies. This interpretation of the kinematic pile up found in Fig. 4.5 clearly hints at quantum effects which due to energy momentum conservation prevent the emission of higher energetic photons.
We may now turn to the case where γ_0 and ξ actually are on the same order of magnitude but not equal. Reminding ourselves of the discussion in section 4.1.1 we remember that in order to observe back-scattering i.e. $\vartheta_{\mathrm{min}} \leq 90°$ we have to consider $\xi \geq 2\gamma_0$. So we choose first of all $\xi = 200$ and $\gamma_0 = 100$ which gives a quantum parameter of approximately $\chi \approx 0.04$. So we expect the emitted frequencies still to be much smaller than the maximally allowed frequencies ω_{Max} and classical calculations to be valid. The resulting spectra are presented in Fig. 4.6.

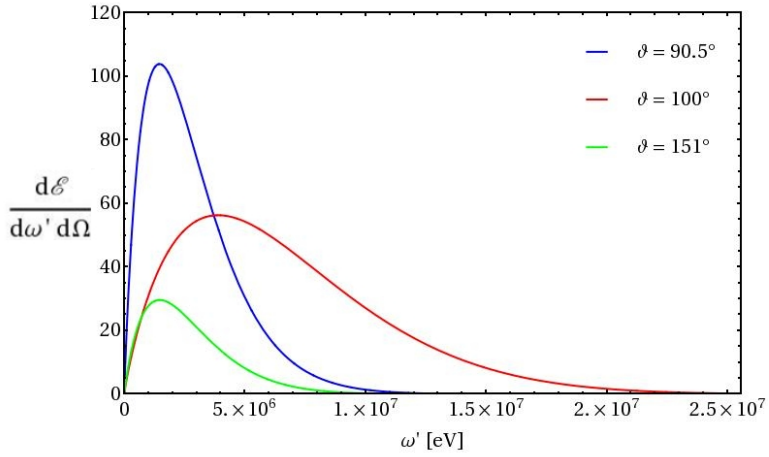

Figure 4.6: Power spectra for different scattering angles and $\xi = 200$ and $\gamma_0 = 100$.

Since these spectra still represent a classical parameter regime it is most sensible to compare Fig. 4.6 to Fig. 4.3. A common feature of these two sets of emission spectra is the decrease of the spectra's amplitudes for observation angles larger than ϑ_{min}. A clear distinction of the two spectra is that in the latter the minimal scattering angle is $\vartheta_{\text{min}} = 90°$ as expected from Eq. (4.12).
To analyze the scattering in the case $\xi = 2\gamma_0$ in a regime where quantum effects have to be taken into account we plot the emission spectra in the case of $\xi = 1000$ and $\gamma_0 = 500$ such that we again will have emission into the same polar angle regime as we had in Fig. 4.6. The quantum parameter χ in turn will be approximately unity as we compute from Eq. (2.34). The spectra are shown in Fig. 4.7.

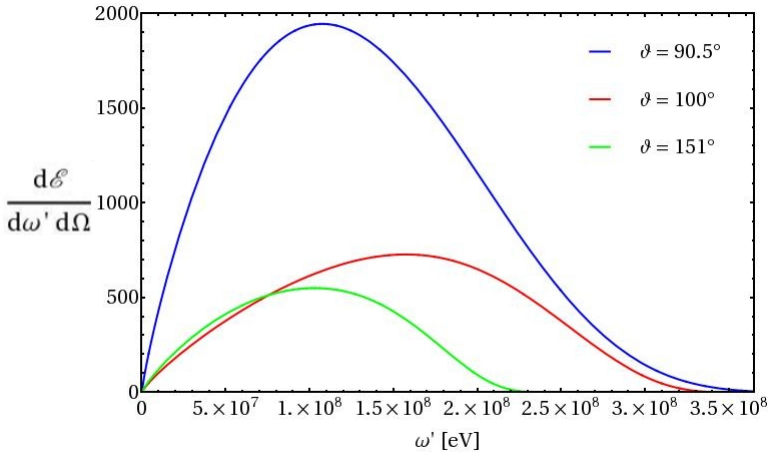

Figure 4.7: Power spectra for different scattering angles and $\xi = 1000$ and $\gamma_0 = 500$.

In these plots we find once again the effect of kinematic pile up for large γ_0 confirmed.

4.1.4 The special case $\vartheta = \pi$

As mentioned in section 3.3 an electron with large γ_0 will emit most of its radiation into a narrow cone around its propagation direction. Furthermore subsequently to Eq. (4.12) we found that for $\xi < 2\,\gamma_0$ in any case we will have $\vartheta_{\min} > 90°$ i.e. emission only into the electron's initial direction of propagation. The spectra for the polar angle $\vartheta = \pi$ hence are of great interest for the understanding of the radiation pattern of an electron moving in a high intensity laser pulse. However, looking back at Eq. (2.33) we find

$$\alpha\big|_{\vartheta=\pi,0} = 0.$$

Consequently our assumption $\alpha \sim \beta \sim K_3$ breaks down and we recapitulate the discussion for $\alpha = 0$. From Eq. (2.33) we derive the explicit expressions for β and K_3 at $\vartheta = \pi$

$$\beta = -\frac{m^2\,\xi^2\,T}{2}\left[\frac{1}{\epsilon + P - 2\omega'} - \frac{1}{\epsilon + P}\right] \tag{4.20}$$

$$K_3 = 2\,T\frac{\omega'\,(\epsilon - P)}{\epsilon + P - 2\omega'} \tag{4.21}$$

which in this special case are connected as

$$\beta = -K_3\frac{\xi^2}{2}. \tag{4.22}$$

Hence we conclude that if $\beta \sim \xi^3$ as generally shown in Eq. (4.5) it must hold $K_3 \sim \xi \ll \xi^3 \sim \beta$. This does not contradict our previous estimates of K_3 as can be seen from the last line of Eq. (4.5). Hence in the large exponent we only have to include the part of $g(x)$ proportional to β. The parameter functions are then given by

$$f_i = \mathrm{e}^{-2\,\mathbb{i}\,\beta}\,2\,\Re\left(\int_0^\infty G_i(x)\,\mathrm{e}^{\mathbb{i}\,K_3 x}\,\mathrm{e}^{-\mathbb{i}\,\beta\,\tanh(2x)}\mathrm{d}\,x\right) \tag{4.23}$$

In this we may treat $G_i(x)\,\exp\left[\mathbb{i}\,K_3 x\right]$ as the preexponential function since it oscillates slowly in comparison to $\exp\left[-\mathbb{i}\,\beta\,\tanh(2x)\right]$. However, because of

$$\frac{\mathrm{d}}{\mathrm{d}x}\tanh(2x) = \frac{2}{\cosh^2(2x)} \neq 0 \text{ f.a. } x \in \mathbb{R}$$

the parameter functions contain no real stationary points for $\vartheta = \pi$. But an integral over a highly oscillating function which features no stationary points is very small. We hence conclude that in the limit of large ξ the radiation emitted into this angular regime will be negligibly small. Physically this can be understood such that a very strong laser scatters even highly relativistic electrons considerably from their initial direction of propagation. Then the electrons will not move towards $\vartheta = \pi$ and thus not radiate significantly into this angular region.

4.2 Constant field approximation

The second parameter regime we consider is called *constant field approximation* and covers parameter configurations in which the pulse duration grows like $T \sim \xi$ the while electron's relativistic parameter γ_0 as well as the electric field strength $\mathcal{E}$ are fixed. This parameter region is the same as considered in [13]. To interpret the physical situation described by the assumption

$$\xi \gg 1 \qquad ; \qquad \gamma_0 \sim \text{const.} \qquad ; \qquad \mathcal{E} \sim \text{const.}$$

we state the realization of this limit as presented in [13]: From Eq. (2.14) it is obvious that the limit $\xi \to \infty$ can be regarded equal to the limit $T \to \infty$ in such a way that the electric field amplitude remains constant in the limit of large ξ. We thus conclude that

$$T \sim \xi \gg 1 \tag{4.24}$$

holds in the constant field limit. As we see from Eq. (2.14) it holds for the electric field amplitude

$$\mathcal{E} \propto \frac{\xi}{T} \sim \text{const. in the limit } \xi \to \infty$$

whence the reason for calling this the *constant field approximation* is evident. To keep the amplitude of the electric field constant while increasing the parameter T corresponds to increase the parameter ξ at the expense of a longer pulse duration. Physically this can be interpreted such that the laser pulse in this approximation is so long that for the time of interaction we may consider its electric field to be constant. But since the parameter T is connected to the temporal duration of the laser pulse its growing large somehow puts constraints on our intention to treat ultra-short laser pulses. However, the constant field limit physically is realized if one does not consider optical but e.g. far-infrared single-cycle laser pulses [43]. Even if such pulses contain only half a cycle of the electric field they feature pulse duration of a few hundred femtoseconds. So their electric fields may considered constant during the emission of a photon by an electron.

4.2.1 Asymptotic behaviour of the process parameters

The contrast between the constant and the strong field approximations will definitely lie in the behaviour of the involved parameters α, β and K_3. So we need to recapitulate the discussion of section 4.1.1 considering the asymptotics of these parameters.
First of all we consider the same classical asymptotics (4.1) as in the strong field limit. We assume $\epsilon + P \sim \gamma_0$ where γ_0 again is the electron's relativistic factor before scattering. Here, however, we find the first important difference to the strong field case namely that this factor will remain fixed in the limit $\xi \to \infty$. Since the electron's initial momentum is fixed in the limit of large ξ it will hold $\xi \gg \gamma_0$ and the electron will absorb much more energy from the laser than it initially carried. So even if initially it was not relativistic it will be accelerated to relativistic velocities inside the laser pulse. Then due to relativistic focussing the electron will emit radiation mainly close to $\vartheta = 0$ in our special reference frame. The polar observation angles at which we expect radiation will then be of the order $\vartheta \sim \xi^{-1}$. Paying attention to

$(\omega^*)^{-1} \propto T \sim \xi$ from the first line of Eq. (4.2) we find that the predominantly emitted photon frequencies classically are expected to scale as

$$\omega' \sim \xi^2. \tag{4.25}$$

Since for $\vartheta \sim \xi^{-1}$ it holds $1-\cos(\vartheta) \sim \xi^{-2}$ the cutoff frequency defined in Eq. (2.32) also scales as

$$\omega_{\mathrm{Max}} = \frac{\epsilon + P}{1-\cos(\vartheta)} \sim \xi^2. \tag{4.26}$$

So the cutoff frequency will asymptotically grow with the same power of ξ as the predominantly emitted frequencies. Consequently it is not necessary to distinguish the regimes $\omega' \ll \omega_{\mathrm{Max}}$ and $\omega' \lesssim \omega_{\mathrm{Max}}$. With this observation in combination with Eqs. (2.31) we complete the asymptotic properties valid in the constant field limit

$$\begin{aligned} \varphi \sim \vartheta &\sim \frac{1}{\xi} \\ p'_1 = -k'_1 &\sim \xi \\ p'_2 = -k'_2 &\sim \text{const.} \\ \omega' - k'_3 &\sim \text{const.} \\ \epsilon' - p'_3 \sim \epsilon + P &\sim \text{const.}. \end{aligned} \tag{4.27}$$

and thus

$$\begin{aligned} \alpha = -m\,\xi\,T\frac{k'_1}{\epsilon' - p'_3} &\sim \xi^3 \\ \beta = -\frac{m^2\,\xi^2\,T}{2}\frac{\omega' - k'_3}{(\epsilon' - p'_3)\,(\epsilon + P)} &\sim \xi^3 \\ K_3 = 2\,T\frac{\omega'\,(\epsilon + P\cos(\vartheta))}{\epsilon' - p'_3} &\sim \xi^3. \end{aligned} \tag{4.28}$$

So also in the constant field approximation α, β and K_3 approximately grow like ξ^3.

4.2.2 Parameter functions

We found that the parameters α, β and K_3 also in the constant field approximation are large. Now we need to recapitulate the discussion of the parameter functions f_i as given in section 4.1.2 for it is not trivially clear that they also will exhibit the same asymptotic behaviour as in the strong field approximation. For this purpose we again start from the expressions (4.7)

$$f_i = \mathrm{e}^{\mathbb{i}\left(\frac{\pi}{2}\alpha - \beta\right)} \int_{-\infty}^{\infty} \mathrm{d}x\, G_i(x)\, \mathrm{e}^{g(x)}. \tag{4.29}$$

Since the argument function of the exponential is the same as in the strong field approximation its derivatives and hence the stationary point as well will be distinguished by

$$\operatorname{sech}(2x_0) = \frac{\alpha}{2\,\beta} - \mathbb{i}\,\frac{\sigma_0}{\xi} \tag{4.30}$$

The minimal observation angle as defined in Eq. (4.12) is found to be

$$\vartheta_{\min} = 2 \operatorname{arccot}\left(\frac{\xi}{\gamma_0 \cos(\varphi)\left(1+\sqrt{1-\frac{1}{\gamma_0^2}}\right)}\right). \tag{4.31}$$

This angle actually scales as $\vartheta_{\min} \sim \xi^{-1}$ what confirms our classical prediction from section 4.1.1 that emission will mainly be detectable in the polar angular regime

$$\boxed{\begin{array}{rcll} \vartheta & \sim & \dfrac{1}{\xi} & \\ \vartheta & \geq & \vartheta_{\min} \ll 1 & (4.32) \end{array}}$$

Looking back at Eq. (4.30) we now essentially have to answer two questions to find the asymptotic expansions of the f_i:
First, is the quantity σ_0 also a constant in the constant field approximation? This would allow us to neglect the imaginary part of x_0 in the asymptotic limit and as long as condition (4.11) is satisfied.
And second, do we have to take the same orders of derivatives of the exponential function $g(x)$ into account i.e. are $g''(x)(x-x_0)^2$ and $g'''(x)(x-x_0)^3$ of the same order as they were in the strong field approximation?
To answer the former question we first of all show that in the constant field approximation $k_2' \sim$ const. indeed is valid. To this end we make use of the first line of Eq. (4.27). Putting these relations together we find $k_2' = \omega' \sin(\vartheta)\sin(\varphi) \sim 1$. Then with the third and the fourth line of Eq. (4.27) we find

$$\sigma_0 \sim \sqrt{1+\gamma_0^2\left(1+\beta_0\right)^2} \sim 1.$$

So also in the constant field limit it holds $\sigma_0 \sim$ const. and for $\xi \to \infty$ we may neglect the imaginary part of the stationary point x_0.
The second question can be answered by looking at the definitions (D.10) and (D.11).

$$g_0'' = \mp 8 \frac{\tanh(2x_0)}{\cosh(2x_0)} \sigma_0 \frac{\beta}{\xi} =: h \tag{4.33}$$

$$g_0''' = -16\mathbb{i}\left(\frac{\tanh(2x_0)}{\cosh(2x_0)}\right)^2 \beta =: -\mathbb{i}\, g \tag{4.34}$$

Now from the first two lines of Eq. (4.28) we know that α and β also in the constant field approximation are of the same asymptotic order. We thus conclude that the stationary point x_0 which goes to $x_0 \to \operatorname{arsech}(\alpha\,/\,(2\beta))$ in the limit $\xi \to \infty$ is asymptotically independent of the intensity parameter ξ. From this observation we deduce

$$h \sim \frac{\beta}{\xi} \sim \xi^2 \qquad ; \qquad g \sim \beta \sim \xi^3 \tag{4.35}$$

as can be seen from Eq. (4.28). Analogously to the line of arguments in section 4.1.2 we conclude that in the integrals (4.29) we have to take into account only those values of the integration variable x for which holds $(x - x_0) \sim \xi^{-1}$ whence we infer

$$g_0'' (x - x_0)^2 \sim g_0''' (x - x_0)^3 \sim 1.$$

We consequently may treat the parameter functions f_i in the constant field limit in exactly the same way as we did in the strong field limit.
So adopting the derivation from appendix D of the asymptotic expansion for the f_i we state that in the constant field approximation for large ξ we may use the formulae (4.17) for the necessary combinations of the parameter functions.
Nevertheless one has to pay attention to the different regimes of the process parameters φ, ϑ and γ_0 one is allowed to consider in contrast to the strong field approximation.

4.2.3 Energy spectrum

Inserting the expansions (4.17) into Eq. (2.29) and using the parameter regimes we found in the previous sections we can plot the power spectrum. As process parameters we choose an electron initially at rest $\gamma_0 = 1 \ll \xi$ and observation directly in the direction of the laser's polarization $\varphi = 0$. Additionally to be consistent with Eq. (4.24) we put $T\left[\mathrm{eV}^{-1}\right] = \xi$.
To verify the last asymptotic relation in Eq. (4.27) we are going to plot the spectra for different intensity parameters ξ. But to do so we need to pay attention to Eq. (4.32). From this relation we conclude that for ever increasing ξ smaller observation angles need to be considered. The asymptotic behaviour $\omega' \sim \xi^2$ will be found only at the respective minimal observation angles $\vartheta_{\mathrm{min}} = \vartheta_{\mathrm{min}}(\xi)$. We begin with presenting the emission spectra at different observation angles ϑ for an intensity parameter $\xi = 100$.

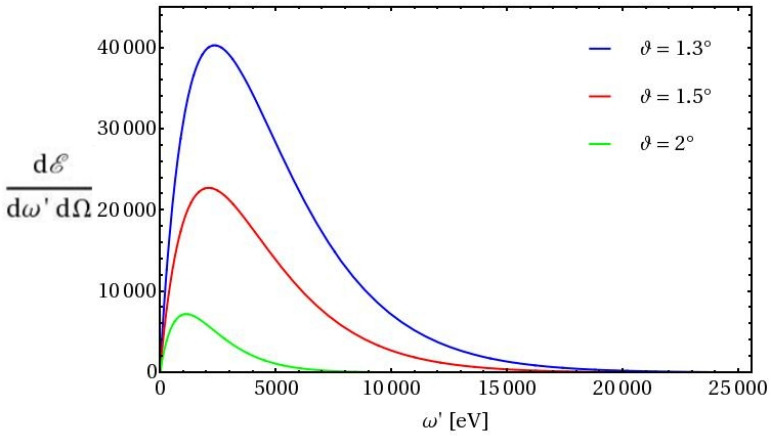

Figure 4.8: Power spectra for different scattering angles and $\xi = 100$ and $\gamma_0 = 1$.

In these spectra we immediately see that for angles $\vartheta > \vartheta_{\mathrm{min}}$ the spectra's amplitudes decrease quite fast. We interpret this behaviour as a proof for the condition that polar observation angles under which we find considerable radiation need to be on the order of $\vartheta \sim \xi^{-1}$ and for

larger angles the radiated power is strongly suppressed. Physically this behaviour also is easily understood since the condition $\xi \gg \gamma_0$ states that the electron absorbs far more energy from the laser pulse than it initially carried. In the case $\gamma_0 = 1$ under consideration here the electron initially even carries only its rest mass energy. Thus the electron will be strongly accelerated into the laser pulse's initial direction of propagation and thus radiate predominantly into the polar angle region close but not equal to $\vartheta = 0$ (compare section 2.6).
Next we plot the emission spectra for small ϑ in the case of $\xi = 200$ and $\xi = 1000$. In the

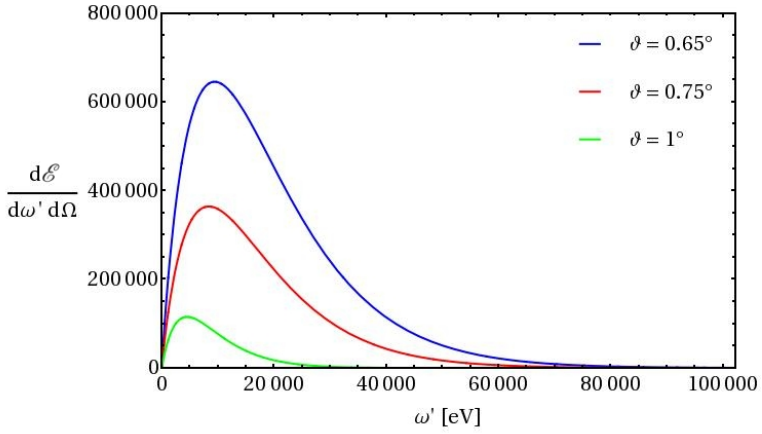

Figure 4.9: Power spectra for different scattering angles and $\xi = 200$.

spectra obtained for $\xi = 200$ we find that except the scaling of the axes and the emission angles nothing has changed in comparison to Fig. 4.8. Even if we increase the intensity parameter to $\xi = 1000$ the shapes of the emission spectra remain unaffected as shown in Fig. 4.10.

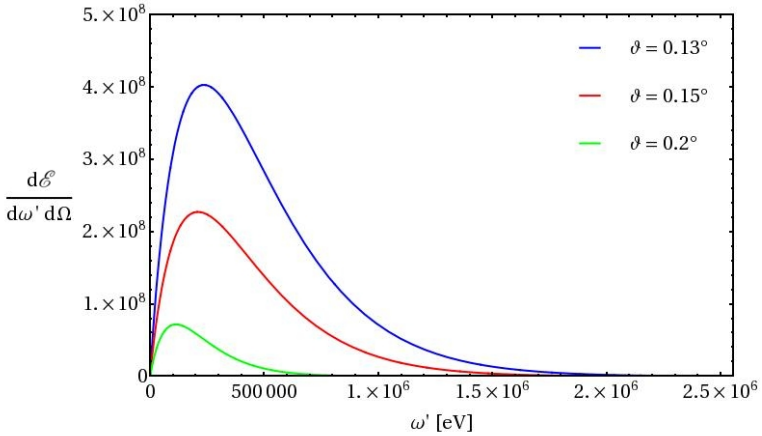

Figure 4.10: Power spectra for different scattering angles and $\xi = 1000$.

This absence of any kinematic pile up is evidence for the unimportance of quantum effects.
Comparing the red spectra in the three figures 4.8 - 4.10 we find the maximally emitted fre-

quencies at angles close to the minimal emission angles

$$\begin{aligned} \omega_{Max}\left(\xi = 100\right) &\approx \quad 2000\,\mathrm{eV} \quad \equiv \omega_{Max,0} \\ \omega_{Max}\left(\xi = 200\right) &\approx \quad 8000\,\mathrm{eV} \quad \approx 4\ \omega_{Max,0} \\ \omega_{Max}\left(\xi = 1000\right) &\approx \quad 2 \cdot 10^5\,\mathrm{eV} \quad \approx 100\ \omega_{Max,0}. \end{aligned}$$

This is in fact the classical scaling with ξ^2 expected from Eq. (4.27). From Eq. (2.34) we conclude that for $\gamma_0 = 1$ and $\xi = 100, 200, 1000$ we obtain the quantum parameter of $\chi \approx \xi \,/\, (2m\,T) \approx 10^{-6}$ if we always consider $T\left[\mathrm{eV}^{-1}\right] = \xi$. We thus could have expected that classical calculations would have given correct results.
However, of course it is possible to observe quantum effects in the constant field limit. In an experimental facility such as ELI promising to provide nonlinearity parameters of the order $\xi \sim 10^4$ in an optical laser system an electron with an initial energy of a few ten MeV would satisfy $\gamma_0 \ll \xi$. Hence the constant field limit should be applicable and quantum effects are expected. Another possible experimental realization of the constant field limit would be an ultra-intense and ultra-short micro-wave laser pulse where the electric field can be considered constant over the time of photon emission.

Chapter 5

The intermediate case

In the case of intermediate values for the parameter ξ none of the approximations employed in sections 3 and 4 is applicable. This is obvious from Eq. (2.33) because the exponent of the parameter functions will neither be small allowing for an perturbation theoretical expansion into a TAYLOR series nor will it be large causing rapid oscillations making an asymptotic expansion feasible. So the only way of obtaining spectra in the intermediate intensity regime will be a numerical evaluation of the parameter functions (2.26) and subsequently the energy spectrum (2.29). We choose the incoming electron momentum to be very large. Recapitulating Eq. (2.34) we find

$$\chi \approx \xi \gamma_0 \frac{\omega}{m}. \tag{5.1}$$

For $\xi \sim 1$ Eq. (5.1) reveals that χ will be on the order of unity for initial electron momenta $\gamma_0 \sim m/\omega$. For optical radiaion ($\omega \approx 1$ eV) this corresponds to an initial electron energy of roughly 250 GeV as already obtained at the SPS at CERN [26]. We will use such large γ-factors to investigate at which values of the parameter χ the regime of applicability of classical calculations is left and quantum effects dominate the emission spectra. It will turn out that as long as $\chi \ll 1$ classical calculations give sensible results what we view as proof that the parameter χ may be used to distinguish the quantum from the classical regime. Additionally $\gamma_0 \gg \xi$ indicates that the electron initially carries much more energy than it can absorb from the laser. Its initial direction of propagation thus will be changed only marginally and we can choose to observe the emitted radiation exclusively at the polar angle $\vartheta = \pi$. In contrast to the previous discussion in section 4.1 this is not problematic since we do not apply any approximation but integrate the parameter functions numerically. So in the following discussion we will always present a spectrum obtained through direct integration of Eqs. (2.26) and compare it to a emission spectrum calculated classically (s. section 2.5).
We begin with spectra obtained for $\gamma_0 = m/(200\,\omega)$ corresponding to an initial electron energy $\epsilon = 1.3$ GeV from which choice we infer the quantum parameter $\chi \approx 5 \cdot 10^{-3}$. We present the results in Fig. 5.1.

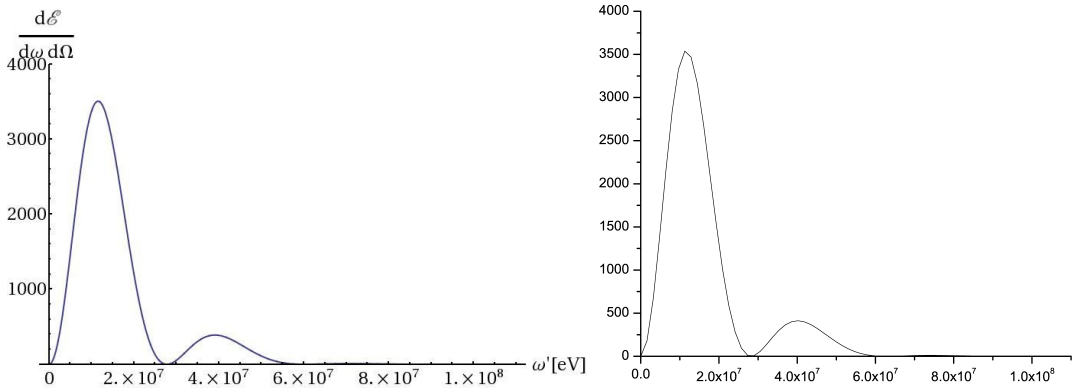

Figure 5.1: Comparison of quantum mechanical (left) and classical (right) emission spectra for $\xi = 1$ and $\gamma_0 = \frac{m}{200\,\omega}$

In these two plots we find perfect matching of the spectra. We conclude that for the chosen parameters the classical and quantum mechanical calculations agree what confirms the classical limit for small quantum parameters χ. Besides validating the classical limit of our calculations we have to explain an additional feature apparent in Fig. 5.1: The second maximum in Fig. 5.1 cannot be attributed to emission of a second harmonic as it lies at roughly four times the frequency of the first maximum. We will show that the minimum between the two emission maxima is due to interference effects. To this end it is legitimate to use classical considerations since $\chi \ll 1$ is fulfilled and in Fig. 5.1 we found excellent agreement with our quantum calculations. The differential energy $\mathrm{d}\mathscr{E}$ emitted from a classical pointlike charge moving accelerated on a given trajectory per frequency interval $\mathrm{d}\omega'$ into the solid angle element $\mathrm{d}\Omega$ lying in the direction $\mathbf{n}$ from the point of emission is calculated via

$$\frac{\mathrm{d}^2\mathscr{E}}{\mathrm{d}\omega'\,\mathrm{d}\Omega} = \frac{e^2}{4\,\pi^2}\left|\int_{-\infty}^{\infty} \frac{\mathbf{n}\times\left[(\mathbf{n}-\boldsymbol{\beta})\times\dot{\boldsymbol{\beta}}\right]}{(1-\boldsymbol{\beta}\cdot\mathbf{n})^2}\mathrm{e}^{\mathrm{i}\,\omega(t-\mathbf{n}\cdot\mathbf{r}(t))}\mathrm{d}t\right|^2 \tag{5.2}$$

which is Eq. (14.67) in [1] with $c \equiv 1$.
Computing the electron's classical trajectory for the given parameters $\gamma_0 = m/(200\,\omega)$ and $\xi = 1$ we find it to lie in the x-z-plane. Since in the azimuthal angular regime $\varphi \approx \pi$ there will not be any radiation we confine our discussion to $\varphi = 0$ and distinguish the direction of observation by the polar angle ϑ. The electron's trajectory was already shown in section 4.1.1 to look like Fig. 4.1. Because of relativistic focussing the emitted radiation observed at a certain angle θ is created mainly at two segments of the trajectory where the electron moves directly into direction $\vartheta = \theta$. This is clarified in Fig. 5.2.

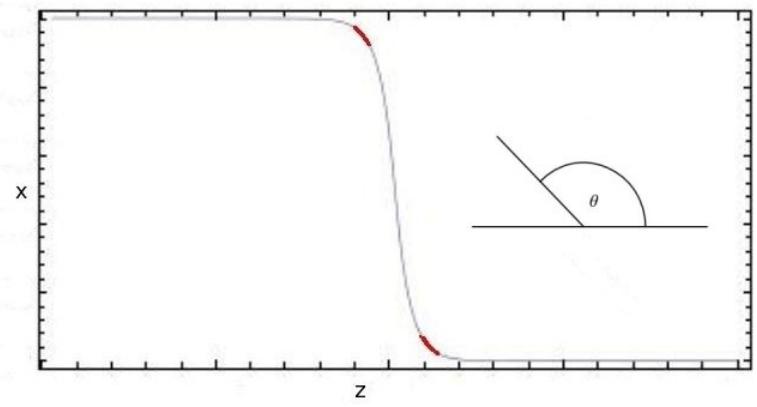

Figure 5.2: Segments of the trajectory where radiation observable at θ is created

Respecting that every point on the trajectory is characterized by a unique value of the invariant phase ϕ we replace the integral in Eq. (5.2) by a sum over the two contributing space points which may be distinguished by the phase values $\phi_1 = t_1 - \mathbf{n}_1 \cdot \mathbf{r}(t_1)$ and $\phi_2 = t_2 - \mathbf{n}_2 \cdot \mathbf{r}(t_2)$

$$\frac{\mathrm{d}^2\mathscr{E}}{\mathrm{d}\omega'\,\mathrm{d}\Omega} \approx \frac{e^2}{4\,\pi^2}\left|\frac{\mathbf{n}_1 \times \Big[(\mathbf{n}_1 - \boldsymbol{\beta}_1) \times \dot{\boldsymbol{\beta}}_1\Big]}{\left(1 - \boldsymbol{\beta}_1 \cdot \mathbf{n}_1\right)^2} \mathrm{e}^{\mathrm{i}\,\omega(t_1 - \mathbf{n}_1 \cdot \mathbf{r}(t_1))} + \frac{\mathbf{n}_2 \times \Big[(\mathbf{n}_2 - \boldsymbol{\beta}_2) \times \dot{\boldsymbol{\beta}}_2\Big]}{\left(1 - \boldsymbol{\beta}_2 \cdot \mathbf{n}_2\right)^2} \mathrm{e}^{\mathrm{i}\,\omega(t_2 - \mathbf{n}_2 \cdot \mathbf{r}(t_2))}\right|^2 . \tag{5.3}$$

This approximation is fulfilled the better the larger γ_0 is i.e. the narrower the emission cone of the electron becomes. To evaluate Eq. (5.3) we note that the points ϕ_1 and ϕ_2 are chosen such that the electron's velocity vectors at both space points are equal $\boldsymbol{\beta}_1 = \boldsymbol{\beta}_2 =: \boldsymbol{\beta}$, the direction of observation is the same $\mathbf{n}_1 = \mathbf{n}_2 =: \boldsymbol{n} = (\sin(\theta), 0, \cos(\theta))$ and that since the electric field is antisymmetric around its zero-point the forces acting on the electron at the two points are exactly opposite $\dot{\boldsymbol{\beta}}_1 = -\dot{\boldsymbol{\beta}}_2 =: \dot{\boldsymbol{\beta}}$. From these considerations we may simplify Eq. (5.3) to give

$$\frac{\mathrm{d}^2\mathscr{E}}{\mathrm{d}\omega'\,\mathrm{d}\Omega} \approx \frac{e^2}{4\,\pi^2}\left|\frac{\mathbf{n} \times \Big[(\mathbf{n} - \boldsymbol{\beta}) \times \dot{\boldsymbol{\beta}}\Big]}{\left(1 - \boldsymbol{\beta} \cdot \mathbf{n}\right)^2} \left(\mathrm{e}^{\mathrm{i}\,\omega(t_1 - \mathbf{n}_1 \cdot \mathbf{r}(t_1))} - \mathrm{e}^{\mathrm{i}\,\omega(t_2 - \mathbf{n}_2 \cdot \mathbf{r}(t_2))}\right)\right|^2 . \tag{5.4}$$

So we note that we will have $\mathrm{d}^2\mathscr{E}/\left(\mathrm{d}\omega'\,\mathrm{d}\Omega\right) = 0$ i.e. the two radiation contributions from ϕ_1 and ϕ_2 interfering destructively at the frequencies ω_n where it holds

$$\begin{aligned} & \omega_n\left(t_1 - \mathbf{n}_1 \cdot \mathbf{r}(t_1)\right) = \omega_n\left(t_2 - \mathbf{n}_2 \cdot \mathbf{r}(t_2)\right) + 2\pi\, n \\ \Rightarrow \qquad & \omega_n = \tfrac{2\pi\, n}{(t_1 - \mathbf{n}_1 \cdot \mathbf{r}(t_1)) - (t_2 - \mathbf{n}_2 \cdot \mathbf{r}(t_2))} \end{aligned} \tag{5.5}$$

because there the term in round brackets in Eq. (5.4) vanishes.
The method described above of course is not rigorously applicable at the polar angle $\vartheta = \pi$ because in this direction there will not be only two but many points on the electron's trajectory where its velocity vector points into the observation direction. However, the frequencies of destructive interference can by found by computing the ω_n at a polar angle $\vartheta = \pi - \varepsilon$ and then considering the limit $\varepsilon \to 0$.
For the parameter choices made to obtain the spectra in Fig. 5.1 we find the first two frequencies of destructive interference to be

n	ω_n
1	$2.57 \cdot 10^7$ eV
2	$5.13 \cdot 10^7$ eV

In every further discussion of destructive interferences it will suffice to compute ω_1 for all higher ω_n will be multiples of it. Comparing the above table with Fig. 5.1 we see that ω_1 matches well with the first minimum in that figure and we attribute this minimum to destructive interference. The previous discussion as well enables us to explain a second feature of Fig. 5.1. Due to $\chi \ll 1$ the maximum frequency of the spectrum still has to be computable via Eq. (3.8). The quantity ω_{Theo} defined there was the maximum frequency of the blue shifted energy distribution of the incident laser pulse. As we argued in section 3.3 in the classical limit corresponding to $\chi \ll 1$ the maximum of the energy spectrum is expected to lie at ω_{Theo}. In Fig. 5.3 we show the quantum mechanically calculated spectrum with an arrow pointing at ω_{Theo} for $\gamma_0 = m/(200\,\omega)$ at $\vartheta = \pi$.

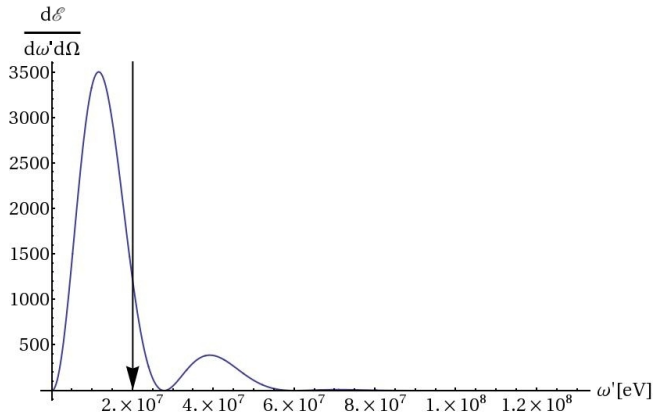

Figure 5.3: Quantum mechanical emission spectrum or $\xi = 1$ and $\gamma_0 = \frac{m}{200\,\omega}$, the arrow marks ω_{Theo}

The proper explanation for the disagreement of the positions of the arrow and the first maximum are the destructive interferences discussed above. Without this effect the spectrum maximum would lie at $\omega_{\text{Theo}} \approx 2 \cdot 10^7$ eV but due to interference effects the spectrum is suppressed at ω_1. So the first maximum of the energy emission probability found in Fig. 5.1 is not a physical maximum but rather interpretable as a pseudo-maximum arising from a distortion of the spectra due to interferences.
By increasing ξ the time points t_1 and t_2 as well as the space points $\boldsymbol{r}_1$ and $\boldsymbol{r}_2$ become more separate and thus, looking back at Eq. (5.5), ω_1 becomes smaller. Hence we expect for increased ξ to observe more interference minima in the spectra. To check this we plot the energy spectra for an increased intensity parameter $\xi = 5$ with every other parameter unchanged. These spectra are presented in Fig. 5.4

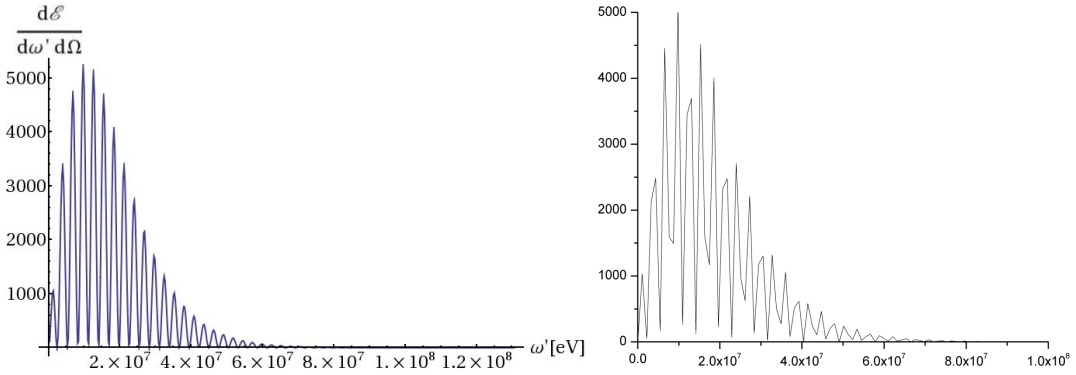

Figure 5.4: Comparison of quantum mechanical (left) and classical (right) emission spectra for $\xi = 5$ and $\gamma_0 = \frac{m}{200\,\omega}$

The rough appearance of the classical spectrum is due to a small numerical resolution. However, the quantum mechanically and classically obtained spectra again agree very well. This is expected because the quantum parameter in this case still is very small $\chi \approx 2.5 \cdot 10^{-2}$. Again computing the first frequency of destructive interference according to Eq. (5.5) we find

$$\omega_1 = 1.55 \cdot 10^7\,\text{eV}$$

with all higher ω_n being integer multiples of this fundamental frequency.
Indeed this first frequency of destructive interference is smaller than it was in the case of $\xi = 1$ but still not as small as it should be looking at Fig. 5.4. This deviation has to be attributed to a numerical uncertainty in our method of determining the ω_n.
What furthermore is remarkable about Fig. 5.4 is the absence of a second harmonic maximum despite a nonlinearity parameter $\xi = 5$. We attribute the nonexistence of such a two-photon absorption maximum to the shortness of the pulse which puts some difficulties on interpreting it as a stream of photons with an frequency distribution according to Eq. (2.17). These difficulties were already present in section 2.4 where we could not expand the transition matrix element into a FOURIER series in which the n^{th} term would have represented absorption of n photons.
Next in Fig. 5.5 we again plot the quantum mechanically obtained spectrum with an inset arrow at the blue shifted central frequency of the incident laser as in Fig. 5.3.

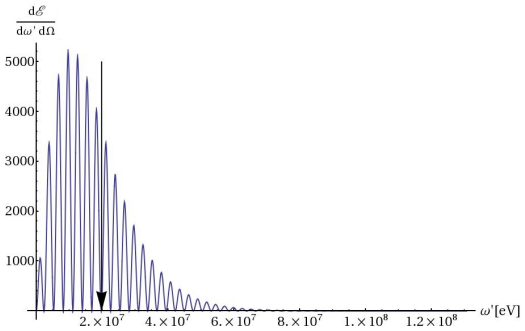

Figure 5.5: Quantum mechanical emission spectrum or $\xi = 5$ and $\gamma_0 = \frac{m}{200\,\omega}$, the arrow marks ω_{Theo}

Here we again explain the seemingly random position of ω_{Theo} in the spectrum by distortion due to the many destructive interferences.
Having now discussed and understood the classical limit of our calculations in detail we pass to parameter regimes where quantum effects become considerable. To this end we plot the emission spectra for increased initial electron momenta. We choose γ_0 to be one order of magnitude larger than in the previous spectra and pay attention to any significant differences between the quantum mechanical and classical results which would hint at an upcoming importance of quantum effects.

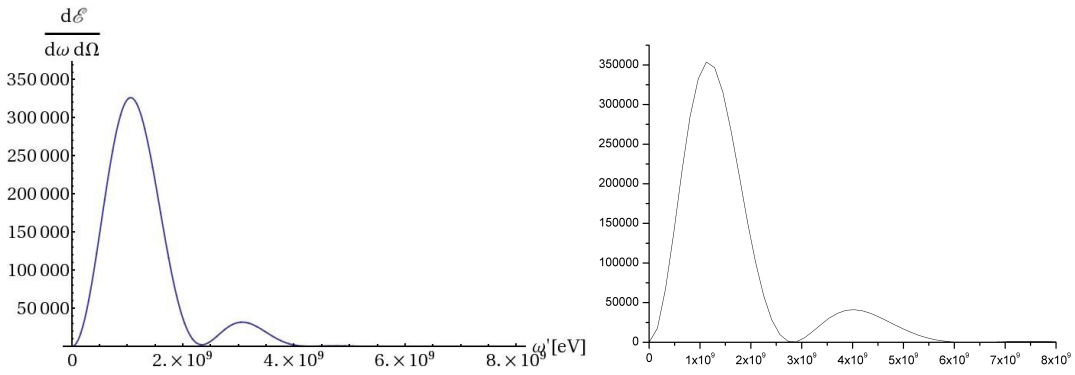

Figure 5.6: Comparison of quantum mechanical (left) and classical (right) emission spectra for $\xi = 1$ and $\gamma_0 = \frac{m}{20\,\omega}$

In Fig. 5.6 we chose an initial relativistic factor of the electron of $\gamma_0 = m/(20\,\omega)$ corresponding to a quantum parameter $\chi \approx 5 \cdot 10^{-2}$. In these spectra we find that even though the shapes of the classical and the quantum mechanical spectrum look quite similar their scaling differs. In the classical calculation the emission probability goes to zero at irradiated photon frequencies of approximately $\omega' \approx 6 \cdot 10^9$ eV. In the quantum calculation, however, the energy spectrum goes to zero around $\omega' \approx 4 \cdot 10^9$ eV. This is a first indication that at quantum parameters larger than $\chi \approx 0.01$ quantum effects become important albeit not so dominant that they would change the spectra's shapes. Computing the first frequency of destructive interference we find $\omega_1 = 2.9 \cdot 10^9$ eV which is in good agreement with the classical spectrum but slightly disagrees with the position of the first minimum in the quantum spectrum. But Eq. (5.5) was obtained through classical considerations and thus will always yield the classical result. So at this point we note the rise of a second class of effects determining the shape of the energy spectra namely quantum effects suppressing emission of high energetic photons. This suppression is due to the energy momentum conservation expressed by Eq. (2.32). As can be concluded from Fig. 5.6 this results in a seeming shift of any distinct feature such as an interference minimum in the energy spectrum to smaller frequencies. So from now on we have to pay attention to not only the classical effect of destructive interference but also the quantum effect of a cutoff in the energy spectra as soon as the emitted photon frequencies approach the threshold given by Eq. (2.32).
If we again plot the spectra for $\xi = 5$ we anew observe that the minima shift to smaller frequencies in comparison to $\xi = 1$ as shown in Fig. 5.7

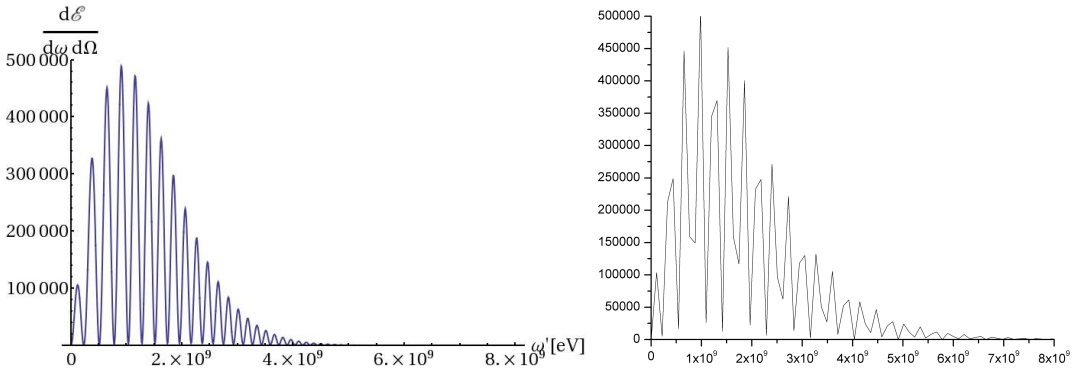

Figure 5.7: Comparison of quantum mechanical (left) and classical (right) emission spectra for $\xi = 5$ and $\gamma_0 = \frac{m}{20\,\omega}$

In these two spectra we find the same differences as in Fig. 5.6 that the classical spectrum extends to somewhat larger photon energies than the quantum mechanical spectrum. Having noticed that for quantum parameters on the order of a few percent quantum effects begin to yield small differences between the quantum mechanical and the classical calculations we now turn to even higher quantum parameters of order unity. In this case already from the four pairs of spectra shown previously we may expect to find major differences in the two spectra. And indeed for the choice of $\gamma_0 = m/\omega$ and $\xi = 1$ corresponding to $\chi \approx 1$ we find the spectra in Fig. 5.8.

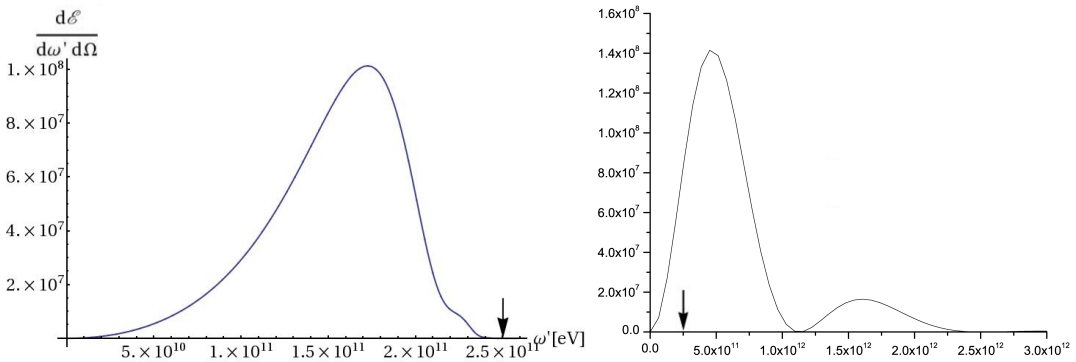

Figure 5.8: Comparison of quantum mechanical (left) and classical (right) emission spectra for $\xi = 1$ and $\gamma_0 = \frac{m}{\omega}$

In these spectra the arrows point to the same emitted photon frequency of roughly $\omega_{\text{Max}} \approx 2.5 \cdot 10^{11}$ eV. At this frequency the quantum spectrum shows a vanishing emission probability while in the classical calculation the spectrum extends to considerably larger photon frequencies. Due to $\xi \ll \gamma_0$ the electron will absorb only very little energy from the laser compared to its initial energy ϵ what in turn may be considered as an upper limit for emitted photon energies. Computing it for the choice of $\gamma_0 = m/\omega$ we find $\epsilon = m^2/\omega \approx 2.5 \cdot 10^{11}$ eV. This is the cutoff frequency found in the quantum mechanical spectrum left in Fig. 5.8. Since in the classical calculation there is no restriction on the emitted photon energies the emission spectrum stretches to photon energies larger than the electron's total energy. This is unphysical

and thus the classical predictions lose validity. So obviously as soon as the quantum parameter χ approaches unity not only the scales of the emission spectra but also their shapes will differ fundamentally from the classical predictions. These differences as can be presumed from Fig. 5.8 arise because the emitted photon energies approach the total energy of the electron. If we again calculate the first frequency of destructive interference ω_1 from Eq. (5.5) we find $\omega_1 = 1.2 \cdot 10^{12}\,\mathrm{eV}$ what is in good agreement with the classical spectrum in Fig. 5.8. In the quantum spectrum on the other hand we don't find any minima at all and additionally have radiation only at emitted photon energies substantially smaller than ω_1. So we note that for $\chi \sim 1$ no longer classical effects such as destructive interference determine the energy spectra but much rather quantum effects as the energy cutoff at ω_{Max}.
An even more interesting graph can be obtained if for the case of χ on the order of unity one increases the intensity parameter to $\xi = 5$. In that case the resulting spectra look as shown in Fig. 5.9

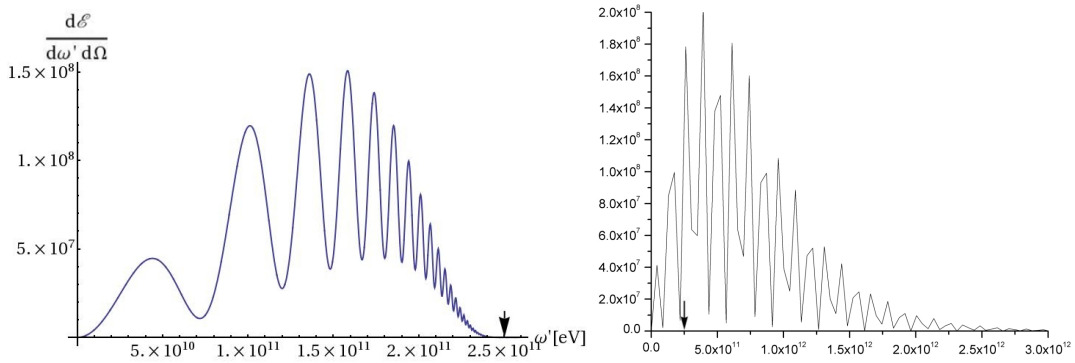

Figure 5.9: Comparison of quantum mechanical (left) and classical (right) emission spectra for $\xi = 5$ and $\gamma_0 = \frac{m}{\omega}$

The arrows again point to the cutoff frequency of the quantum spectrum and obviously the classical spectrum is unphysical. In the quantum spectrum we find two classes of effects at once. These are on the one hand the classically explainable destructive interferences leading to the emission minima and on the other hand a quantum mechanical energy cutoff shifting these minima to seemingly smaller photon frequencies ω'. This shift additionally causes the minima to lie closer together the closer these minima lie to the cutoff frequency.
Summing up all this discussion we have seen that the quantum parameter χ is well suited to distinguish processes in which we may neglect or have to respect quantum effects. Furthermore we have seen that the energy spectra especially in the case of $\chi \sim 1$ exhibit a rich structure due to classical as well as quantum mechanical effects.

Chapter 6

Changed carrier-envelope-phase

Up to now we only considered the case where the *carrier-envelope-phase* (CEP) was fixed. We can assume it was zero. However, since for laser pulses as short as we are considering in this work it is complicated to control this phase experimentally it is of great importance to understand the influence of a changed CEP on the emission patterns. In fact, as we will see in this section, from the angular distribution of the spectrum one can obtain information about the CEP of the ultra-strong and ultra-short laser pulse.
To obtain energy spectra in the case of a changed CEP we basically follow the procedure from sections 2.3 and 2.4 albeit in an abbreviated form. The pulse described by the electric field shape (2.12) can be imagined as a sine shaped by a hyperbolic secans as envelope function $\boldsymbol{E}(\phi) \propto \sin(\phi)\mathrm{sech}(\phi)$. Introducing a relative phase between the carrier wave and the envelope then corresponds to considering the electric field $\boldsymbol{E}(\phi) \propto \sin(\phi+\phi_0)\mathrm{sech}(\phi)$. We can decompose this according to $\sin(\phi+\phi_0) = \sin(\phi)\cos(\phi_0)+\cos(\phi)\sin(\phi_0)$ into a superposition of two electric fields $\boldsymbol{E}_1(\phi) \propto \sin(\phi)\mathrm{sech}(\phi)$ and $\boldsymbol{E}_2(\phi) \propto \cos(\phi)\mathrm{sech}(\phi) = \sin(\phi+\pi/2)\mathrm{sech}(\phi)$.
Since the case $\phi_0 = 0$ has already been covered it is sufficient to consider the case of $\phi_0 = \pi/2$ and to expect that the electron's dynamics in a laser pulse with arbitrary CEP will be determinable from these two cases. The electric field shape $\boldsymbol{E}_2(\phi)$ is depicted in Fig. 6.1

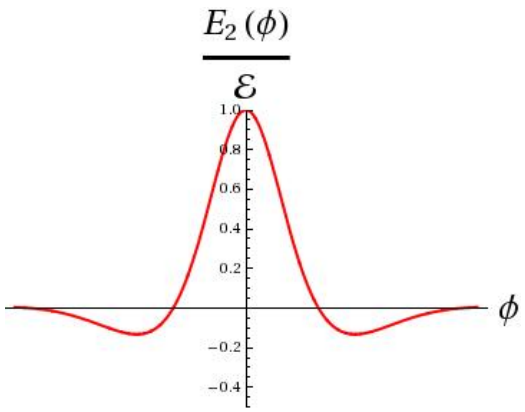

Figure 6.1: Electric field shape for $\phi_0 = \frac{\pi}{2}$

We model such a laser pulse with a CEP $\phi_0 = \pi/2$ by the four potential

$$A^\mu \;=\; a^\mu \,\frac{\tanh(\phi)}{\cosh\left(\phi\right)} \tag{6.1}$$

corresponding to the electric field

$$\boldsymbol{E}(\phi) = \frac{\mathcal{E}}{T}\mathrm{sech}\left(\phi\right)\left(2\mathrm{sech}^2\left(\phi\right)-1\right)\boldsymbol{n} \tag{6.2}$$

where $\boldsymbol{n}$ again is a three-dimensional normalized vector pointing into the laser pulse's direction of polarization and $\mathcal{E}$ is the electric field's maximal amplitude. The electric field (6.2) looks in dependence of the invariant phase ϕ as shown in Fig. 6.2

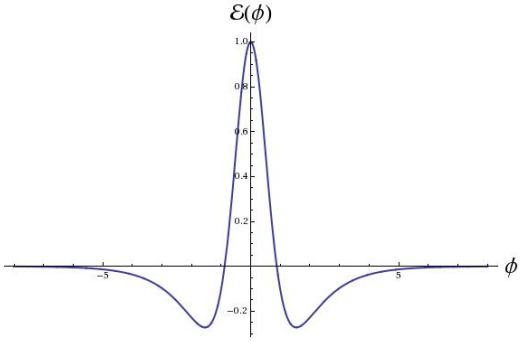

Figure 6.2: The electric field arising from (6.1)

This field shape is in good agreement with Fig. 6.1. We additionally note that the function $\mathrm{sech}\left(\phi\right)\left(2\mathrm{sech}^2\left(\phi\right)-1\right)$ has a maximum value of 1 as can be seen from Fig. 6.2. Thus the connection between the electric field's maximal amplitude $\mathcal{E}$ and the intensity parameter ξ looks a bit different from the case of vanishing CEP inasmuch as in Eq. (2.14) we may drop the additional factor 2 and thus write

$$\xi \;=\; -\frac{\mathcal{A}\,e}{m} = -\frac{e\,\mathcal{E}}{m\omega}. \tag{6.3}$$

To further characterize the laser pulse described by Eq. (6.1) we have to determine the central frequency of the frequency distribution contained in it. To this end we FOURIER transform the electric field as in section 2.3. The frequency dependent electric field reads

$$\widetilde{\boldsymbol{E}}(\omega) = \frac{\mathcal{E}}{T\sqrt{2\pi}}\pi\omega^2\mathrm{sech}\left(\frac{\pi\omega}{2}\right)\boldsymbol{n}.$$

The energy distribution is proportional to $\mathscr{E}(\omega) \propto \omega^4\mathrm{sech}^2\left(\frac{\pi\omega}{2}\right)$ which is peaked at $\omega^* \approx 1.3$ eV. Such differences in the maximum frequencies of the frequency distributions naturally occur in ultra-short pulses due to the distortions of the electric field by the envelope function.
The choice (6.1) leads to the same mathematical structure of the energy spectrum as derived in Eq. (2.29) if only the parameter functions are defined as

$$f_i = \mathrm{e}^{-\mathbb{i}\,\rho}\int_{-\infty}^{\infty}\mathrm{d}x \qquad \mathrm{e}^{-\mathbb{i}\left[\alpha\,\mathrm{sech}(2x)+\rho\,\tanh^3(2\,x)\right]}\mathrm{e}^{i\,K_3 x}\;\left(\frac{\tanh\left(2x\right)}{\cosh\left(2x\right)}\right)^i. \tag{6.4}$$

The parameters α and K_3 have been defined in Eq. (2.33) while the last parameter is defined as $\rho := \beta/3$. Also for these parameter functions it holds the important equality

$$f_0 \;=\; -\frac{2}{K_3}\left(\alpha\, f_1 - \beta\, f_2\right). \tag{6.5}$$

So now we turn to compute the parameter functions f_i in the three intensity regimes we considered for the case of a CEP equal to zero. We again start with the perturbative regime $\xi \ll 1$.

6.1 Perturbation theory

For $\xi \ll 1$ we expand the exponential in the f_i as in section 3.2. The parameter functions then become

$$\begin{aligned} f_{1,2} &= \int_{-\infty}^{\infty} \left(1 - \mathbb{i}\,\left(\alpha\,\mathrm{sech}(2x) - \rho\tanh^3(2x)\right) - \frac{\alpha^2}{2}\mathrm{sech}^2(2x)\right)\left(\frac{\tanh(2x)}{\cosh(2x)}\right)^{1,2} \mathrm{e}^{\mathbb{i}\,K_3 x}\mathrm{d}x + \mathcal{O}\left(\xi^3\right) \\ f_0 &= -\frac{2}{K_3}\left(\alpha\, f_1 - 3\rho\, f_2\right). \end{aligned}$$

With these expressions for the parameter functions we may compute the combinations $|f_0|^2$, $|f_1|^2$, $\Re\left(f_0 f_1^*\right)$ and $\Re\left(f_0 f_2^*\right)$ which are needed to compute $|S_{\mathrm{fi}}|^2$. However in this case we will not write down the expression for the transition probability but rather present the resulting energy spectra directly.
We again plot the differentially emitted energy per unit cosine of the polar angle $\mathcal{T} = \cos(\vartheta)$ and frequency interval $\mathrm{d}\mathscr{E}/\left(\mathrm{d}\mathcal{T}\,\mathrm{d}\omega'\right)$ over the outgoing photon's frequency ω'. As in section 3.3 we will perform the calculations for a laser intensity of $I = 10^{16}\,\mathrm{W/cm^2}$ corresponding to an intensity parameter of roughly $\xi \approx 0.07$. We begin with an electron initially at rest ($\gamma_0 = 1$) and the resulting spectra look like shown in Fig. 6.3.

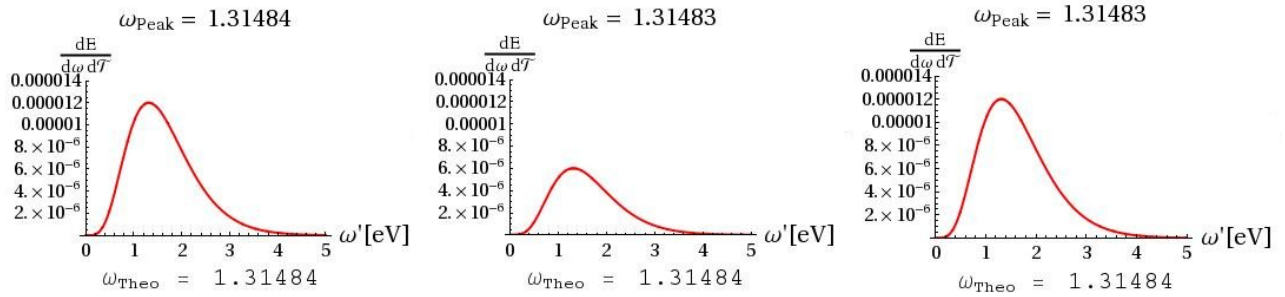

Figure 6.3: Emitted frequency spectra for $\gamma_0 = 1$ eV for the polar angles from left to right $\vartheta = 0, \frac{\pi}{2}, \pi$

In these spectra we find two noteworthy features comparing it to Fig. 3.2: First of all we find the spectra to be peaked at the incident laser pulse's central frequency $\omega_{\mathrm{Peak}} \approx 1.3$ eV. In section 3.3 we found the same quantitative behaviour that an electron at rest scattered off a weak laser pulse basically reproduces the incident frequency distribution and interpreted it as

the well-known THOMSON scattering.
The second interesting observation in Fig. 6.3 can be drawn regarding the spectra's amplitudes. The maximal differentially emitted energy $\mathrm{d}\mathscr{E}$ is roughly $1.2 \cdot 10^{-5}$ eV at $\vartheta = 0, \pi$ and $6 \cdot 10^{-6}$ eV at $\vartheta = \pi/2$. But looking back at Fig. 3.2 we find that there the energy spectra exhibit exactly the same amplitudes.
From these two facts we infer that for an electron initially at rest changing the CEP qualitatively leaves the energy spectra unchanged. But this is expected for the limit $\xi \ll 1$ corresponds to a very weak laser pulse and in the limit of a small amplitude of the electric field its particular temporal and spatial shape cannot have great influence on the energy spectra.
Next we need to find possible differences arising from changing the CEP for an electron initially moving at relativistic speeds. To this end we plot the energy spectra at the three polar angles $\vartheta = 0, \pi/2$ and π for an initial relativistic factor of the electron of $\gamma_0 = 10^5$ corresponding to an initial energy of $\epsilon \approx 50$ GeV and compare the resulting spectra to Fig. 3.5.

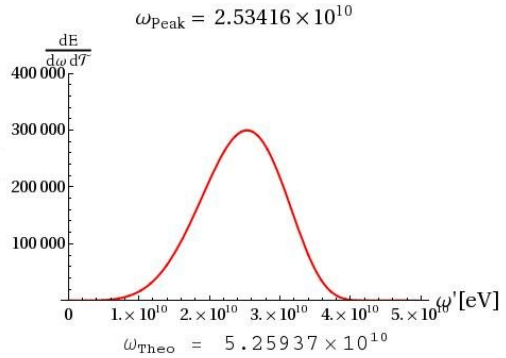

Figure 6.4: The emission spectra for $\gamma_0 = 10^5 \Leftrightarrow P \approx 50\,\mathrm{GeV}$ for $\vartheta = \pi$

In this spectrum we again don't find any deviations from the behaviour observed in Fig. 3.5 despite the different central frequency of the laser pulse we already explained. But the same features as in section 3.3 are determining the energy spectra namely the relativistic focussing, the blue shift of the pulse's central frequency and the kinematic pile up as can be found in Fig. 6.4.
So we conclude that in the limit of weak laser intensities a changed CEP does not influence the qualitative structure of the energy spectra.

6.2 Strong field limit

For $\xi \sim \gamma_0 \gg 1$ we employed the method of stationary phase as described in section 4.1.2 to find asymptotically correct approximations for the parameter functions f_i. To this end first of all we had to find the asymptotic behaviour of the process parameters α, ρ and K_3 in the limit $\xi \to \infty$. Since in the case of a changed CEP these parameters are unchanged we can adopt the expressions we found in section 4.1.1 for their asymptotic development namely $\alpha \sim \rho \sim K_3 \sim \xi^3$.
So we may directly begin by applying the method of stationary phase to obtain expressions for

the parameter functions f_i. As a beginning we state the exponential function

$$g(x) = -\mathbb{i}\,\left(\alpha\,\mathrm{sech}(2x) + \rho\,\tanh^3(2\,x) - K_3\,x\right) \tag{6.6}$$

as well as the three preexponential functions

$$\begin{aligned} G_0(x) &= -\frac{2}{K_3}\left(\alpha\,G_1(x) - 3\rho\,G_2(x)\right) \\ G_1(x) &= \frac{\tanh(2x)}{\cosh(2x)} \\ G_2(x) &= \left(\frac{\tanh(2x)}{\cosh(2x)}\right)^2. \end{aligned} \tag{6.7}$$

In appendix E we will show that at the stationary point it holds

$$\frac{\tanh(2x_0)}{\cosh(2x_0)} = \frac{\alpha}{2\,\beta} \pm \mathbb{i}\,\frac{\sigma_0}{\xi}$$

with the asymptotic behaviour $\alpha\,/\,(2\,\beta) \sim \sigma_0 \sim$ const. what already strongly reminds us of relation (4.10) which we found in the case of a vanishing CEP. The condition for real stationary points in the limit of large ξ, however, will be given by

$$-0.5 \leq \frac{\alpha}{2\beta} \leq 0.5.$$

Just as we did in section 4.1.2 we may translate this restriction into an angular confinement of the emitted radiation

$$\boxed{\vartheta \;\geq\; \vartheta_{\min} = 2\;\mathrm{arccot}\left(\frac{\xi}{4\,\gamma_0}\right).} \tag{6.8}$$

This condition corresponds to a backscattering condition of $\xi \geq 4\,\gamma$ unlike in the case of a zero CEP where we found $\xi \geq 2\,\gamma$ as a condition for observing radiation at polar angles $\vartheta \leq \frac{\pi}{2}$. However, since the ratio $\alpha/\,(2\beta)$ for a changed CEP may be smaller than zero the condition (6.8) may be met in the azimuthal angular regimes $\varphi \sim \xi^{-1}$ and $\varphi - \pi \sim \xi^{-1}$ corresponding to observation of radiation at positive as well as negative x-coordinates.
The expectation that there will be emission also detectable at $\varphi \approx \pi$ again can be interpreted classically. By solving the equations of motions one finds that the trajectory will still lie in the x-z-plane but look like shown in Fig. 6.5.

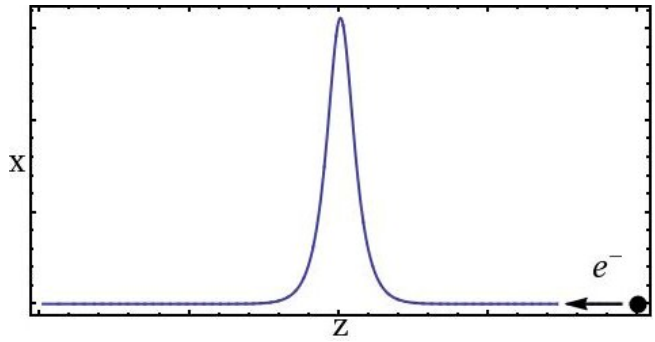

Figure 6.5: Classical electron trajectory for changed CEP

Here we find a clear distinction in comparison to e.g. Fig. 4.1 where we plotted the electron trajectory for a vanishing CEP. The electron namely will not exclusively propagate towards positive but also negative values of x and thus also radiate into the azimuthal angular region around $\varphi = \pi$. The differences in the angular distribution of emission consequently can be attributed to different electron dynamics during the scattering process.
Now as reasoned in section 4.1.2 once we have found a stationary point x_0 we may expand the exponential as well as the preexponential functions in orders of $(x - x_0)$ to obtain an expression analogous to Eq. (4.16). But as a complication in comparison to the treatment in section 4.1.2 it will turn out that the exponential function (6.6) will lead to two stationary points $x_{0,1}$ and $x_{0,2}$ within the integration range. To treat two separate stationary points with the method of stationary phase on the other hand is quite straightforward as the two contributions may simply be added up [42].
Doing so the parameter functions can be written analogously to Eq. (4.17) as

$$f_i \sim \mathrm{e}^{\mathrm{i}\left(\frac{\pi}{2}\alpha-\beta\right)} \sum_{j=1}^{2} G_{i,j}\mathcal{H}_0^j + G'_{i,j}\mathcal{H}_1^j + \frac{1}{2}G''_{i,j}\mathcal{H}_2^j \tag{6.9}$$

where now we defined $G_{i,j}^{(n)} = G_i^{(n)}(x_{0,j})$ for the preexponential functions and their first two derivatives evaluated at the stationary points $x_{0,j}$. The integrals $\mathcal{H}_i^j$, however, are defined as

$$\mathcal{H}_i^j := \int_{-\infty}^{\infty} (x - x_{0,j})^i \, \mathrm{e}^{g_{\mathrm{T},j}(x)} \, \mathrm{d}x.$$

Here the expanded exponential functions are

$$g_{\mathrm{T},j} := g_{0,j} + g'_{0,j}(x - x_{0,j}) + \frac{1}{2}g''_{0,j}(x - x_{0,j})^2$$

with the exponential function $g(x)$ and their derivatives taken at the respective stationary point $x_{0,j}$. The computation of the $\mathcal{H}_i^j$ again is possible on grounds of the method of stationary phase and performed in appendix E. Now we turn to present the resulting energy spectra.
We begin with the parameter choices $\gamma_0 = \xi = 100$ corresponding to a quantum parameter of $\chi \approx 0.02$. From Eq. (6.8) we derive that this corresponds to a minimal scattering angle of $\vartheta_{\min} = 151.9°$ what reveals that for the changed CEP the radiation will be narrower confined

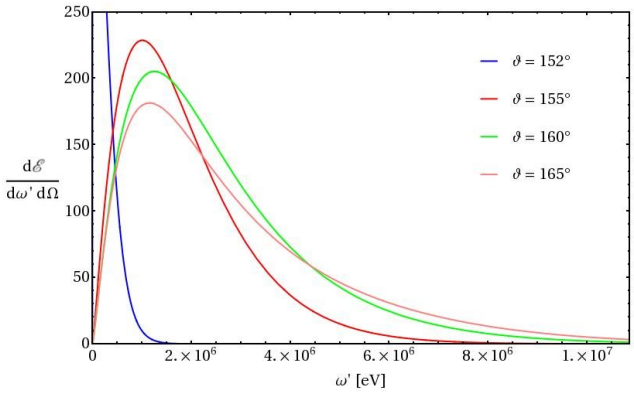

Figure 6.6: Energy spectrum for $\gamma_0 = \xi = 100$

to the z-axis. The resulting energy spectrum is presented in Fig. 6.6.
Comparing this spectrum to Fig. 4.3 which was obtained for the same parameters for vanishing CEP we find that the emitted frequencies are on the same order of magnitude but the spectra's amplitudes differ distinctly. We attribute this difference to the closer confinement of the emission in the case of a changed CEP. However, there is yet another difference in the angular distribution of the emission in comparison to section 4.1: We expect to observe radiation also in negative x-direction as discussed above. So we plot the emission spectrum at the same polar angles but at the azimuthal angle $\varphi = \pi$ and show the result in Fig. 6.7

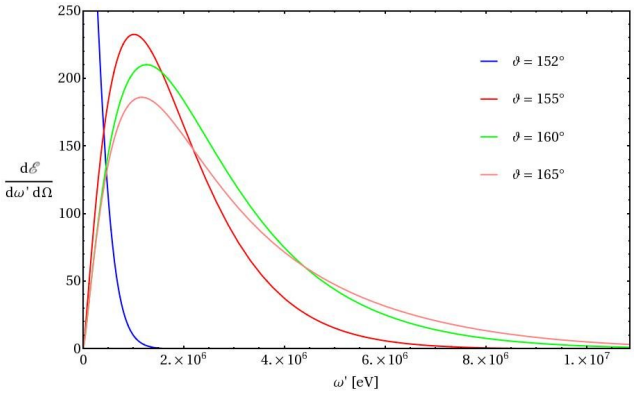

Figure 6.7: Energy spectrum for $\gamma_0 = \xi = 100$ at $\varphi = \pi$

These energy spectra agree very well with the ones shown in Fig. 6.6 whence we conclude that the emission will be symmetrically distributed around the z-axis.
We find analogous differences between the spectra for a vanishing and a finite CEP for parameter choices where quantum effects are important. To test this we plot the energy spectra for $\gamma_0 = \xi = 1000$ at $\varphi = 0$ as well as at $\varphi = \pi$ and show the resulting spectra in Fig. 6.8.

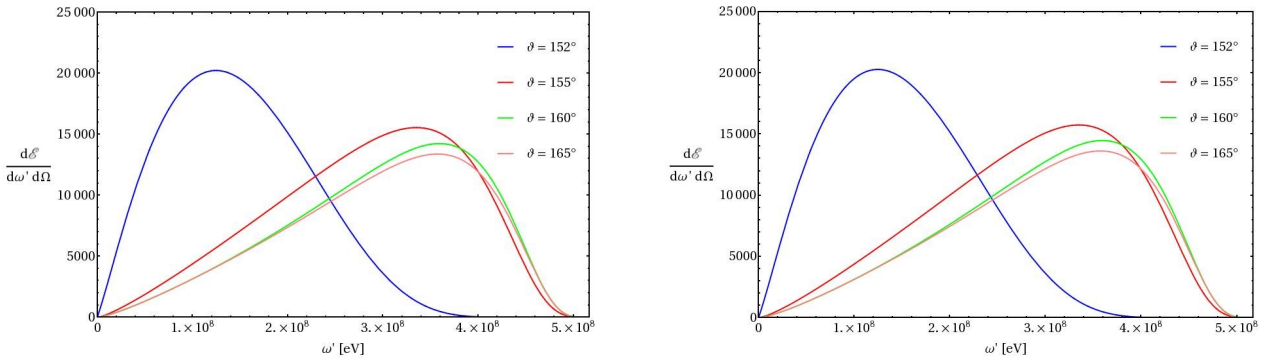

Figure 6.8: Energy spectrum for $\gamma_0 = \xi = 1000$ for $\varphi = 0$ (left) and $\varphi = \pi$ (right)

Here we find agreement with Fig. 4.5 concerning the kinematic pileup and disagreement concerning the symmetric distribution of radiation at t $\varphi = 0$ and at $\varphi = \pi$. The difference in the spectra's amplitude again is due to the narrow confinement of emission in the case of a changed CEP.

6.3 Constant field limit

For obtaining the parameter functions in the constant field regime $\xi \gg 1$, $\gamma_0 \sim$ const. basically all work is already done. In section 4.2.1 we stated the asymptotic behaviour of the important process parameters in the constant field limit to be $\alpha, \beta, K_3 \sim \xi^3$. Second in section 4.2.2 we could show that in the constant field regime the f_i may be asymptotically expanded in exactly the same way as in the strong field regime. And this expansion we obtained as Eq. (E.6) in appendix E. So we simply adopt that formula and pay attention to the different parameter regimes we may consider in the constant field regime and directly turn to discussing the resulting energy spectra.
For the constant field limit we will plot the energy spectra for electrons initially at rest $\gamma_0 = 1$. We begin with the parameter choice $\xi = T = 100$ corresponding to a minimal scattering angle $\vartheta_{\text{min}} = 2.3°$ and a quantum parameter of $\chi \approx 10^{-6}$. The resulting energy spectrum is given in Fig. 6.9.

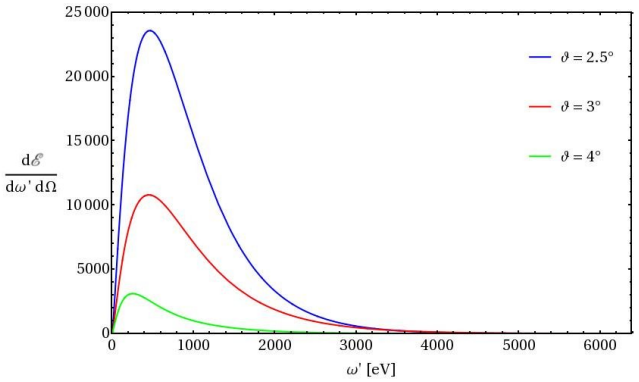

Figure 6.9: Energy spectra for $\xi = 100$

We compare these spectra to those obtained for $\xi = 1000$ corresponding to a minimal scattering angle $\vartheta_{\min} = 0.23°$ which are shown in Fig. 6.10.

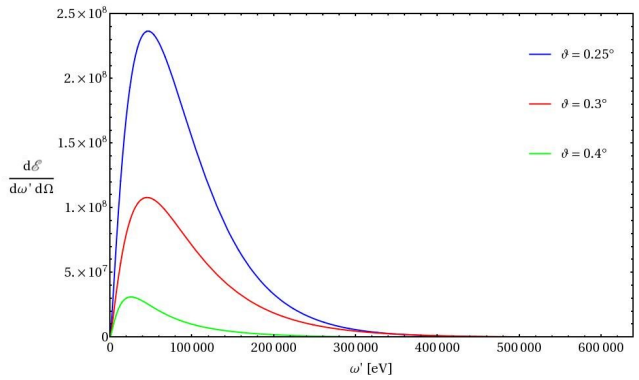

Figure 6.10: Energy spectra for $\xi = 1000$

As discussed in section 4.2.3 the quantum parameter χ is unchanged as long as we consider $\xi = T$. In comparing Figs. 6.9 and 6.10 we again find the classically expected scalings $\vartheta \sim \xi^{-1}$ and $\omega' \sim \xi^2$ confirmed. There will again be emission into $\varphi = \pi$ unlike in the case of a vanishing CEP but we discussed the interpretation of this observation already in section 6.2.

6.4 The intermediate case

As already reasoned in section 5 in the intermediate regime $\xi \sim 1$ neither a perturbative nor an asymptotic expansion of the parameter functions is feasible. So once again we will have to integrate the integrals in Eq. (6.4) out numerically to obtain values for the f_i which in turn can be inserted into Eq. (2.29) to yield energy spectra.
In section 5 we found that the order of magnitude of the quantum parameter χ is a good measure for the degree of agreement that may be expected between classical and quantum mechanical calculations. So we start our discussion by presenting energy spectra calculated for the case $\chi \ll 1$ end then go over to the case $\chi \approx 1$. Additionally we will compute the energy spectra for

two different values of the intensity parameter $\xi = 1, 5$ and discuss qualitative differences. As we motivated in section 5 on the basis of Eq. (5.1) comparatively large electron momenta are needed to access the regime of $\chi \sim 1$. We additionally state that from Eq. (6.3) one derives that in the case of changed CEP Eq. (5.1) needs to be written as

$$\chi = \xi\gamma_0 (1 + \beta) \frac{\omega}{m}. \tag{6.10}$$

As a consequence we take a start by computing the energy emission spectrum for the case of $\xi = 1$ and an initial relativistic electron factor of $\gamma_0 = m/(200\,\omega)$ what in this case corresponds to $\chi = 10^{-2}$. As observation angle we chose $\vartheta = \pi$ again due to $\gamma_0 \gg \xi$ and the electron thus changing its initial direction of propagation only little. The result is presented in Fig. 6.11 and as in section 5 it is compared to the spectrum resulting from a classical computation to its right.

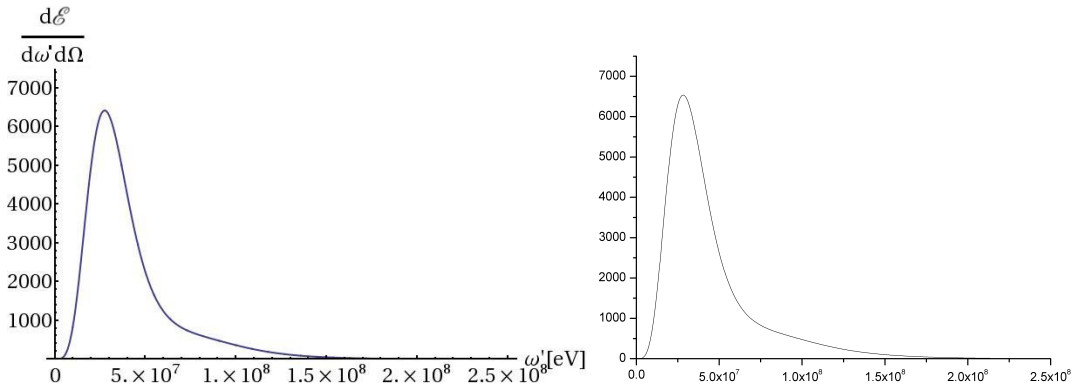

Figure 6.11: Comparison of quantum mechanical (left) and classical (right) emission spectra for a changed CEP with $\xi = 1$ and $\gamma_0 = \frac{m}{200\,\omega}$

First of all in these two spectra we find perfect matching of quantum mechanical and classical calculations as was expected since $\chi \ll 1$. Furthermore we note that there are no minima present in the energy spectra for the case of changed CEP. In section 5 we attributed the minima in the spectra in destructive interferences. But for too small values of ξ the frequencies of destructive interference may be too large to cause significant minima in the energy spectra. So we increase the intensity parameter to $\xi = 5$ and present the results in Fig. 6.12. This choice of parameters corresponds to a quantum parameter of $\chi = 5 \cdot 10^{-2}$.

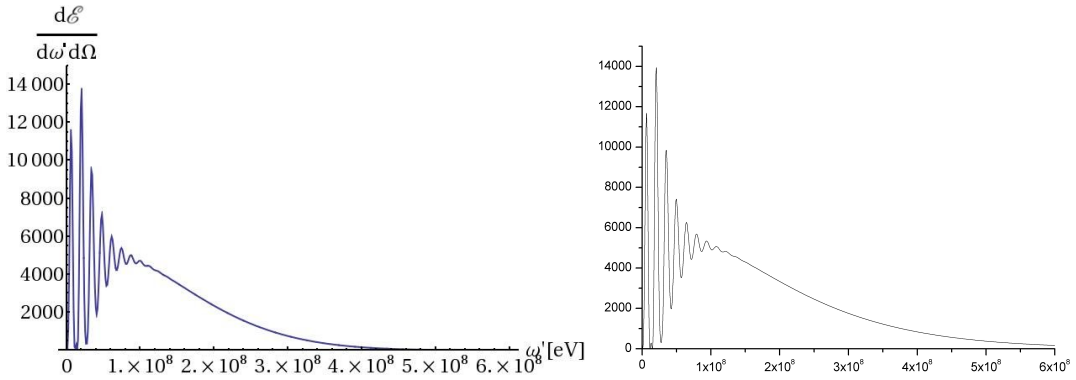

Figure 6.12: Comparison of quantum mechanical (left) and classical (right) emission spectra for a changed CEP with $\xi = 5$ and $\gamma_0 = \frac{m}{200\,\omega}$

In these two plots again we find very good agreement between the two spectra. We may consequently claim that our calculations yield the correct classical limit for small χ. Furthermore we find a number of minima in the spectra. Unlike in section 5 in the spectra in Fig. 6.12 there is a narrow sequence of minima up to $\omega' \approx 1 \cdot 10^9$ eV followed by a very smooth and slow decrease of energy emission probability. But if we now plot the quantum spectrum only up to the frequency where the oscillations die out as is shown in Fig. 6.13 we find that these oscillations lie equally spaced.

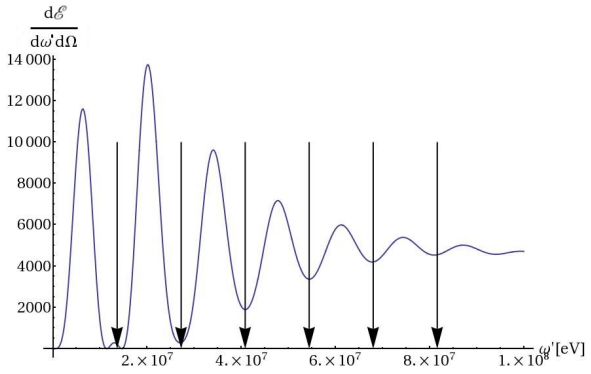

Figure 6.13: Energy spectrum for a changed CEP with $\xi = 5$ and $\gamma_0 = \frac{m}{200\,\omega}$ up to $\omega' = 10^8$ eV.

The only exception is the small bump to be found in the spectrum's first minimum which can be attributed to the complicated trajectory a classical electron takes in a electric field shaped as Eq. (6.2) (comp. Fig. 6.5). Furthermore this feature is so small that it will hardly be identified in any experimental setup. So from the combination of the Figs. 6.12 and 6.13 we conclude that the energy spectrum for larger values of ξ is a combination of a smooth curve and an interference pattern which dies out when the ω' become too large. We interpret this such that interferences become less complete the larger the outgoing photon frequencies are. We did not observe such an effect in the spectra shown in section 5. This discrepancy may be explained by the fact that unlike in the discussion in that section the electron will not only propagate towards $\vartheta = \pi$ before entering and after leaving the laser pulse. Much rather as can be seen from Fig. 6.5 there are three segments of the electron's trajectory contributing significantly to

the radiation detectable at $\vartheta = \pi$. Since for larger emission frequencies ω' the coherence length of the emitted radiation becomes shorter the displacement of the points where the radiation is emitted may become too large for all the three contributions to interfere completely destructively.
We are not going to present the resulting energy spectra for the case of an slightly increased initial electron momentum $\gamma_0 = m/(20\,\omega)$ for it gives no additional insight compared to section 5. We rather go on to plot the quantum mechanical and classical spectra for the case of a quantum parameter of order unity. As done in the case of vanishing CEP we choose $\gamma_0 = m/\omega$ what in connection with an intensity parameter $\xi = 1$ according to Eq. (6.10) yields a quantum parameter of $\chi = 2$. The spectra are shown in Fig. 6.14.

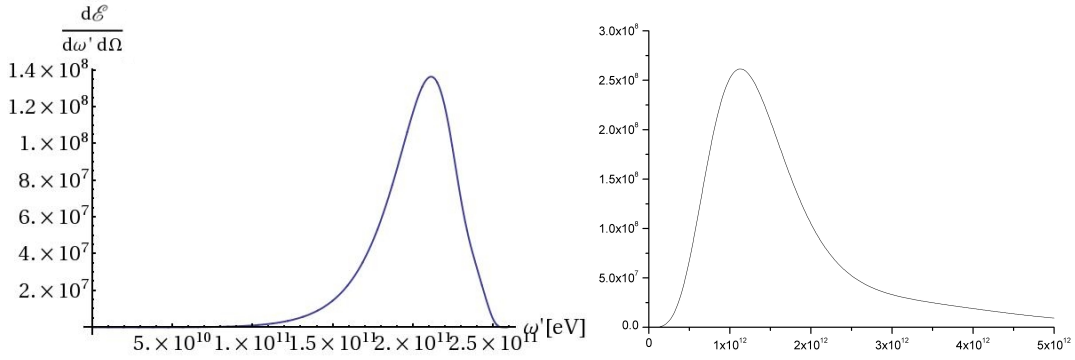

Figure 6.14: Comparison of quantum mechanical (left) and classical (right) emission spectra for a changed CEP with $\xi = 1$ and $\gamma_0 = \frac{m}{\omega}$

In these two spectra there appear significant differences between the quantum and the classical calculations. But looking back at Fig. 5.8 and the discussion below it we realize that the cutoff frequency apparent in the quantum mechanical spectrum on the left of Fig. 6.14 is roughly $\omega_{\text{cutoff}} \approx 2.5 \cdot 10^{11}$ eV what exactly corresponds to the cutoff frequency found in the former figure. But there we interpreted the presence of a cutoff ω_{cutoff} as a quantum effect namely that the electron transfers basically all its kinetic energy to the emitted photon. Higher photon energies are not possible due to energy momentum conservation.
For the next pair of energy spectra we increase the nonlinearity parameter to $\xi = 5$ corresponding to a quantum parameter of $\chi = 10$. As in Fig. 5.9 in this case we expect serious overlay of quantum and interference effects. Indeed for the given parameter choices the energy spectra look as given in Fig. 6.15.

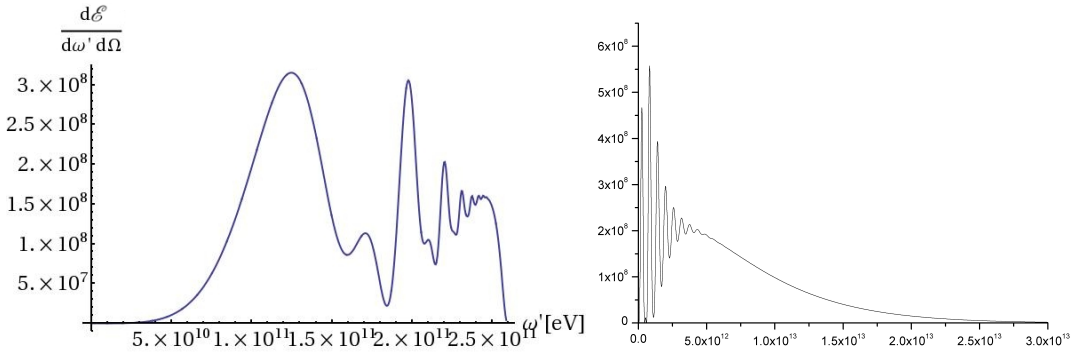

Figure 6.15: Comparison of quantum mechanical (left) and classical (right) emission spectra for a changed CEP with $\xi = 5$ and $\gamma_0 = \frac{m}{\omega}$

The classical spectrum in this case does not need any attention due to the undeniable importance of quantum effects. So we focus our discussion on the quantum spectrum shown left in Fig. 6.15. As in the case of a vanishing CEP the energy spectrum exhibits a complicated structure. But as in Fig. 5.9 this structure is resolvable. It is essentially created by a compression of the emission maxima with the smaller bumps in the intermediate minima towards smaller emission frequencies. In section 5 we argued that such a distortion of the energy spectra for large χ is clear evidence for quantum effects which inhibit the emission of large photon frequencies ω'.
So even though the actual shape of the energy spectra is significantly changed by introducing a finite CEP there is no qualitative difference in the origin of the spectra's shapes. In both cases the emission spectra are determined by interference and quantum effects.

Chapter 7

Conclusions

This section is devoted to a concise overlook of the effects arising in the scattering of an electron and an ultra-short laser pulse as found in this diploma thesis.

7.1 Effects characteristic of ultra-short laser pulses

As we mentioned in the introduction there has already been a lot of work on electron scattering from monochromatic [10–13] or long pulsed [14] lasers. Comparing our results to these works we find some agreement as well as some differences. We obtain analogous qualitative behaviour in our emission spectra concerning the rise of nonlinear quantum effects in the scattering process. Specifically by the discussion in section 5 we could show that the parameter χ also in the case of ultra-short laser pulses is suitable to characterize the onset of nonlinear quantum effects.
However, we could unveil two major differences between these earlier treatments and our analysis. First of all in section 2.4 we found the momentum conserving δ-functions contained in the transition matrix element to differ from those obtained for scattering off monochromatic laser waves or long pulses. We interpreted this as the absence of a dressed mass effect. Additionally we pointed out that this prediction could be tested by not only detecting the photons emitted in the scattering process but also the scattered electron. Then by measuring the outgoing momenta one could judge if the electron propagated with a dressed mass inside the pulse or not.
Second in both parts of section 4 as well as in section 5 we found no multiphoton peaks in our spectra. The several peaks in the emission spectra for larger ξ in the latter section were due to destructive interferences. The spectra's envelopes, however, were peaked only close to the first harmonic frequency as shown in Figs. 5.3 and 5.5. From this observation one can conclude that an electron scattering off an ultra-short laser pulse does not emit higher harmonic frequencies. Physically this phenomenon can be understood such that for ultra-short durations a laser pulse can no longer be viewed to be composed of many photons with the same energy. In the works [10–14], however, the absorption of many of such quasi-monoenergetic photons led to the many multiphoton peaks in the emission spectra.
These two features are the effects we find to be typically expectable when considering ultra-short pulses in an electron-laser scattering event.

7.2 The effect of changing the CEP

In comparing the results of section 6 to the previous parts of this work we could show that there arise clear differences in the emission spectra by changing the CEP. The most apparent difference between figs. 5.1 -5.9 and figs. 6.11 - 6.15 of course would be the changed shape of the energy spectra $\mathrm{d}\mathscr{E}/(\mathrm{d}\omega'\mathrm{d}\Omega)$ when plotted over the emitted photon frequencies ω'. As we could show in section 5 these shapes are mainly caused by interference effects and thus the differences are caused by the different dynamics the electron exhibits inside the laser pulse. Thinking of a classical pointlike electron this can be viewed as the electron moving on different trajectories each being uniquely connected to a particular pulseshape or equivalently CEP.
But the experimentally far more relevant difference between the emission spectra for the two different values of the CEP is the angular distribution of the emitted photons. So in section 6.4 we could show that for a CEP of $\pi/2$ due to the changed trajectory a relativistic electron emits into the regimes of the azimuthal angle $\varphi \sim 0$ and $\varphi \sim \pi$. In section 5 we saw that for a vanishing CEP a relativistic electron emits into the angular region close to $\varphi = 0$ exclusively. Furthermore in section 4.1.2 we could analytically show that for an ultra-strong incident laser pulse with vanishing carrier-envelope-phsae the emission will be suppressed at $\varphi < 0$.
This distinction in the angular distributions hints at a method of how the absolute phase of a ultra-short high intensity laser pulse might be detected easily. By measuring the angular distributions of the emitted photons and comparing it to the results presented in this work one could possibly infer the absolute phase of the incident laser pulse. In addition the suggested method to determine the CEP could be applicable to ultra-strong lasers what up to now is a challenging experimental task.

Appendix A

General procedure of obtaining transition probabilities in QED

Quantum electrodynamics describes the interaction of charged elementary particles with photons. The transition from an initial to a final state $|i\rangle \rightarrow |f\rangle$ is characterized by the matrix elements of the operator $\hat{S}$ which in the interaction picture is defined as

$$\hat{S} = \hat{\mathrm{T}}\, \mathrm{e}^{-\mathbb{i}\, e \int \hat{V} \mathrm{d}t} \tag{A.1}$$

where $\hat{T}$ is the operator of time ordering and $\hat{V}$ is the operator of the interaction [33, 36]. In QED the interaction is electromagnetic and its operator is

$$\hat{V} = e \int \hat{\bar{\psi}}\, \gamma_\mu\, \hat{\psi} \hat{A}^\mu \ \mathrm{d}^3 x. \tag{A.2}$$

The operators of the electromagnetic and the DIRAC field read

$$\hat{A}^\mu = \sum_{\boldsymbol{k},\epsilon^\mu} \hat{c}_{\boldsymbol{k},\epsilon^\mu} A^\mu_{\boldsymbol{k},\epsilon^\mu}(x) + \hat{c}^+_{\boldsymbol{k},\epsilon^\mu} A^{\mu *}_{\boldsymbol{k},\epsilon^\mu}(x) \tag{A.3}$$

$$\hat{\psi} = \sum_{\boldsymbol{p}\sigma} \hat{a}_{\boldsymbol{p}\sigma}\, \psi_{\boldsymbol{p}\sigma} + \hat{b}^+_{\boldsymbol{p}\sigma} \psi_{-\boldsymbol{p}-\sigma}, \tag{A.4}$$

respectively. For the electromagnetic field the indices $\boldsymbol{k}$ and ϵ^μ label the field mode's spatial wave vector and polarization, respectively. For the DIRAC field the indices $\boldsymbol{p}$ and σ label the particles' spatial momentum and spin, respectively. The amplitudes of electromagnetic field modes read

$$A^\mu_{\boldsymbol{k}\epsilon^\mu} = \sqrt{4\pi} \frac{\epsilon^\mu}{\sqrt{2\omega}} e^{-\mathbb{i}\ (\omega\, t - \boldsymbol{k}\boldsymbol{r})}, \tag{A.5}$$

while the $\psi_{\boldsymbol{p}\sigma}$ are the wave functions of the DIRAC particles. Inserting Eqs. (A.3-A.5) into Eq. (A.1) we find the first order approximation of the matrix element of an electromagnetic scattering process where an electron changes its spatial momentum from $\boldsymbol{p}$ to $\boldsymbol{p}'$ under emission of a photon of four wave vector $k^\mu = (\omega, \boldsymbol{k})$ and polarization ϵ^μ to look like

$$S_{\mathrm{fi}} = -\mathbb{i}\ e \int \bar{\psi}_{\boldsymbol{p}'\sigma'}\, \gamma_\mu\, \psi_{\boldsymbol{p}\sigma} \sqrt{4\pi} \frac{\epsilon^\mu}{\sqrt{2\omega}} e^{\mathbb{i}\ k_\mu x^\mu} \mathrm{d}^4 x. \tag{A.6}$$

Appendix B

Decomposing f_0 into a convergent and a singular part

In this paragraph we will show how to decompose the first parameter function f_0 into a convergent part and a part proportional to a δ-function. A similar procedure is described in [44]. For any arbitrary integrable function $G(x) \in L^\infty$ we may write

$$\begin{aligned} g_0 &= \int_{-\infty}^{\infty} \mathrm{d}x \; \mathrm{e}^{\mathbb{i}\, G(x)} \; \mathrm{e}^{\mathbb{i}\, K_3\, x} \\ &= \int_{-\infty}^{0} \lim_{\epsilon\to 0} \mathrm{d}x \; \mathrm{e}^{\mathbb{i}\, G(x)} \; \mathrm{e}^{\mathbb{i}\,(K_3 - \mathbb{i}\,\epsilon)\, x} + \int_{0}^{\infty} \lim_{\epsilon\to 0} \mathrm{d}x \; \mathrm{e}^{\mathbb{i}\, G(x)} \; \mathrm{e}^{\mathbb{i}\,(K_3 + \mathbb{i}\,\epsilon)\, x} \end{aligned} \tag{B.1}$$

Since we are going to need the specific function $G(x)$ from Eq. (2.26) as well as its derivative we state them here

$$\begin{aligned} G(x) &= 2\,\alpha \arctan\left(\tanh\left(x\right)\right) - \beta\, \tanh\left(2\,x\right) \\ G'(x) &= 2\,\mathrm{sech}(2x)(\alpha - \beta\,\mathrm{sech}(2x)) \end{aligned}$$

We now integrate Eq. (B.1) by parts

$$\begin{aligned} g_0 &= -\lim_{\epsilon\to 0} \frac{\dot{\mathbb{i}}}{K_3 - \mathbb{i}\,\epsilon} \mathrm{e}^{\mathbb{i}\, G(x)} \; \mathrm{e}^{\mathbb{i}\,(K_3 - \mathbb{i}\,\epsilon)x}\Big|_{-\infty}^{0} - \int_{-\infty}^{0} \mathrm{d}x \; \lim_{\epsilon\to 0} \frac{G'(x)}{K_3 - \mathbb{i}\,\epsilon} \; \mathrm{e}^{\mathbb{i}\, G(x)} \; \mathrm{e}^{\mathbb{i}\,(K_3 - \mathbb{i}\,\epsilon)x} \\ &\quad -\lim_{\epsilon\to 0} \frac{\dot{\mathbb{i}}}{K_3 + \mathbb{i}\,\epsilon} \mathrm{e}^{\mathbb{i}\, G(x)} \; \mathrm{e}^{\mathbb{i}\,(K_3 + \mathbb{i}\,\epsilon)x}\Big|_{0}^{\infty} - \int_{0}^{\infty} \mathrm{d}x \; \lim_{\epsilon\to 0} \frac{G'(x)}{K_3 + \mathbb{i}\,\epsilon} \; \mathrm{e}^{\mathbb{i}\, G(x)} \; \mathrm{e}^{\mathbb{i}\,(K_3 + \mathbb{i}\,\epsilon)x} \\ &= -\lim_{\epsilon\to 0} \frac{\dot{\mathbb{i}}}{K_3 - \mathbb{i}\,\epsilon} \left(\mathrm{e}^{\mathbb{i}\, G(0)} - \underbrace{\mathrm{e}^{\mathbb{i}\, G(-\infty)} \mathrm{e}^{-\mathbb{i}\,(K_3 - \mathbb{i}\,\epsilon)\infty}}_{=0} \right) \qquad \text{(B.2)} \\ &\quad -\lim_{\epsilon\to 0} \frac{\dot{\mathbb{i}}}{K_3 + \mathbb{i}\,\epsilon} \left(\underbrace{\mathrm{e}^{\mathbb{i}\, G(\infty)} \mathrm{e}^{\mathbb{i}\,(K_3 + \mathbb{i}\,\epsilon)\infty}}_{=0} - \mathrm{e}^{\mathbb{i}\, G(0)} \right) \\ &\quad - \int_{-\infty}^{0} \mathrm{d}x \; \lim_{\epsilon\to 0} \frac{1}{K_3 - \mathbb{i}\,\epsilon} G'(x) \; \mathrm{e}^{\mathbb{i}\, G(x)} \; \mathrm{e}^{\mathbb{i}\,(K_3 - \mathbb{i}\,\epsilon)} x \qquad \text{(B.3)} \\ &\quad - \int_{0}^{\infty} \mathrm{d}x \; \lim_{\epsilon\to 0} \frac{1}{K_3 + \mathbb{i}\,\epsilon} G'(x) \; \mathrm{e}^{\mathbb{i}\, G(x)} \; \mathrm{e}^{\mathbb{i}\,(K_3 + \mathbb{i}\,\epsilon)} x \qquad \text{(B.4)} \end{aligned}$$

Now we use the SOKHOTSKI - PLEMELJI relation [42, p. 37]

$$\lim_{\epsilon\to 0}\frac{1}{x\pm \mathbb{i}\,\epsilon}=\mathcal{P}\left(\frac{1}{x}\right)\mp \mathbb{i}\,\pi\,\delta(x)$$

Here $\mathcal{P}$ denotes the CAUCHY principal value and δ the DIRAC δ-distribution. We need to stress that this relation is valid in the language of distributions only.
Plugging this into Eq. (B.4) yields

$$\begin{aligned} g_0 &= -\mathbb{i}\left[\mathcal{P}\left(\frac{1}{K_3}\right)+\mathbb{i}\,\pi\,\delta\left(K_3\right)\right]\mathrm{e}^{\mathbb{i}\,G(0)}+\mathbb{i}\left[\mathcal{P}\left(\frac{1}{K_3}\right)-\mathbb{i}\,\pi\,\delta\left(K_3\right)\right]\mathrm{e}^{\mathbb{i}\,G(0)}\\ &\quad -\mathcal{P}\left(\frac{1}{K_3}\right)\int_{-\infty}^{\infty}\mathrm{d}x\;G'(x)\,\mathrm{e}^{\mathbb{i}\,G(x)}\;\mathrm{e}^{\mathbb{i}\,K_3\,x}\\ &\quad -\mathbb{i}\,\pi\,\delta\left(K_3\right)\int_{-\infty}^{0}\mathrm{d}x\;\underbrace{G'(x)\,\mathrm{e}^{\mathbb{i}\,G(x)}}_{=\frac{1}{\mathbb{i}}\frac{\mathrm{d}}{\mathrm{d}x}\mathrm{e}^{\mathbb{i}\,G(x)}}+\mathbb{i}\,\pi\,\delta\left(K_3\right)\int_{0}^{\infty}\mathrm{d}x\;\underbrace{G'(x)\,\mathrm{e}^{\mathbb{i}\,G(x)}}_{=\frac{1}{\mathbb{i}}\frac{\mathrm{d}}{\mathrm{d}x}\mathrm{e}^{\mathbb{i}\,G(x)}}\\ &= \pi\,\delta\left(K_3\right)\left[\mathrm{e}^{\mathbb{i}\,G(-\infty)}+\mathrm{e}^{\mathbb{i}\,G(\infty)}\right]-\mathcal{P}\left(\frac{1}{K_3}\right)\int_{-\infty}^{\infty}\mathrm{d}x\;G'(x)\,\mathrm{e}^{\mathbb{i}\,G(x)}\;\mathrm{e}^{\mathbb{i}\,K_3\,x}. \end{aligned}\tag{B.5}$$

Now we remind ourselves of the function $G(x)$ to find the asymptotic behaviour

$$\lim_{x\to\pm\infty}G(x) \;=\; \pm\left(\alpha\frac{\pi}{2}-\beta\right)$$

Using this and the form for $G'(x)$ stated earlier in Eq. (B.5) we find

$$\begin{aligned} g_0 &= \pi\,\delta\left(K_3\right)\left(\mathrm{e}^{\mathbb{i}\left(\frac{\pi}{2}\alpha-\beta\right)}+\mathrm{e}^{-\mathbb{i}\left(\frac{\pi}{2}\alpha-\beta\right)}\right)\\ &- \mathcal{P}\left(\frac{1}{K_3}\right)\int_{-\infty}^{\infty}\mathrm{d}x\;2\,\mathrm{sech}(2x)(\alpha-\beta\,\mathrm{sech}(2x))\\ &\quad\times\mathrm{e}^{\mathbb{i}\,(2\,\alpha\arctan(\tanh(x))-\beta\,\tanh(2\,x))}\;\mathrm{e}^{\mathbb{i}\,K_3\,x}. \end{aligned}\tag{B.6}$$

Since

$$f_0=\mathrm{e}^{\mathbb{i}\left(\frac{\pi}{2}\alpha-\beta\right)}g_0$$

we may finally conclude that

$$\begin{aligned} f_0 &= \pi\,\delta\left(K_3\right)\left(1+\mathrm{e}^{\mathbb{i}\,(\pi\,\alpha-2\beta)}\right)\\ &- \mathrm{e}^{\mathbb{i}\left(\frac{\pi}{2}\alpha-\beta\right)}\,\mathcal{P}\left(\frac{1}{K_3}\right)\int_{-\infty}^{\infty}\mathrm{d}x\;\mathrm{e}^{\mathbb{i}\,(2\,\alpha\arctan(\tanh(x))-\beta\,\tanh(2\,x))}\;\mathrm{e}^{\mathbb{i}\,K_3\,x}\\ &\quad\times 2\,\mathrm{sech}(2x)(\alpha-\beta\,\mathrm{sech}(2x)). \end{aligned}\tag{B.7}$$

Appendix C

Computation of the spin summed and averaged modulus square $|S_{\mathrm{fi}}|^2$

We want to compute the modulus square of the expression (2.25) and to sum and average the result over final and initial spin states, respectively. In this calculation we keep the parameter functions f_i as mere parameters. To this purpose we define

$$\mathcal{Z} = \not{\epsilon}'^{*}\ f_0 + A_1\ f_1 - A_2\ f_2 \tag{C.1}$$

As is well known for any scattering amplitude of the form

$$S_{\mathrm{fi},\sigma\sigma'} = \mathcal{K}\ \bar{u}_{p'\sigma'}\,\mathcal{Z}\,u_{p\sigma}$$

with an arbitrary prefactor $\mathcal{K}$ containing no diracmatrices the modulus square is summed and averaged over final and initial electron spin states, respectively, as follows [36, p. 236]

$$\frac{1}{2}\sum_{\sigma,\sigma'=1}^{2}|S_{fi,\sigma\sigma'}|^2 = |\mathcal{K}|^2\mathrm{tr}\left(\rho'\,\mathcal{Z}\,\rho\,\bar{\mathcal{Z}}\right) \tag{C.2}$$

Where ρ' and ρ represent the density matrices of the electron in its final and the initial states

$$\rho = \frac{1}{2}\left(\not{p}+m\right) \tag{C.3}$$

$$\rho' = \not{p}'+m. \tag{C.4}$$

The difference of a factor 1/2 is due to that in the former expression we take the *average* over the spin directions while in the latter we *sum* over them.
In our case there is

$$\bar{\mathcal{Z}} = \gamma^0\mathcal{Z}^\dagger\gamma^0 = \not{\epsilon}'\ f_0^* + e\left(\frac{\not{\epsilon}'\not{k}\not{a}}{2(kp')}+\frac{\not{a}\not{k}\not{\epsilon}'}{2(kp)}\right)\ f_1^* - \frac{e^2\,a^2\ (k\epsilon')\,\not{k}}{2(kp)(kp')}f_2^*.$$

We thus find

$$\frac{1}{2}\sum_{\sigma,\sigma'=1}^{2}|S_{fi,\sigma\sigma'}|^2 = \frac{e^2\,2\pi\,T^4\,n^2}{\omega'\,p_0'\,p_0V^3}(2\pi)^4\left(\delta_\perp^{(2)}\left(p'+k'-p\right)\left(\frac{2\pi}{T}\delta\left(p_0'+\omega'-p_0-(p_3'+k_3'-p_3)\right)\right)\right)^2$$
$$\times\frac{1}{2}\mathrm{tr}\left[\left(\not{p}'+m\right)\left[\not{\epsilon}'^{*}\,f_0+A_1\,f_1-A_2\,f_2\right]\left(\not{p}+m\right)\left[\not{\epsilon}'\,f_0^*+\bar{A}_1\,f_1^*-\bar{A}_2\,f_2^*\right]\right]. \tag{C.5}$$

Here $\delta_\perp^{(2)}$ denotes the two-dimensional δ-function over the spatial vector components perpendicular to the laser's direction of propagation. From now on we drop the sum sign in front of $|S_{\mathrm{fi},\sigma\sigma'}|^2$ and refer to the spin summed and averaged result as *the transition number* $|S_{\mathrm{fi}}|^2$. We expand the second line of Eq. (C.5) to get

$$
\begin{aligned}
|S_{fi}|^2 = \quad & \frac{e^2\,\pi\,T^4\,n^2}{\omega'\,p_0'\,p_0 V^3}(2\pi)^4\left(\delta_\perp^{(2)}\left(p'+k'-p\right)\left(\frac{2\pi}{T}\delta\left(p_0'+\omega'-p_0-(p_3'+k_3'-p_3)\right)\right)\right)^2 \\
\times \quad & \mathrm{tr}\Bigg[\not p'\not\epsilon'^*\not p\not\epsilon'|f_0|^2+\not p'\not\epsilon'^* \not p e\left(\frac{\not\epsilon'\not k\not a}{2(kp')}+\frac{\not a\not k\not\epsilon'}{2(kp)}\right)f_0 f_1^* \\
& -\not p'\not\epsilon'^*\not p\frac{e^2\,a^2\;(k\epsilon')\not k}{2(kp)(kp')}f_0 f_2^*+\not p' e\left(\frac{\not a\not k\not\epsilon'^*}{2(kp')}+\frac{\not\epsilon'^*\not k\not a}{2(kp)}\right)\not p\not\epsilon' f_1 f_0^* \\
& +\not p' e^2\left(\frac{\not a\not k\not\epsilon'^*}{2(kp')}+\frac{\not\epsilon'^*\not k\not a}{2(kp)}\right)\not p\left(\frac{\not\epsilon'\not k\not a}{2(kp')}+\frac{\not a\not k\not\epsilon'}{2(kp)}\right)|f_1|^2 \\
& -\not p' e\left(\frac{\not a\not k\not\epsilon'^*}{2(kp')}+\frac{\not\epsilon'^*\not k\not a}{2(kp)}\right)\not p\frac{e^2\,a^2\;(k\epsilon')\not k}{2(kp)(kp')}f_1 f_2^* \\
& -\not p'\frac{e^2\,a^2\;(k\epsilon'^*)\not k}{2(kp)(kp')}\not p\not\epsilon' f_2 f_0^*-\not p'\frac{e^2\,a^2\;(k\epsilon'^*)\not k}{2(kp)(kp')}\not p e\left(\frac{\not\epsilon'\not k\not a}{2(kp')}+\frac{\not a\not k\not\epsilon'}{2(kp)}\right)f_2 f_1^* \\
& +\not p'\frac{e^4\,a^4\;(k\epsilon'^*)\,(k\epsilon')\not k\not k}{4(kp)^2(kp')^2}|f_2|^2 \\
+m^2 \quad & \Bigg(\not\epsilon'^*\not\epsilon'|f_0|^2+\not\epsilon'^* e\left(\frac{\not\epsilon'\not k\not a}{2(kp')}+\frac{\not a\not k\not\epsilon'}{2(kp)}\right)f_0 f_1^* \\
& -\not\epsilon'^*\frac{e^2\,a^2\;(k\epsilon'^*)\not k}{2(kp)(kp')}f_0 f_2^*+e\left(\frac{\not a\not k\not\epsilon'^*}{2(kp')}+\frac{\not\epsilon'^*\not k\not a}{2(kp)}\right)\not\epsilon' f_1 f_0^* \\
& +e^2\left(\frac{\not a\not k\not\epsilon'^*}{2(kp')}+\frac{\not\epsilon'^*\not k\not a}{2(kp)}\right)\left(\frac{\not\epsilon'\not k\not a}{2(kp')}+\frac{\not a\not k\not\epsilon'}{2(kp)}\right)|f_1|^2 \\
& -e\left(\frac{\not a\not k\not\epsilon'^*}{2(kp')}+\frac{\not\epsilon'^*\not k\not a}{2(kp)}\right)\frac{e^2\,a^2\;(k\epsilon')\not k}{2(kp)(kp')}f_1 f_2^* \\
& -\frac{e^2\,a^2\;(k\epsilon'^*)\not k}{2(kp)(kp')}\not\epsilon' f_2 f_0^*-\frac{e^2\,a^2\;(k\epsilon'^*)\not k}{2(kp)(kp')}e\left(\frac{\not\epsilon'\not k\not a}{2(kp')}+\frac{\not a\not k\not\epsilon'}{2(kp)}\right)f_2 f_1^* \\
& +\frac{e^4\,a^4\;(k\epsilon'^*)\,(k\epsilon')}{4(kp)^2(kp')^2}\not k\not k|f_2|^2\Bigg)\Bigg]
\end{aligned}
\tag{C.6}
$$

Here all terms containing an odd number of gamma matrices were omitted since they vanish in the trace. By pulling out the factors $\epsilon_\mu'^*$ and ϵ_μ' we may replace

$$k\epsilon' \to k^\mu \qquad , \qquad \not\epsilon' \to \gamma^\mu$$

and we obtain an overall factor $\epsilon_\mu'^*\epsilon_\nu'$ where the indices denote the final state polarization. By summing over the polarizations we may replace

$$\sum_{\mu,\nu}\epsilon_\mu'^*\epsilon_\nu' \to -g_{\mu\nu}$$

Thus Eq. (C.6) yields

$$
\begin{aligned}
|S_{fi}|^2 &= \frac{e^2\,\pi\,T^4\,n^2}{\omega'\,p_0'\,p_0 V^3}(2\pi)^4\left(\delta_\perp^{(2)}\left(p'+k'-p\right)\left(\frac{2\pi}{T}\delta\left(p_0'+\omega'-p_0-(p_3'+k_3'-p_3)\right)\right)\right)^2 \\
&\times\ (-1)\ \mathrm{tr}\left[\not p'\gamma_\mu\not p\gamma^\mu|f_0|^2+\not p'\gamma_\mu\not p e\left(\frac{\gamma^\mu\not k\not a}{2(kp')}+\frac{\not a\not k\gamma^\mu}{2(kp)}\right)f_0 f_1^*\right. \\
&\quad -\not p'\gamma_\mu\not p\frac{e^2\,a^2\ (k^\mu)\not k}{2(kp)(kp')}f_0 f_2^*+\ p' e\left(\frac{\not a\not k\gamma_\mu}{2(kp')}+\frac{\gamma_\mu\not k\not a}{2(kp)}\right)\not p\gamma^\mu f_1 f_0^* \\
&\quad +\not p' e^2\left(\frac{\not a\not k\gamma_\mu}{2(kp')}+\frac{\gamma_\mu\not k\not a}{2(kp)}\right)\not p\left(\frac{\gamma^\mu\not k\not a}{2(kp')}+\frac{\not a\not k\gamma^\mu}{2(kp)}\right)|f_1|^2 \\
&\quad -\not p' e\left(\frac{\not a\not k\gamma_\mu}{2(kp')}+\frac{\gamma_\mu\not k\not a}{2(kp)}\right)\not p\frac{e^2\,a^2\ (k^\mu)\not k}{2(kp)(kp')}f_1 f_2^* \\
&\quad -\not p'\frac{e^2\,a^2\ (k_\mu)\not k}{2(kp)(kp')}\not p\gamma^\mu f_2 f_0^*-\not p'\frac{e^2\,a^2\ (k_\mu)\not k}{2(kp)(kp')}\not p e\left(\frac{\gamma^\mu\not k\not a}{2(kp')}+\frac{\not a\not k\gamma^\mu}{2(kp)}\right)f_2 f_1^* \\
&\quad +m^2\left(\gamma_\mu\gamma^\mu|f_0|^2+\gamma_\mu e\left(\frac{\gamma^\mu\not k\not a}{2(kp')}+\frac{\not a\not k\gamma^\mu}{2(kp)}\right)f_0 f_1^*\right. \\
&\quad -\gamma_\mu\frac{e^2\,a^2\ (k^\mu)\not k}{2(kp)(kp')}f_0 f_2^*+e\left(\frac{\not a\not k\gamma_\mu}{2(kp')}+\frac{\gamma_\mu\not k\not a}{2(kp)}\right)\gamma^\mu f_1 f_0^* \\
&\quad +e^2\left(\frac{\not a\not k\gamma_\mu}{2(kp')}+\frac{\gamma_\mu\not k\not a}{2(kp)}\right)\left(\frac{\gamma^\mu\not k\not a}{2(kp')}+\frac{\not a\not k\gamma^\mu}{2(kp)}\right)|f_1|^2 \\
&\quad -e\left(\frac{\not a\not k\gamma_\mu}{2(kp')}+\frac{\gamma_\mu\not k\not a}{2(kp)}\right)\frac{e^2\,a^2\ (k^\mu)\not k}{2(kp)(kp')}f_1 f_2^* \\
&\quad \left.\left.-\frac{e^2\,a^2\ (k_\mu)\not k}{2(kp)(kp')}\gamma^\mu f_2 f_0^*-\frac{e^2\,a^2\ (k_\mu)\not k}{2(kp)(kp')}e\left(\frac{\gamma^\mu\not k\not a}{2(kp')}+\frac{\not a\not k\gamma^\mu}{2(kp)}\right)f_2 f_1^*\right]\right. \qquad \text{(C.7)}
\end{aligned}
$$

The square of the δ-functions can be evaluated by the standard method as described in e.g. [36]. Using additionally the properties of the γ-matrices and their traces [36, p. 77] we can simplify Eq. (C.7) to give

$$
\begin{aligned}
|S_{fi}|^2 &= \frac{e^2\,\pi\,T^2\,n^2}{\omega'\,\epsilon'\,p_0 V^2}\,(2\pi)^3\,\delta_{D,\perp}^{(2)}\left(p'+k'\right)\delta_D\left(\epsilon'+\omega'-\epsilon-(p_3'+k_3'+P)\right) \\
&\times\ 8\left[\left(\epsilon\,\epsilon'+P\,p_3'-2m^2\right)|f_0|^2-\mathcal{A}\,p_1'\left(\frac{\epsilon+P}{\epsilon'-p_3'}-1\right)\Re\left(f_0 f_1^*\right)-e^2\,\mathcal{A}^2\Re\left(f_0 f_2^*\right)\right. \\
&\quad \left.+\frac{e^2\,\mathcal{A}^2}{2}\left[\frac{\epsilon'-p_3'}{\epsilon+P}+\frac{\epsilon+P}{\epsilon'-p_3'}\right]|f_1|^2\right]. \qquad \text{(C.8)}
\end{aligned}
$$

To obtain the transition probability we have to integrate Eq. (C.8) over all the phase space of the final particles. Doing so the factor V^{-2} with the normalization volume V drops out.

Appendix D

Computation of the integrals $\mathcal{I}_i$

The integrals $\mathcal{I}_i$ are defined as

$$\mathcal{I}_i = \int_{-\infty}^{\infty} (x - x_0)^i \mathrm{e}^{g(x)}\,\mathrm{d}x \approx \int_{-\infty}^{\infty} (x - x_0)^i \mathrm{e}^{g_\mathrm{T}(x)}\,\mathrm{d}x. \tag{D.1}$$

It will turn out that the computation of $\mathcal{I}_1$ and $\mathcal{I}_2$ is rather simple once $\mathcal{I}_0$ is known. Hence we start by computing this integral.
First of all we exploit the symmetry of the integral $\mathcal{I}_0$ to further simplify it

$$\mathcal{I}_0 = \int_{-\infty}^{\infty} \mathrm{e}^{g(x)}\mathrm{d}\,x \;=\; \int_{-\infty}^{0} \mathrm{e}^{g(x)}\mathrm{d}x + \int_{0}^{\infty} \mathrm{e}^{g(x)}\mathrm{d}x = 2\,\Re\left(\int_{0}^{\infty} \mathrm{e}^{g(x)}\mathrm{d}x\right)$$

Now we apply the method of stationary phase by replacing the exponential function $g(x)$ by $g_\mathrm{T}(x)$ (see section 4.1.2).
To evaluate $g_\mathrm{T}(x)$ we have to calculate the first three derivatives of Eq. (4.8)

$$\begin{aligned}
g'(x) &= 2\,\mathbb{i}\left[\frac{\alpha}{\cosh(2x)} - \frac{\beta}{\cosh^2(2x)} + \frac{K_3}{2}\right] \\
g''(x) &= 4\,\mathbb{i}\,\frac{\tanh(2x)}{\cosh(2x)}\left(\frac{2\,\beta}{\cosh(2x)} - \alpha\right) \\
g'''(x) &= 8\mathbb{i}\,\frac{1-\sinh^2(2x)}{\cosh^3(2x)}\left(\frac{2\beta}{\cosh(2x)} - \alpha\right) - 16\,\mathbb{i}\,\beta\frac{\tanh^2(2x)}{\cosh^2(2x)}
\end{aligned} \tag{D.2}$$

and to find the stationary point x_0 of the function $g(x)$ as usually by

$$g'(x)|_{x=x_0} \stackrel{!}{=} 0.$$

This equation is solved by

$$y_{0_{1,2}} = \frac{\alpha}{2\,\beta} \pm \sqrt{\left(\frac{\alpha}{2\,\beta}\right)^2 + \frac{K_3}{2\,\beta}}. \tag{D.3}$$

with $y_0 = \mathrm{sech}(2x_0)$. For the determinant of this quadratic equation

$$\Delta := \left(\frac{\alpha}{2\,\beta}\right)^2 + \frac{K_3}{2\,\beta} \tag{D.4}$$

it can be shown that in the strong and constant field limits it holds

$$\Delta = -\frac{1}{(m\,\xi)^2}\left[m^2 + k_2'^2\left(\frac{E+P}{\omega' - k_3'}\right)^2\right] \sim \frac{1}{\xi^2}$$

and that Δ is always smaller than zero. Thus Eq. (D.3) has no real but two complex solutions which can be expressed as

$$\begin{aligned} y_{1,2} &= = \frac{\alpha}{2\,\beta} \pm \mathbb{i}\,\frac{\sigma_0}{\xi} \\ \text{with } \sigma_0 &:= \sqrt{1 + \frac{k_2'^2}{m^2}\left(\frac{E+P}{\omega' - k_3'}\right)^2}. \end{aligned} \tag{D.5}$$

Later on it will turn out that we have to choose the minus sign to obtain convergent integrals for the parameter functions. In the limit $\xi \to \infty$ it holds $\alpha/(2\beta) \sim \sigma_0 \sim$ const. and thus the real part remains constant with respect to ξ while the imaginary part of y_0 vanishes and the hyperbolic secans of twice the stationary point tends to the unique solution

$$\operatorname{sech}(2x_0) \xrightarrow{\xi\to\infty} \frac{\alpha}{2\,\beta} \tag{D.6}$$

Any such defined x_0 is real only for

$$0 < \frac{\alpha}{2\,\beta} \leq 1. \tag{D.7}$$

However, the parameter function will be exponentially damped in case that x_0 is complex in the limit $\xi \to \infty$. This is obvious since every parameter function involves a term $\propto \exp[\mathbb{i}\,K_3\,x_0]$ with $K_3 \sim \xi^3$. If now x_0 contains an imaginary part independent of ξ this factor will result in an exponential damping. Consequently we consider only such processes where condition (D.7) is fulfilled. So because our formulas become valid only in the limit of large ξ we confine the integration in Eq. (D.1) to the real axis. This is an important observation since it allows us to bypass the rather involved formalism of the method of steepest descend in favour of the simpler stationary phase method. The integral $\mathcal{I}_0$ accordingly becomes

$$\begin{aligned} \mathcal{I}_0 &\sim 2\Re\left(\int_0^\infty \mathrm{d}x\ \exp\left[\Re\,(g_0) + \mathbb{i}\,\Im\,(g_0) + g_0''\frac{(x-x_0)^2}{2} + g_0'''\frac{(x-x_0)^3}{6}\right]\right) \\ &= 2\Re\left(\int_{-x_0-b}^\infty \mathrm{d}y \exp\left[g_0 + \frac{1}{3}\frac{g_0''^3}{g_0'''^2} - \frac{1}{2}\frac{g_0''^2}{g_0'''}y + \frac{g_0'''}{6}y^3\right]\right) \\ &= 2\Re\left(\exp\left[g_0 + \frac{1}{3}\frac{g_0''^3}{g_0'''^2}\right]\int_{-x_0-b}^\infty \mathrm{d}y\ \exp\left[\frac{g_0'''}{6}y^3 - \frac{1}{2}\frac{g_0''^2}{g_0'''}y\right]\right) \end{aligned} \tag{D.8}$$

where we made the definitions

$$b = -\frac{g_0''}{g_0'''} \qquad ; \qquad y = x - x_0 - b.$$

In the spirit of the stationary phase method we extend the lower integration limit in Eq. (D.8) to $-\infty$. This will cause no large error in the final result for the integral is predominantly

determined by its values close to its point of stationary phase and points far away from x_0 will yield only negligible contributions. We write

$$\mathcal{I}_0 \sim 2\Re\left[\exp\left(g_0+\frac{1}{3}\frac{g_0''^3}{g_0'''^2}\right)\int_{-\infty}^{\infty}\mathrm{d}y\ \exp\left(\frac{g_0'''}{6}y^3-\frac{1}{2}\frac{g_0''^2}{g_0'''}y\right)\right]. \tag{D.9}$$

The explicit representations for g_0'' and g_0''' are

$$g_0'' = 8\frac{\tanh(2x_0)}{\cosh(2x_0)}\sigma_0\frac{\beta}{\xi} =: h \sim \xi^2 \tag{D.10}$$

$$g_0''' = -16\mathbb{i}\left(\frac{\tanh(2x_0)}{\cosh(2x_0)}\right)^2\beta =: -\mathbb{i}\ g \sim \xi^3. \tag{D.11}$$

This postfactum justifies why in Eq. (4.14) we had to take into account the second and the third derivative alike. From Eq. (2.33) we see $h, g < 0$. what justifies the choice of the sign of κ for otherwise Eq. (D.10) would have led to $g_0'' > 0$ which in turn would have given an asymptotically diverging integral. From Eqs. (D.10) and (D.11) we obtain that in the limit $\xi \to \infty$ it holds $-h^3/3\,g^2 = -\Re\left(g(x_0)\right)$. So for the exponential independent of the integration variable in Eq. (D.9) we find

$$\mathrm{e}^{g_0+\frac{1}{3}\frac{g_0''^3}{g_0'''^2}} \xrightarrow{\xi\to\infty} \mathrm{e}^{\mathbb{i}\,\Im(g_0)}$$

Eq. (D.8) in the asymptotic limit then gives

$$\mathcal{I}_0 \sim 4\,\cos\left(\Im(g_0)\right)\left(-\frac{2\,\pi^3}{g}\right)^{\frac{1}{3}}\mathrm{Ai}\left(\eta\right) \tag{D.12}$$

with the first AIRY function $\mathrm{Ai}(x)$ [45] and its argument defined as

$$\eta = \left(-\frac{h^3}{2\,g^2}\right)^{\frac{2}{3}}. \tag{D.13}$$

Having obtained this expression for the first integral $\mathcal{I}_0$ we now turn to the computation of the other two integrals $\mathcal{I}_1$ and $\mathcal{I}_2$. In doing so it is favourable to start with the latter for it can be obtained as a derivative from $\mathcal{I}_0$. From the first line of Eq. (D.8) we find that it holds

$$\mathcal{I}_2 = 2\,\frac{\partial}{\partial\,g''(x_0)}\mathcal{I}_0 \sim 8\cos\left(\Im(g_0)\right)\left(-\frac{2}{g}\right)^{\frac{1}{3}}\frac{\pi}{h}\left(\eta^{\frac{3}{2}}\,\mathrm{Ai}\left(\eta\right)+\eta\,\mathrm{Ai}'\left(\eta\right)\right). \tag{D.14}$$

From Eq. (4.8) in combination with Eqs. (D.10) and (D.11) we find that the real part of the TAYLOR expansion $g_{\mathrm{T}}(x)$ at $x=\pm\infty$ function is $\Re\left(g_{\mathrm{T}}(x)\right)|_{x=\pm\infty} = -\infty$ whence we conclude

$$\int_{g_{\mathrm{T}}(-\infty)}^{g_{\mathrm{T}}(\infty)}\mathrm{d}g_{\mathrm{T}}(x)\mathrm{e}^{g_{\mathrm{T}}(x)} = g_0''\underbrace{\int_{-\infty}^{\infty}(x-x_0)\mathrm{e}^{g_{\mathrm{T}}(x)}}_{=\mathcal{I}_1}+\frac{1}{2}g_0'''\underbrace{\int_{-\infty}^{\infty}(x-x_0)^2\mathrm{e}^{g_{\mathrm{T}}(x)}}_{=\mathcal{I}_2} = 0. \tag{D.15}$$

Then we obtain

$$\mathcal{I}_1 = -\frac{g_0'''}{2\,g_0''}\mathcal{I}_2. \tag{D.16}$$

Appendix E

Computation of the integrals $\mathcal{H}_i^j$ for a changed CEP

The integrals $\mathcal{H}_i^j$ are defined as

$$\mathcal{H}_i^j = \int_{-\infty}^{\infty} (x - x_{0,j})^i \mathrm{e}^{g_{\mathrm{T},j}(x)} \,\mathrm{d}x. \tag{E.1}$$

Here the functions $g_{\mathrm{T},j}(x)$ are defined as in section 4.1.2, however, derived from the changed exponential function

$$g(x) = -\mathbb{i}\ \left(\alpha \,\mathrm{sech}(2x) + \rho\, \tanh^3(2\,x) - K_3 x\right). \tag{E.2}$$

Paying attention to the changed exponential function the integrals $\mathcal{H}_i^j$ can be computed analogously to the $\mathcal{I}_i$. The derivatives of Eq. (E.2) are

$$\begin{aligned}
g'(x) &= 2\mathbb{i}\ \mathrm{sech}(2x)\tanh(2x)\left(\alpha - 3\rho \mathrm{sech}(2x)\tanh(2x)\right) + \mathbb{i}\ K_3 \\
g''(x) &= 2\mathbb{i}\ \left(2\,\mathrm{sech}^2(2x) - 1\right)\mathrm{sech}(2x)\left[2\alpha - 12\rho\ \tanh(2x)\mathrm{sech}(2x)\right] \\
g'''(x) &= \mathbb{i}\ \left(8\mathrm{sech}^3(2x)\tanh(2x) + 2\mathrm{sech}(2x)\left(2\mathrm{sech}^2(2x) - 1\right)\tanh(2x)\right)\left[12\rho\ \tanh(2x)\mathrm{sech}(2x)\right] \\
&\quad -48\rho\left(2\mathrm{sech}^2(2x) - 1\right)^2 \mathrm{sech}^2(2x).
\end{aligned} \tag{E.3}$$

All the stationary points $x_{0,j}$ will be distinguished by the condition

$$\mathrm{sech}(2x_{0,j})\tanh(2x_{0,j}) = \frac{\alpha}{6\,\rho} \pm \mathbb{i}\,\frac{1}{\xi}\sqrt{1 + \frac{k_2'^2}{m^2}\left(\frac{E+P}{\omega' - k_3'}\right)^2} \tag{E.4}$$

This equation is solved by four values of x_0 only two of which give asymptotically convergent integrals. These points x_{0_1} and x_{0_2} are the two respective stationary points. Unlike in Eq. (4.11) the reality condition for the stationary points will be given by

$$-0.5 \leq \frac{\alpha}{2\beta} \leq 0.5. \tag{E.5}$$

Apart from this the calculations are analogous to appendix D and we find the $\mathcal{H}_i^j$ to be given by

$$\mathcal{H}_0^j \sim \mathrm{e}^{-\mathbb{i}\,\rho}\,\mathrm{e}^{\mathbb{i}\,\Im(g_{0,j})}\left(-\frac{2\,\pi^3}{g_j}\right)^{\frac{1}{3}}\mathrm{Ai}\left(\eta_j\right) \tag{E.6}$$

$$\mathcal{H}_2^j \sim 8\cos\left(\Im(g_{0,j})\right)\left(-\frac{2}{g_j}\right)^{\frac{1}{3}}\frac{\pi}{h_j}\left(\eta^{\frac{3}{2}}\,\mathrm{Ai}\left(\eta_j\right)+\eta\,\mathrm{Ai}'\left(\eta_j\right)\right) \tag{E.7}$$

$$\mathcal{H}_1^j = -\frac{g_{0,j}'''}{2\,g_{0,j}''}\mathcal{H}_2^j. \tag{E.8}$$

with the definitions according to those in appendix D

$$\eta_j = \left|\frac{h_j^3}{2\,g_j^2}\right|^{\frac{2}{3}} \quad ; \quad h = g''(x_{0,j})\,|_{\xi\to\infty} \quad ; \quad g_j = \mathbb{i}\,g'''(x_{0,j})\,|_{\xi\to\infty}\,.$$

Bibliography

[1] Jackson, J. D. *Classical Electrodynamics.* John Wiley & Sons, New York, 2nd edition, (1975).

[2] Thomson, J. *Conduction of electricity through gases.* Cambridge Univ. Press, (1906).

[3] Sarachik, E. S. and Schappert, G. T. *Phys. Rev. D* **1**(10), 2738–2753 (1970).

[4] Vachaspati. *Phys. Rev.* **128**(2), 664–666 (1962).

[5] Eberly, J. and Sleeper, A. *Phys. Rev.* **176**(5), 1570–1573 (1968).

[6] Salamin, Y. I. and Faisal, F. H. M. *Phys. Rev. A* **54**(5), 4383–4395 (1996).

[7] Salamin, Y. and Faisal, F. *Phys. Rev. A* **55**(5), 3678–3683 (1997).

[8] Narozhnyi, N. and Fofanov, M. *J. Exp. Theo. Phys.* **90**(5), 753–768 (2000).

[9] Zel'dovich, Y. *Sov. Phys. - Uspekhi* **18**(2), 79–98 (1975).

[10] Nikishov, A. and Ritus, V. *Sov. Phys. JETP-USSR* **19**(2), 529–541 (1964).

[11] Baier, V., Mil'shtein, A., and Strakhovenko, V. *Sov. Phys. JETP* **42**(6), 961–965 (1976).

[12] Brown, L. S. and Kibble, T. W. B. *Phys. Rev.* **133**(3A), A705–A719 (1964).

[13] Ritus, V. *Journal of Russian Laser Research* **6**(5), 497–617 (1985).

[14] Narozhnyi, N. and Fofanov, M. *Zh. Eksp. Teo. Fiz.* **110**(1), 26–46 (1996).

[15] Tajima, T. and Mourou, G. *Phys. Rev. ST Accel. Beams* **5**(3), 031301 (2002).

[16] Englert, T. J. and Rinehart, E. A. *Phys. Rev. A* **28**(3), 1539–1545 (1983).

[17] Moore, C., Knauer, J., and Meyerhofer, D. *Phys. Rev. Lett.* **74**(13), 2439–2442 (1995).

[18] Meyerhofer, D. *IEEE Journal of Quantum Electronics* **33**(11), 1935–1941 (1997).

[19] Chen, S., Maksimchuk, A., and Umstadter, D. *Nature* **396**(6712), 653–655 (1998).

[20] Babzien, M., Ben-Zvi, I., Kusche, K., Pavlishin, I., Pogorelsky, I., Siddons, D., Yakimenko, V., Cline, D., Zhou, F., Hirose, T., Kamiya, Y., Kumita, T., Omori, T., Urakawa, J., and Yokoya, K. *Phys. Rev. Lett.* **96**(5) (2006).

[21] Kumita, T., Kamiya, Y., Babzien, M., Ben-Zvi, I., Kusche, K., Pavlishin, I. V., Pogorelsky, I. V., Siddons, D. P., Yakimenko, V., Hirose, T., Omori, T., Urakawa, J., Yokoya, K., Cline, D., and Zhou, F. *Laser Physics* **16**(2), 267–271 (2006).

[22] Einstein, A. *Physikalische Gesellschaft Zürich, Mitteilungen 18* (1916).

[23] Compton, A. H. *Phys. Rev.* **21**(5), 483–502 (1923).

[24] Sauter, F. *Zeitschrift für Physik* **69**(11-12), 742–764 (1931).

[25] Heisenberg, W. and Euler, H. *Zeitschrift für Physik* **98**, 714 (1936).

[26] Medenwaldt, R., Møller, S., Jensen, B., Strakhovenko, V., Uggerhøj, E., Worm, T., Elsener, K., Sona, P., Connell, S., Sellschopp, J., Avakian, R., Avetisian, A., and Taroian, S. *Phys. Lett. B* **281**(1-2), 153–158 (1992).

[27] Uggerhøj, U. *Rev. Mod. Phys.* **77**(4), 1131–1171 (2005).

[28] Bula, C., McDonald, K. T., Prebys, E. J., Bamber, C., Boege, S., Kotseroglou, T., Melissinos, A. C., Meyerhofer, D. D., Ragg, W., Burke, D. L., Field, R. C., Horton-Smith, G., Odian, A. C., Spencer, J. E., Walz, D., Berridge, S. C., Bugg, W. M., Shmakov, K., and Weidemann, A. W. *Phys. Rev. Lett.* **76**(17), 3116–3119 (1996).

[29] Yanovsky, V., Chvykov, V., Kalinchenko, G., Rousseau, P., Planchon, T., Matsuoka, T., Maksimchuk, A., Nees, J., Cheriaux, G., Mourou, G., and Krushelnick, K. *Opt. Express* **16**(3), 2109–2114 (2008).

[30] http://www.extreme-light-infrastructure.eu/.

[31] Bonvalet, A., Joffre, M., Martin, J. L., and Migus, A. *Appl. Phys. Lett.* **67**(20), 2907–2909 (1995).

[32] Sansone, G., Benedetti, E., Calegari, F., Vozzi, C., Avaldi, L., Flammini, R., Poletto, L., Villoresi, P., Altucci, C., Velotta, R., Stagira, S., De Silvestri, S., and Nisoli, M. *Science* **314**(5798), 443–446 (2006).

[33] Peskin, M. E. and Schroeder, D. V. *An introduction to Quantum Field Theory.* Westview Press, Boulder, (1995).

[34] Furry, W. H. *Phys. Rev.* **81**(1), 115–124 (1951).

[35] Volkov, D. *Zeitschrift für Physik* **94**(3-4), 250–260 (1935).

[36] Landau, L. and Lifschitz, E. *Lehrbuch der Theoretischen Physik - Band 4: Quantenelektrodynamik.* Akademie Verlag, Berlin, 7$^{\text{th}}$ edition, (1991).

[37] http://slac.stanford.edu/.

[38] Hartemann, F., Siders, C. W., and Barty, C. P. J. *Phys. Rev. Lett.* **100** (2008).

[39] http://www.desy.de.

[40] http://www.bessy.de.

[41] Landau, L. and Lifschitz, E. *Lehrbuch der Theoretischen Physik - Band 2: Klassische Feldtheorie*. Akademie Verlag, Berlin, 12$^{\text{th}}$ edition, (1997).

[42] Blanchard, P. and Bruening, E. *Mathematical Methods in Physics*. Birkhäuser, Boston, 1$^{\text{st}}$ edition, (2003).

[43] Greene, B. I., Federici, J. F., Dykaar, D. R., Jones, R. R., and Bucksbaum, P. H. *Applied Physics Letters* **59**(8), 893–895 (1991).

[44] Fried, Z., Baker, A., and Korff, D. *Phys. Rev.* **151**(4), 1040–1048 (1966).

[45] Abramowitz, M. and Stegun, I. A. *Handbook of Mathematical Functions with Formulas, Graphs, and Mathematical Tables*. Dover, New York, (1964).

Acknowledgements

I wish to express my thanks to all persons who made this work possible:

First of all I thank Prof. Christoph H. Keitel for accepting me in his group at the MPI for Nuclear Physics and supervising this work. Also I thank him for providing ideal surroundings for scientific work and sending me to the DPG Frühjahrstagung in Hamburg this year.
I particularly thank Dr. Antonino Di Piazza for his inspiring and sometimes irreplaceably needed scientific advice as well as for his humorous and at any time pleasant personal behaviour. He is notably among the "World's Best Advisors".
Also I thank Dr. PD Georg Wolschin for being the second reviewer of this work.

I thank Peter for solving any computer problems and Vera and Sibel for making administrative issues a little more understandable to me.

Of course I thank all the people from our group who made my hitherto stay at the MPI a pleasurable and memorable time especially Adriana, Benedikt, Matthias, Ruggi and Sarah for Avernion, "Die Bettwurst I+II", lots of coffee, great cooking, numerous great evenings and "The Kohlfahrt" as well as valuable discussion and technical and formal advice.

Last but not least I thank my girlfriend Tamara for the strong support she provides and for keeping me from going insane during the past few days.

My deepest thanks, however, go to my parents and my siblings Hanna, Jule and Lise for making my studies possible, being the greatest family in this world celebrating the best family parties imaginable and for always just being there.

Erklärung

Hiermit versichere ich, dass ich die vorliegende Arbeit selbst angefertigt und keine anderen als die angegebenen Hilfsmittel benutzt habe.

Heidelberg, den _____ _____

Kai Felix Mackenroth